Validation of Nuclear Data for High Burn-up MOX Fuels

(VALMOX)

Servais PILATE, Benoît LANCE, Hélène GABAIEFF
Belgonucléaire S.A. , Brussels (BE)

Alain SANTAMARINA, Robert JACQMIN, David BERNARD
Commissariat à l'Energie Atomique, Centre de Cadarache (FR)

Bernard VERBOOMEN, Wim HAECK
Studie Centrum voor Kernergie/Centre d'Etude de l'Energie Nucléaire, Mol (BE)

Jim C. KUIJPER, Dirceu da CRUZ
Nuclear Research and Consultancy Group, Petten (NL)

Contract n° FIKS-CT-00191
Final Report

March 2005

EXECUTIVE SUMMARY

Scope

This Validation of Nuclear Data for High Burn-up MOX Fuels, or "VALMOX", took place from October 2001 to September 2004 as part of the research on Nuclear Fission Safety in the 5th R&D Framework Programme of the European Commission (1999-2004) under contract number FIKS-CT-00191. VALMOX was one of the projects of the cluster EVOL (Evolutionary Fuel Concepts: High Burn-up and MOX Fuels).

Based on the most significant irradiations of MOX fuel at high burn-up (up to 60 GWd/t) in European Light Water Reactors, VALMOX comprised the evaluation of the actinide inventory in spent MOX fuel, with special attention placed on helium production.

This study started with a validation of the calculation methods employed by the partners (BELGONUCLEAIRE, CEA, NRG, SCK-CEN) and concluded with precise recommendations to revise some neutron cross-sections in the new basic data file JEFF3 developed under the auspices of OECD/NEA.

Validation of methods

Chapter A first lists the computer code packages used: APOLLO2 at CEA, WIMS8 at BN and NRG, and ALEPH at SCK-CEN. A benchmark case with MOX fuel irradiated up to 48 GWd/t was calculated by all partners.

It is concluded that APOLLO2 yields results of good accuracy while fully usable for design calculations. This is supported by an extensive validation work, including comparisons with the Monte-Carlo code ALEPH. The inventory is well predicted for most actinide isotopes. The agreement is excellent, within 1%, for the U isotopes, for the Pu isotopes (except of Pu238) and Am241. Some deviations (up to 4%) are identified for Pu238, Am243 and the Cm isotopes, however.

Compared to APOLLO2, WIMS8 results are in general in satisfactory agreement: within 1% for U235 and 236, Pu238, 240 and 242; within 3% for Am241, and 4% for Am243 and the Cm isotopes. The only really significant deviations concern Pu239 (+4%) and Pu241 (+3%). This is due to some approximations in the resonance treatment. Part of these approximations have been eliminated in WIMS9, now available.

Analyses of MOX fuel irradiations

Chapter B describes the analyses of MOX fuel irradiated up to 57 GWd/t in the PWR of Beznau-1 (ARIANE programme). In general, recalculations of actinide concentrations in spent fuel done with WIMS8 at BN agree well with the measured values. The C/E ratios are close to unity, with the exceptions of Pu239 (overestimated by 7%), Am241 at End-of-Life (overestimated by 20% and more), and Am243 and all Cm isotopes (underestimated by 5 to 15%).

With ALEPH at SCK-CEN, C/E ratios are closer to unity. The major improvements compared to WIMS are observed for Pu239, Np237, Am241, Am242m and Am243. The large overestimate for Am241 at EoL (about 1.20) remains, while all Cm isotopes are still underestimated. Recalculations with a test version JEFF3.0 were also done at SCK. C/E ratios are improved for U235, U236, Np237, Pu242 and Cm245, as a result of the changes brought to basic data.

The question of measurement errors was addressed in details. It can be observed that the uncertainty on the C/E ratios for the actinides is of the order of ±2%; when larger biases are obtained between calculation and measurement, they should be due to deficiencies in the cross-section data, not to the methods.

An analysis of MOX fuel irradiation in a BWR (Dodewaard) is also presented. It corresponds to MOX pins inserted in UOX fuel. The trends, although more pronounced than in PWR conditions, go in the same direction as above.

Chapter C describes the analyses of MOX fuel irradiations in the French PWRs of Saint-Laurent-des-Eaux B1 and Dampierre 2, two of the twenty 900-MWe reactors loaded with 1/3 MOX fuel, containing well characterised MOX pins extracted for detailed measurements. In SLB1 MOX fuel was irradiated up to 45 GWd/t, and in Dampierre up to 60 GWd/t.

When comparing APOLLO2 calculations for SLB1 and DA using the reference JEF2.2 data file (used by all partners), one can observe quite similar results except for:

- Pu239, for which the overestimate of 3% in SLB1 becomes 5% in DA;
- Am241, for which the excellent C/E in SLB1 is not consistent with the large overestimate (1.17) in DA; the latter results, which are based on more reliable measurements, exhibit the same large overestimate as above.

The APOLLO2 calculations were repeated with a test version of the new data file JEFF3 (JEFF3.0). The consequences of cross-section changes could easily be identified (predictions improved for U236, Np237, Pu242, Am243 and Cm244). The two major observations made above for Pu239 and Am241 remain.

Sensitivity evaluations

A large effort, illustrated in **Chapter D**, was made at CEA and NRG to identify the sensitivities of final atom densities to the initial ones and to the cross-sections used.

At CEA the automated code RDN (Re-estimation of Nuclear Data) was used to check the consistency between integral measurements and spent chemical assays and JEF2.2 evaluations, in order to suggest nuclear data modifications to be introduced in new JEFF3 evaluations. A large series of spent UOX fuel measurements is taken into account. The work done contributed to firm up the recommendations of cross-section modifications in JEFF3.

At NRG a computer code CASEMATE was written to calculate the sensitivities. NRG used a combination of basic cross-section uncertainty values either from the EAF file or provided by CEA. The method was applied to the benchmark case and to typical MOX samples calculated at BN (Beznau-1) and CEA (Dampierre). The sensitivities are very similar for these two samples (the initial plutonium vector was also very similar, and so are the neutron spectra in both cases).
This code was used to investigate the dependence of the helium produced by a-decay as a function of the fuel actinide content.

Helium production and build-up

In **Chapter E**, particular attention is given to the production and build-up of helium (a-particles), which is much stronger in MOX fuels than in UOX fuels. The presence of helium grows largely after irradiation during storage time.

Using the results obtained in Chapters B, C and D, it is shown that the helium build-up:
- is underestimated by -3 ±6% at EoL and by -2 ±4% for a cooling time of 10 years ; Cm242, Cm244, Pu238 and Am241 are the dominant sources of helium just after the end of irradiation ;
- it is very well predicted and its uncertainty is ± 2% (1s) for a storage time of 100 years and ±1% after 1000 years and longer; the dominant sources become the plutonium isotopes Pu240 and Pu241, which are indeed very well calculated.

Conclusions

The main conclusions of this work, given in **Chapter F**, are in the form of recommended changes to some cross-sections in the recent JEFF3.0 file (even if some improvements, such as the increase of ^{235}U and ^{241}Pu resonant capture, are already included) :

- A decrease by 1% of the ^{238}U-resonance integral, in order to lower by 1% the Pu239 content at 45 GWd/t.
- An increase by +15% of the $^{241}Am(n,\gamma)$ capture cross-section in the [0 – 1.5 eV] thermal and epithermal range.

These recommendations are addressed to the JEFF3 evaluators' group of the NEA Databank. With such changes the major part of the biases in C/E ratios found here should disappear.

The whole community of users of this file (designers, fuel vendors, electricity utilities, national regulatory bodies) will benefit from these improvements.

TABLE OF CONTENTS

List of Figures

List of Tables

INTRODUCTION

VALMOX

VALMOX, an acronym for Validation of Nuclear Data for High Burnup Mixed Uranium-Plutonium Oxide Fuels, is one of the projects of the cluster EVOL (Evolutionary Fuel Concepts: High Burnup and MOX Fuels), which is part of the Fifth Framework research programme on Nuclear Energy, Safety of the Existing Installations.

Entirely devoted to MOX assemblies in Light Water Reactors, VALMOX comprises the evaluation of the actinide inventory of spent MOX fuel at high burnup (45 to 60 GWd/t), with special attention to the helium production. Calculated values for the spent fuel isotopic masses were compared to the measured ones, with sensitivity analyses made in support. The European JEF 2.2 evaluated nuclear data file was taken as a basis for the calculations, with some of them repeated with a preliminary version of the new JEFF3 data file.

High burn-up MOX fuels

Achievement of high burn-up with Mixed Oxide Fuels is favourable for clear economic reasons: about 25% of the electricity generation costs in present-day Light Water Reactors is due to fuel cycle costs, and an increase in fuel burn-up reduces them.

A gradual raise in burn-up is authorised by the Safety Authorities on the basis of experimental irradiations followed by post-irradiation examinations, which give as major results the fuel isotopic mass balances following irradiation, and also the amount of helium gas and fission product gases released in the fuel, which determine the internal pin pressure.

Partnership

The following four companies decided to combine their resources and complementary expertise in the VALMOX Project:
- the French *Commissariat à l'Energie Atomique (CEA)*, whose expertise covers a.o. nuclear electricity generation, optimisation of the fuel cycle, nuclear safety and nuclear fusion; staff at Cadarache have strong ties with the JEFF project at the NEA Data Bank of OECD ;
- the Belgian nuclear research centre SCK-CEN of Mol with its mission focused on nuclear safety, radiation protection and safeguards and radioactive waste research;
- the Dutch research centre at Petten, NRG, which provides services in support of the safe, ecological and efficient use of nuclear installations;

- and Belgonucléaire which owns a MOX fuel manufacturing plant delivering up to 40 t MOX fuel per year, and design offices for fuel design and safety, licensing applications and treatment of nuclear waste.

The group was co-ordinated by Belgonucléaire (BN) as was already the case for a similar study contract in the Fourth Framework Programme (1995-1998), entitled 'Nuclear Data for Advanced MOX Fuels', FI4I-CT95-0002. Actually VALMOX may be seen as a follow-up of the former project, the results of which have been reported in [1], with some salient issues presented in [2].

Work planned

The work was subdivided into three Work Packages:
WP1: Evaluation of MOX Fuel Irradiation in Light Water Reactors (one PWR, one BWR), by BN and SCK
WP2: Evaluation of MOX Fuel Irradiation in Light Water Reactors (two PWRs), by CEA
WP3: Intercomparisons, sensitivity analyses and final assessment, by all partners.
The work was started using cross-sections derived from the JEF2.2 file. The code packages used for most of the calculations were WIMS8 [3], APOLLO2 [4] and ALEPH [5].

Work objectives

The general objective of the VALMOX project is to validate the calculations of MOX fuel at high burn-up in Light Water Reactors. Nowadays MOX fuel is generally licensed for burn-ups up to 45 GWd/t. It is planned to progressively raise this limit to 60 GWd/t, by first allowing the same limit as for UO2 fuel (MOX parity objective), which would ease fuel management strategies in MOX-fuelled reactors.

To justify any burn-up increase, it is needed to analyse the results of available high burn-up irradiations. The partners in this project share their evaluations by comparing the trends they observe in the isotopic mass balances at fuel discharge. A number of sensitivity calculations are done to identify the reasons for discrepancies between experimental values (E) and calculated values (C) and to correlate them with deficiencies in nuclear data. The build-up of the minor actinides americium and curium is larger in MOX fuels than in UO2 fuels; moreover their formation grows more than linearly with burn-up.

Innovations

With respect to former work like the one reported in [1], the experimental basis is given by irradiations of MOX fuels up to 60 GWd/t in commercial Light Water Reactors. In addition, the focus is no longer on transmutation but on practical fuel burn-up limits. Lessons learned from past interpretations are used to improve the modelling of the irradiations, so that the remaining discrepancies can be

specifically attributed to cross-sections. The goal is to indicate to the OECD/NEA group in charge of creating the new JEFF3 file which actinide cross-sections should deserve improvements and corrections.

Particular attention is given to the build-up of helium (alpha particles), strongly influenced by the formation in MOX of Pu238, Am and Cm isotopes. Helium gas continues to be generated long after the end of irradiation and is thus a potential concern in spent fuel cooling and storage situations.[1]

Schedule and meetings held

The VALMOX project, originally planned for 30 months, eventually covered 36 months from October 2001 to September 2004.

The following group meetings were held:

1. 17 October 2001 in Brussels (kick-off)
2. 30 April 2002 in Cadarache
3. 30 October 2002 in Petten
4. 18 March 2003 in Mol
5. 28-29 October 2003 in Cadarache
6. 11 May 2004 in Brussels
7. 17 September 2004 in Petten.

Minutes are available, numbered EVOL-VALMOX-M 001 to 007, respectively.

Reports issued

The following reports were issued, numbered EVOL-VALMOX-P 001 to P-006:

Half-yearly Progress Report, October 2001 to March 2002 (P-001)
Yearly Progress Report, Year 1, October 2001 to September 2002 (P-002)
VALMOX: Mid-Term Assessment Report, April 2003 (P-003)
VALMOX: Technological Implementation Plan (TIP) Draft Report (P-004)
Yearly Progress Report, Year 2, October 2002 to September 2003 (P-005)
Half-yearly Progress Report, October 2003 to March 2004 (P-006)

In addition, a presentation was given at the FISA-2003 Seminar in Luxembourg [6], and a paper was sent for publication to Nuclear Engineering and Design [7].

Benchmark study

When the work was started, it was felt necessary to first pay careful attention to the differences in the methods of calculation used: although similar in principle, these methods were not identical. Therefore it was decided that all partners should first calculate the OECD/NEA benchmark exercise BUC-IV with MOX fuel [8] and compare their results. This comparison provided a validation of the methods.

[1] The fraction of gas release is not part of this study, as it depends on fuel temperature and microstructure.

Structure of the report

The validation of methods is reported in Chapter A.

Chapters B and C describe the evaluations of MOX fuel irradiations made by BN and SCK on the one hand and CEA on the other hand. The Light Water Reactors considered were mainly Pressurised Water Reactors, for which the methods are best adapted. Some complementary checks concern irradiation in a BWR.
Chapter D gathers the sensitivity and uncertainty analyses made respectively by CEA and by NRG.
The helium production is specially dealt with in Chapter E.
Chapter F contains the global assessment and the conclusions.

The original intent had been to issue 3 separate reports corresponding to the 3 WPs. But it was later decided to combine these into a single report, including also the benchmark analyses, because of the strong correlation between all these contributions.

References

[1] Nuclear Data for Advanced MOX Fuels, Final Report of Contract n° FI4I-CT95-0002, by S. Pilate et al., EUR 19126 EN, 2000
[2] Validation of Nuclear Data for Transmutation from the Evaluation of MOX Fuel Irradiations, by S. Pilate, R. Jacqmin et al, PHYSOR2000 Conf., Pittsburgh, May2000
[3] WIMS, the ANSWERS Software Package, A General Purpose Neutronics Code, AEA Technology, 1999
[4] APOLLO Twelve Years After, by S. Loubière, R. Sanchez et al, Int. Top. Meeting on Mathematics and Computation, M&C99, Madrid, Sept. 1999
[5] ALEPH, a Monte Carlo Burn-up Code developed at SCK-CEN, by W. Haeck and B. Verboomen.
[6] Validation of high burn-up MOX Fuels Calculations, by S. Pilate et al, FISA-2003 Symposium, Luxembourg, 10-12 November 2003.
[7] VALMOX, Validation of Nuclear Data for High Burn-up MOX Fuels, by B. Lance et al, paper proposed for publication in Nuclear Engineering and Design.
[8] OECD/NEA-NSC Burn-up Credit Benchmark Phase IV-B: Mixed Oxide (MOX) Fuels, updated Feb. 2002, by P.R. Thorne, G.J. O'Connor, R.L. Boden

CHAPTER A

VALIDATION OF COMPUTER CODES FOR MOX CALCULATIONS

A.1 Codes and calculation schemes

A.1.1 APOLLO 2

The recent code APOLLO2.5/CEA93.V6 developed by CEA [**1**] is a French versatile neutronics tool: it is used in the Cycle code package DARWIN, in the Criticality-Safety code package CRISTAL and in the French Reactor Physics code systems. Hereafter we will mainly describe the Reactor utilization and focus on the reference calculation route for detailed irradiated fuel rod analyses

.

The APOLLO2.5 assembly code is currently implemented in the modern PWR calculation tools of Framatome-ANP and Electricité de France, SCIENCE.V2 and N3C respectively. APOLLO2 is also extensively used at CEA for studies of Thermal Reactors (PWR, BWR, VVER, naval propulsion reactors, HCPWR[2], HTR, CANDU, Graphite-moderated reactors), as well as Irradiation reactors and Safety experimental reactors.

The Reference “CEA-97” calculation scheme

The “CEA-97” Reference scheme was defined in order to meet the target accuracy for every LWR design parameter. In a second step, the “CEA-97” scheme was optimized to reach computing times acceptable for design calculations. For instance, the “CEA-97” scheme associated with the evolution of 17x17 UO_2 assemblies is able to reproduce ^{239}Pu build-up and pin-by-pin power within 1% accuracy (up to 70Gwd/t), in 15 mn CPU time on a COMPAQ SC232 computer (Alpha EV67 processor 667 MHz).

The optimized “CEA-97” scheme was validated via the Validation Machine MACH2 of APOLLO2. We have to stress that this “CEA-97” scheme is used in the analysis of integral experiments, therefore it is the unique scheme calibrated for LWR design parameter calculation at CEA.

The APOLLO2.5/CEA93V6 product utilizes the CEA93 multigroup cross-section library, processed by NJOY from the JEF2.2 evaluations. The “CEA-97” scheme recommends the use of the European X-MAS 172-group structure (99-group libraries are also available).

[2] High Converter PWR with tight lattice

The recommendations for the flux calculation are the following:

- Spatial calculation for PWR assemblies is achieved using a UP1 accurate anisotropic interface current method. The inter-assembly water gap is integrated inside the peripheral rectangular cells
- In order to reduce the calculation cost, a grouping of cells with similar flux into a unique 'physical cell' is recommended. In 17x17 UOX assemblies, there are 18 physical fuel cells, 2 physical "tube-guide" cells and one physical "instrumentation tube" cell [**2**]
- Assembly with UO_2-Gd_2O_3 rods is calculated without cell-grouping .
- The fuel pellet is split into 4 rings (50%, 30%, 15% and 5% of the total volume of the pellet) in order to give a faithful representation of the resonant absorption of ^{238}U inside the pin and of the actinide and fission product concentration profiles. This leads to the determination of 72 evolving media.
- MOX assembly depletion calculation is carried out with surrounding UOX assemblies.

The recommendations for the self-shielding calculations are the following:

- ^{238}U, ^{235}U, ^{236}U, ^{239}Pu, ^{239}Pu, ^{240}Pu, ^{241}Pu, ^{242}Pu, ^{241}Am and Zr are self shielded. For Gd poison pins, ^{155}Gd, ^{156}Gd, ^{157}Gd and ^{158}Gd isotopes are self-shielded
- Self-shielding of the ^{238}U large resonances is taken into account by the accurate UP_1 model. The UP_0 approximation with isotropic interface angular flux is adequate to ensure good quality self-shielding results for the other isotopes
- Space-dependent self-shielding using the Background Matrix method: rim effect is accounted for by 4 concentric rings in each fuel rod, and the differences in the Dancoff effect linked to guide-tube vicinity is accounted for.

The recommendations for the assembly depletion calculation are the following:

- Evolution steps : 0, 37, 75, 112.5, 150, 325, 500, 750, 1000, 1500, 2000, 2500, 3000, then constant step of 1000 MWd/t_m
- If the LWR assembly contains UO_2-Gd_2O_3 rods, the evolution steps are more discretized. Each poison pellet is divided into 11 evolving concentric zones. Thus, the assembly depletion calculation is carried out on 210 evolving media.
- Self-shielding calculations are repeated at the following steps: 4, 8, 12, 24, 36, 48,...GWd/t_m
- The recommended depletion chain describes explicitly 20 Actinides ($^{234}U \rightarrow {}^{247}Cm$) and 85 Fission Products

The recommendations for cross-section collapsing and homogenisation are the following:

- Energy collapsing from 172 groups down to 20-groups [**3**]
- Cell by cell homogenisation
- Use of the equivalent homogenisation SPH which preserves reaction rates

The recommendations for core calculations are the following:

- Transport calculation in S8 quadrature (pin by pin pattern, 20 energy groups)
- Anisotropic scattering accounted for in P1 expansion

- Linear-linear nodal scheme: one mesh-point/cell is well suited for spatial discretization
- Specific scheme based on cluster Pij calculation, followed by SPH equivalent homogenization, are recommended for core calculations including control rod cluster [**4**].

More details are given in the **Appendix** for what concerns the verification, validation and qualification process of APOLLO2.

A.1.2 WIMS

The neutronics code package used at BN is WIMS8a [**5**], developed by Serco Assurance (formerly AEA Technology), combined with the library WIMS'97 (JEF 2.2) composed either of 69 or 172 energy groups. The latter group structure is the recommended one for MOX fuel and will be considered herein.

WIMS8a is a modular software in which the numerical information is transmitted from one module to another by means of standardized binary interface files. This gives the code a large flexibility.

WIMS multigroup library

The resonance integrals and other quantities needed to evaluate the effective broad group average cross-sections are read by WIMS from a nuclear data library generated using the NJOY code.
In this context, NJOY solves the neutron slowing down equation for a simple homogeneous mixture of a single resonance absorbing isotope and a fictitious nuclide which has the scattering properties of hydrogen. The NJOY solution is effectively a continuous energy solution which can be used to average cross-sections or resonance integrals over a broad group energy structure specified by the user.

Each execution of NJOY provides energy group data for a specific isotope, temperature and ratio of the resonance absorbing isotope to the fictitious hydrogen like scattering nuclide (σ_p value). The nuclear data library is therefore assembled from many executions of the NJOY code to give a full temperature and σ_p parameterisation.

In the case of non-resonant nuclides, with no temperature dependent thermal cross-sections, only a single execution of NJOY is required in which the flux is assumed to have the shape of the fission spectrum at high energy, to be of the form 1/E in the resonance range and to have a Maxwellian thermal energy dependence.

WIMS modules

- Module HEAD

HEAD is the first and mandatory module to every depletion calculation. Material and geometry data are introduced and resonance treatment of the fuel rods within their lattice is performed by equivalence theory (default option). The resonance treatment is overwritten by another sequence (PRES-CACTUS-RES) in the "subgroup scheme route" (see further).

Each effective rod type of the geometrical model is at least considered as a distinct rod type for the calculation. The rod type can differ either by the material content or by the geometrical data (e.g. 1 = High Pu content MOX, 2 = Medium Pu content MOX, 3 = Low Pu content MOX, 4 = guide Tube, 5 = instrumented Tube).
The distinct rod definition in HEAD is needed in order to associate at each mesh an appropriate flux and spectrum that will be used in the depletion calculation.

The rods are generally described as a two-mesh element, one for the pellet and the other for the cladding.

In standard depletion calculation, the whole pellet is indeed considered as one mesh, since equivalence theory is applied. This implies that the depletion calculation provides the material inventory for the whole pellet, without information about the radial distribution of nuclides (e.g. the strong Pu239 build-up at pellet periphery), neither radial distribution of the power.

For strong absorbers (AIC, B_4C, Hf, etc.) and burnable poisons (UO_2-Gd_2O_3), however, a refined radial meshing is necessary. The default procedure consists to subdivide the absorbing region into 7 annuli of equal surface (RODSUB keyword). Each rod sub part is filled with a different material in order to take into account large difference in material absorption rates, from the centre to the periphery .

If one wants to avoid the use of equivalence theory and/or one is interested in material inventory as a function of radial region, the fuel pellet must be subdivided in the same way as strong absorbers, e.g : the pellet can be subdivided into 4 radial regions whose radius is calculated to get surfaces of 50, 30, 15, 5 % of the total pellet surface (CEA methodology).

By doing this, the external region is thinner and can account of the rim effect. In such a procedure, a subgroup and space dependent treatment of resonant nuclides is applied, as explained hereafter.

• Module PRES and RES

Those two modules are invoked when resonance treatment by equivalence theory is felt not appropriate (radial power and inventory assessed or special geometries). They are used within the sequence “HEAD $\rightarrow$ PRES $\rightarrow$ CACTUS $\rightarrow$ RES” or “HEAD $\rightarrow$ PRES $\rightarrow$ THESEUS $\rightarrow$ RES” (for cell calculation) and allow a resonance treatment by subgroup method. PRES creates an interface file containing the subgroup cross sections fed into the following module that performs the subgroup flux solution. RES computes the broad group (69 or 172 g) resonance cross sections to be used in the next steps of the WIMS scheme.

The user is requested to specify the nuclides for which a subgroup treatment is desired. Typically, no more than 4 nuclides (U235, U238, Pu239 and Pu240) are specified.

• Module PERSEUS and PIP

PERSEUS module deals with the collision probabilities calculation, within a multicell formalism. PIP performs a flux calculation in the library energy structure (69 or 172 groups). So far the geometry is only an approximate one, as collision probabilities have been deduced on the basis of the contact surfaces of the various cells in the model. In the other hand the energy structure is kept as in the original library (WIMS’97).

• Module CONDENSE

This module performs the flux and cross sections condensation, up to a few energy groups chosen by the user. This step aims at saving computer time in the following main transport calculation. It is not necessary for pin cell model but becomes indispensable as soon as more complex geometries are considered, as assembly and super cell models.

Three group structures were so far recommended by Serco Assurance :

- 6 groups (8.2×10^5, 9.118×10^3, 4.0, 0.625 and 0.14 eV), for PWR-UO2 fuel,
- 8 groups (8.2×10^5, 9.118×10^3, 367.262, 48.052, 4.0, 0.625 and 0.14 eV), for BWR-UO2 fuel,
- 21 groups, recently recommended [**6**] for MOX fuel.

- Module DIFF

The DIFF module of WIMS is used to allow the depletion of each rod in a different manner, according to the flux level and to the condensed (6, 8 or 21 groups) spectrum obtained in the main characteristics transport calculation (CACTUS module). The user must create as many new materials as there are pins in the geometry model, introducing the DIFF module before CACTUS.
Then, after the main transport calculation and the depletion calculation itself by the BURNUP module, DIFF must be set once again in order to calculate the average irradiated pin compositions that will be introduced in HEAD for the following calculation step. In this way, resonance treatment will be applied on the few rod types involved in the model, instead of performing a pin wise resonance treatment. This reveals to be a good approximation.

- Module CACTUS

CACTUS performs the main transport calculation, using a characteristics lines method. This is a numerical approach in which the differential form of the Boltzmann equation is integrated along explicit tracks through the geometry and the neutron flux is obtained by a summation of the contributions made by a selected sample of such tracks. The tracking definition is to be defined by the user.

One of the main features of the method is that it allows to consider complex and explicit geometries. For instance, one is not restricted to standard XY calculations for which the pellet, clad and moderator are smeared together to form square cell cross sections sets. Instead, the pellet and the clad are explicitely represented within their respective cell.

- Module BURNUP

This module computes the depletion of the fuel according to the flux distribution in the geometric model. The resulting fuel composition is fed into the HEAD module for the next time step. This leads to a cyclic calculation in which resonance treatment is performed at several time steps, since the composition of the fuel has an important impact on self-shielding.

Additional details are given in the **Appendix** concerning the resonance treatment and the definition of the calculation routes with WIMS8.

A.1.3 ALEPH

ALEPH [**7**] is a Monte Carlo burn up code developed at SCK-CEN, capable of using any version of MCNP(X) [**8**, **9**] for spectral calculations, a slightly modified version of ORIGEN 2.2 [**10**] for evolution calculations and data read from the ENDF-VI format by using NJOY 99.90 [**11**].

The application of the MC (Monte Carlo) method to the field of burn-up calculations leads to powerful tools with a broad area of applications: from simple 1-D to complex 3-D geometries, either normal critical systems or sub-critical systems with an external fixed source. The use of MC also allows for multi-particle physics, complex interaction laws and detailed energy-angle descriptions which can be of crucial importance in applications such as ADS (Accelerator Driven Systems).

These tools are however quite demanding on calculation time because the reaction rates required for burn up calculations (about 1E+3 per space-mesh and per time step) are always calculated “on the fly” within an MC code (this time is roughly proportional to the number of reaction rates and to the total number of neutron interactions). Examples are MONTEBURNS [**12**], MOCUP [**13**], MCB [**14**] and OCTOPUS [**15**].

The primary purpose of the MC code in an MC burn up code is to calculate the spectrum weighted microscopic reaction rates s_{ijk} for every nuclide (i), reaction (j) and space-cell (k) considered in the transmutation chain:

$$\sigma_{ijk} = \frac{\int_{cell(k)} dV \int dE\, \sigma_{ij}(E)\Phi(P,E)}{\int_{cell(k)} dV \int dE\, \Phi(P,E)} \quad (1)$$

in which $s_{ij}(E)$ is the continuous energy cross section for nuclide (i) and reaction (j) and ? is the neutron energy flux at position P in the cell(s) with the material that we wish to burn. A code such as MCNP(X) estimates these quantities (track length estimator [**16**]) as a sum over all histories (h) and interactions (i) going through the cell in which we want to know the reaction rate :

$$\int_{cell(k)} dV \int dE\, \sigma_{ij}(E)\Phi(P,E) = \frac{1}{N}\sum_h \sum_i L_{i,h} W_{i,h} \sigma(E_{i,h}) \quad (2)$$

$$\int_{cell(k)} dV \int dE\, \Phi(P,E) = \frac{1}{N}\sum_h \sum_i L_{i,h} W_{i,h} \quad (3)$$

where $E_{i,h}$ is the energy of a particle during his free flight within the cell (k) where we want to calculate the reaction rate with a corresponding track length $L_{i,h}$ and weight $W_{i,h}$.

In MCNP(X), these quantities are accumulated during the simulation of all the particles. As such, the following operations have to be performed for every history, every interaction and for every reaction rate that we want:

- § calculate the cross section value s ($E_{i,h}$) (that is, look for the right interval and perform a linear interpolation)
- § calculate the product $L_{i,h} W_{i,h} s (E_{i,h})$ and add it to the previous result

If the number of interactions and histories is large, looking up the cross section value every time will become a very time consuming operation. If we calculate for instance the (n,?) reaction rate of U-238 we already see an increase of 8 % in calculation time. Adding more reaction rates only makes it worse: when calculating about 1000 reaction rates (which are required for burn up calculations) we can observe an increase in calculation time of a factor 30.

A solution to this problem would be to calculate the required reaction rates after the MC calculation finished - allowing us to reduce the number of operations required and thus reduce the total calculation time. For this purpose we have developed a multi group approach to the problem which has been implemented in ALEPH.

This is described in the **Appendix**; the calculation flow with ALEPH is also shown.

A.2 Benchmark description

In order to discuss the C/E trends reported by the different VALMOX partners, each working with a different code, a useful first step is to perform a theoretical depletion calculation benchmark. In this way, the calculation biases in fuel inventory prediction among participants (using the same nuclear data library JEF2.2) can be exactly quantified.

To this aim, it was decided to study the OECD/NEA BUC IVB benchmark [**17**]. This benchmark had been proposed by the expert group on Burnup Credit (BUC) of the Working Party on Nuclear Criticality Safety (NEA – WPNCS).

It consists of several kinds of depletion calculations for MOX fuel, namely by order of complexity (see **Fig. A.1**):

- a pin cell model,
- an assembly model,
- a supercell model.

Fig. A.1
The 3 geometrical models considered in the NEA BUC IV B benchmark

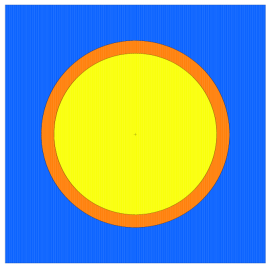

Pin cell model

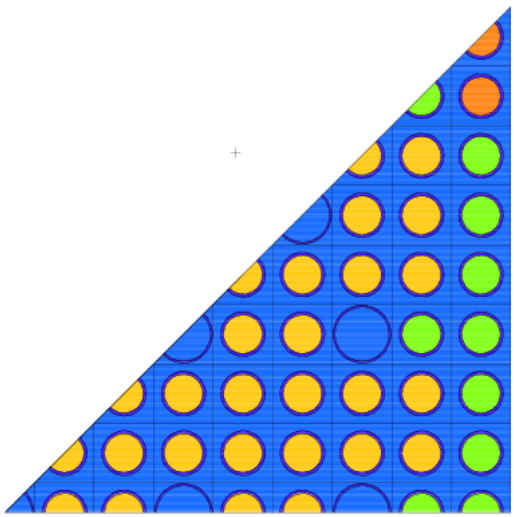

Assembly model

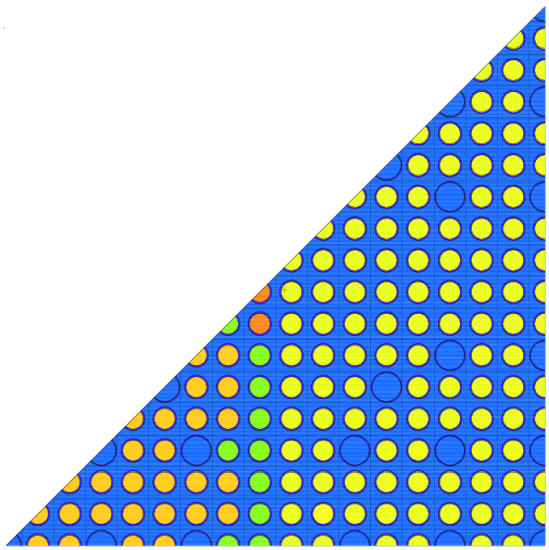

Super cell model

In the first model, one represents a single pin in a moderator cell, with reflection boundary conditions. This model is thus representative of an infinite medium and provides information about reactivity and fuel inventory as a function of burnup. The pitch of the cell must be modified to take into account the assembly global moderation ratio that the pin cell calculation simulates.

The assembly model simulates the assembly with reflection or translation boundary conditions, within a 2D calculation. This model provides more information than the pin cell model, since pinwise power distribution and pinwise material inventory can be computed. The assembly calculation is a standard calculation step in a complete design core calculation, as done for reshuffling.

Finally the supercell model is the most sophisticated depletion calculation, that aims to calculate a fuel assembly while taking into account its environment. It is especially recommended when dealing with MOX fuel, as this type of fuel is loaded in cores filled with a larger number of UO2 fuel assemblies: the MOX fuel assembly behaviour thus depends on the neutron spectrum that is established in the UO2 fuel. In particular, power peaking at the MOX fuel assembly border needs to be carefully assessed.

Two types of MOX fuels were considered in the benchmark specifications: MOX made with Reactor-Grade Plutonium (RG-MOX) and MOX made with Weapon-Grade Plutonium (WG-MOX). In this latter case, the Plutonium content is lower in account of the better fissile quality, as compared to the RG-MOX.

The depletion was assumed to be at constant power and the irradiation history included three cycles, each of 420 days, with 30 days shutdown periods. The material inventory was requested at each End of Cycle states (EOC), as well as End of Irradiation (EOI = EOC-3) with a cooling time of 5 years. The spent fuel is characterized by a final burnup of 48 GWd/t.

A.3 Benchmark results

In order to clarify the discussion, only results for Reactor Grade MOX at EOC-3 state (Bu = 48 GWd/t) are hereunder reported. No significant discontinuity of material inventory as a function of time was found and the comparisons performed at this final burnup are relevant for the forthcoming analysis against experimental results. Moreover WG-MOX is not representative of the samples that were analysed and this material is not further considered in this chapter.

A.3.1 Pin cell model

The results are presented in **Table A.I**. The atomic concentration obtained by the 3 codes are given, along with the relative difference (%) with respect to the APOLLO-2 entry, here considered as the reference.

The agreement between ALEPH and APOLLO-2 is especially good for the Pu isotopes, whereas WIMS8a predicts higher concentrations (~ 3 %) for Pu239 and Pu241 (as well as Am241 mainly arising from Pu241 decay).
The Np237 content is computed lower and higher respectively by WIMS8a and ALEPH, as compared to APOLLO2 (notice that the Np237 build-up is mainly linked to U238(n,2n) reaction for MOX fuel).

Due to Pu241 overestimation, Am241 and its daughter Cm242 are computed higher by ~ 3 % by WIMS; however, the heavier isotope Am242m seems to be underestimated, probably because of a different branching ratio value towards this metastable state. It was verified that this difference between WIMS8a and APOLLO-2 did not originate from the Am241 capture cross sections. Concerning Am243 build-up, WIMS8a and APOLLO-2 disagree by 4% probably due to self-shielding calculation in the E_{Pu242} = 2.7eV resonance.

Finally, a global agreement between WIMS and APOLLO is observed for the fission products, especially for the Samarium isotopes.

For WIMS, a parametric study with respect to the group structure prior to the transport calculation has been performed. This was motivated by the fact that WIMS developers detected that CONDENSE module does not preserve accurately the reaction rates and previously studied the impact on reactivity [**6**].

Table A.II presents the impact of the condensation procedure on the actinides inventory, still compared to the APOLLO2 entry. A degradation of the results is observed with the decrease in the number of energy groups, as compared to the "best" calculation involving no condensation. Accordingly the 21-g condensation should be preferred for MOX fuel, but CPU requirements (21-g makes the computation ~ 3 $\times$ longer) still make the 6-g condensation the standard procedure and this choice will be considered in the frame of C/E analysis in the next Chapter.

More precisely, one focuses on the fissile isotopes U235, Pu239 and Pu241 and on the strong Am241 absorber. The lower the number of energy groups considered, the higher the overestimation of those isotopes. A better agreement between WIMS and APOLLO2 is observed using both WIMS9 self-shielding improvements and refined 172-group structure. However, WIMS/APOLLO2 consistency is not improved for Np237, Am242m and Am243 prediction.

The WIMS9 version under development was received for testing. Such a code answers some WIMS8a shortcomings but is also more time- and memory-consuming than WIMS8a. However results are hereunder reported for the cell approach. They confirm that WIMS9 is in closer agreement with APOLLO-2, thanks to the improvements achieved in the models.

A sketch of the neutron spectrum computed by ALEPH is given at **Fig. A.2**.

Table A.I
Results and comparisons for the **pin cell** model of BUC IV B benchmark

Isotope	APOLLO2	WIMS8a	ALEPH	(W-AP2)/AP2	(AL-AP2)/AP2
	atoms/barn/cm			(%)	
U -234	1.019E-06	1.052E-06	1.011E-06	3.3	-0.7
U -235	2.707E-05	2.736E-05	2.711E-05	1.1	0.1
U -236	5.907E-06	5.842E-06	5.850E-06	-1.1	-1.0
U -238	2.067E-02	2.065E-02	2.066E-02	-0.1	0.0
Pu-238	3.951E-05	3.992E-05	4.115E-05	1.0	4.2
Pu-239	5.218E-04	5.419E-04	5.217E-04	3.9	0.0
Pu-240	4.150E-04	4.050E-04	4.154E-04	-2.4	0.1
Pu-241	2.332E-04	2.405E-04	2.378E-04	3.2	2.0
Pu-242	1.520E-04	1.544E-04	1.512E-04	1.5	-0.5
Np-237	3.511E-06	3.238E-06	3.955E-06	-7.8	12.6
Am-241	1.878E-05	1.938E-05	1.905E-05	3.2	1.5
Am-242m	4.272E-07	3.928E-07	4.302E-07	-8.1	0.7
Am-243	3.954E-05	3.788E-05	4.084E-05	-4.2	3.3
Cm-242	3.856E-06	3.997E-06	3.921E-06	3.7	1.7
Cm-243	1.395E-07	1.452E-07	1.428E-07	4.1	2.4
Cm-244	2.392E-05	2.350E-05	2.391E-05	-1.8	-0.1
Cm-245	3.060E-06	3.059E-06	3.035E-06	0.0	-0.8
Mo-95	4.479E-05	4.466E-05	4.497E-05	-0.3	0.4
Tc-99	6.094E-05	6.097E-05	6.086E-05	0.0	-0.1
Ru-101	6.637E-05	6.587E-05	6.463E-05	-0.7	-2.6
Rh-103	5.458E-05	5.429E-05	5.253E-05	-0.5	-3.8
Ag-109	1.298E-05	1.304E-05	1.240E-05	0.4	-4.5
Cs-133	6.450E-05	6.416E-05	6.547E-05	-0.5	1.5
Nd-143	4.351E-05	4.357E-05	4.399E-05	0.2	1.1
Nd-145	3.200E-05	3.181E-05	3.201E-05	-0.6	0.0
Sm-147	4.091E-06	4.057E-06	4.086E-06	-0.8	-0.1
Sm-149	3.497E-07	3.578E-07	3.204E-07	2.3	-8.4
Sm-150	1.570E-05	1.546E-05	1.649E-05	-1.5	5.0
Sm-151	1.835E-06	1.870E-06	1.691E-06	1.9	-7.8
Sm-152	7.097E-06	6.963E-06	6.699E-06	-1.9	-5.6
Eu-153	8.582E-06	8.433E-06	8.404E-06	-1.7	-2.1
Gd-155	3.031E-08	2.845E-08	2.898E-08	-6.2	-4.4

* APOLLO-2 entry considered as reference

Table A.II
Effect of the energy group condensation for the WIMS pin cell depletion calculation

Code Condensation	WIMS8a 172 → 6 g	WIMS8a 172 → 21 g	WIMS8a 172 g	WIMS9 172 → 6 g
U –234	3.3	3.0	3.3	3.3
U –235	1.1	0.7	0.8	0.8
U –236	-1.1	-1.0	-1.2	-1.6
U –238	-0.1	-0.1	0.0	0.0
Pu-238	1.0	0.6	0.5	0.9
Pu-239	3.9	3.4	2.8	2.4
Pu-240	-2.4	-1.0	-1.1	-2.2
Pu-241	3.2	1.7	1.8	3.1
Pu-242	1.5	1.8	2.2	1.4
Np-237	-7.8	-7.9	-8.3	-14.1
Am-241	3.2	1.9	2.2	2.9
Am-242m	-8.1	-10.0	-10.4	-8.3
Am-243	-4.2	-4.8	-5.2	-3.6
Cm-242	3.7	2.6	2.6	4.1
Cm-243	4.1	3.4	3.1	4.2
Cm-244	-1.8	-3.7	-4.8	-1.0
Cm-245	0.0	-2.1	-4.2	1.3

* Comparisons performed against APOLLO-2

Fig. A.2 Neutron energy spectrum used by ALEPH for the single pin model at begin of life and end of life (1320 days - 48 GWd/t). One clearly sees the self-shielding effects of the Pu 239 resonance at 0.3 eV and the Pu240 resonance at 1.06 eV

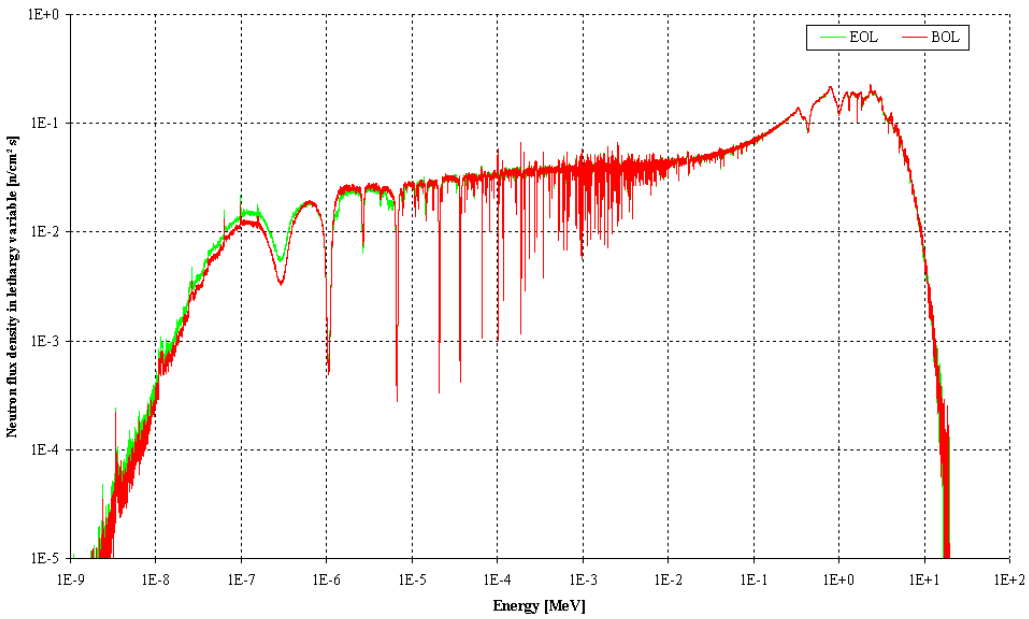

A.3.2 Assembly model

The assembly results (**Table A.III**) show roughly the same trend, but the agreement between WIMS and APOLLO-2 is slightly better than for the pin cell approach, for the important nuclides U235, Pu239, Pu241 and Am241.
The same trend is also observed for ALEPH, which tends to further depelete the fissile isotopes Pu239 and Pu241 than in the pin cell model.

Table A.III
Results and comparisons for the **assembly** model of BUC IV B benchmark

Isotope	APOLLO2	WIMS8a	ALEPH	(W-AP2)/AP2	(AL-AP2)/AP2
	atoms/barn/cm			(%)	
U -234	1.018E-06	1.051E-06	1.011E-06	3.3	-0.7
U -235	2.694E-05	2.714E-05	2.695E-05	0.7	0.1
U -236	5.918E-06	5.860E-06	5.852E-06	-1.0	-1.1
U -238	2.067E-02	2.066E-02	2.068E-02	0.0	0.0
Pu-238	3.941E-05	3.967E-05	4.088E-05	0.6	3.7
Pu-239	5.198E-04	5.343E-04	5.106E-04	2.8	-1.8
Pu-240	4.165E-04	4.084E-04	4.164E-04	-1.9	0.0
Pu-241	2.316E-04	2.370E-04	2.344E-04	2.3	1.2
Pu-242	1.523E-04	1.554E-04	1.521E-04	2.1	-0.1
Np-237	3.485E-06	3.140E-06	3.911E-06	-9.9	12.2
Am-241	1.869E-05	1.919E-05	1.881E-05	2.7	0.7
Am-242m	4.221E-07	3.793E-07	4.169E-07	-10.1	-1.2
Am-243	3.944E-05	3.761E-05	4.043E-05	-4.6	2.5
Cm-242	3.839E-06	3.968E-06	3.892E-06	3.4	1.4
Cm-243	1.389E-07	1.437E-07	1.403E-07	3.4	1.0
Cm-244	2.382E-05	2.317E-05	2.338E-05	-2.7	-1.8
Cm-245	3.035E-06	2.963E-06	2.913E-06	-2.3	-4.0
Mo-95	4.479E-05	4.466E-05	4.494E-05	-0.3	0.3
Tc-99	6.094E-05	6.101E-05	6.088E-05	0.1	-0.1
Ru-101	6.636E-05	6.587E-05	6.467E-05	-0.7	-2.6
Rh-103	5.458E-05	5.437E-05	5.254E-05	-0.4	-3.7
Ag-109	1.299E-05	1.310E-05	1.242E-05	0.8	-4.4
Cs-133	6.449E-05	6.423E-05	6.549E-05	-0.4	1.5
Nd-143	4.345E-05	4.345E-05	4.388E-05	0.0	1.0
Nd-145	3.199E-05	3.180E-05	3.202E-05	-0.6	0.1
Sm-147	4.090E-06	4.068E-06	4.110E-06	-0.5	0.5
Sm-149	3.451E-07	3.406E-07	3.078E-07	-1.3	-10.8
Sm-150	1.571E-05	1.547E-05	1.648E-05	-1.5	4.9
Sm-151	1.821E-06	1.816E-06	1.652E-06	-0.3	-9.3
Sm-152	7.103E-06	7.022E-06	6.763E-06	-1.1	-4.8
Eu-153	8.586E-06	8.440E-06	8.401E-06	-1.7	-2.2
Gd-155	2.987E-08	2.669E-08	2.740E-08	-10.6	-8.3

A.3.3 Super cell model

Finally **Table A.IV** shows the comparisons for the MOX assembly average inventory, within the super cell model. Once again the observations are consistent with those made for the pin cell and assembly calculations. Those results are quite relevant for VALMOX analysis, since the MOX samples studied in the chapter B were calculated according to such an approach.

Table A.IV

Results and comparisons for the **super cell** model of BUC IV B benchmark

Isotope	APOLLO2	WIMS8a	ALEPH	(W-AP2)/AP2	(AL-AP2)/AP2
	atoms/barn/cm			(%)	
U -234	1.027E-06	1.059E-06	1.013E-06	3.2	-1.3
U -235	2.636E-05	2.664E-05	2.621E-05	1.1	-0.6
U -236	5.867E-06	5.816E-06	5.850E-06	-0.9	-0.3
U -238	2.071E-02	2.070E-02	2.071E-02	-0.1	0.0
Pu-238	3.875E-05	3.914E-05	4.022E-05	1.0	3.8
Pu-239	4.793E-04	5.001E-04	4.747E-04	4.3	-1.0
Pu-240	4.195E-04	4.111E-04	4.166E-04	-2.0	-0.7
Pu-241	2.230E-04	2.294E-04	2.269E-04	2.9	1.8
Pu-242	1.572E-04	1.589E-04	1.563E-04	1.1	-0.6
Np-237	3.208E-06	2.972E-06	3.590E-06	-7.4	11.9
Am-241	1.806E-05	1.866E-05	1.813E-05	3.3	0.4
Am-242m	3.850E-07	3.510E-07	3.846E-07	-8.8	-0.1
Am-243	3.899E-05	3.732E-05	4.044E-05	-4.3	3.7
Cm-242	3.811E-06	3.935E-06	3.896E-06	3.3	2.2
Cm-243	1.326E-07	1.374E-07	1.371E-07	3.6	3.4
Cm-244	2.241E-05	2.216E-05	2.285E-05	-1.1	1.9
Cm-245	2.601E-06	2.618E-06	2.687E-06	0.7	3.3
Mo-95	4.489E-05	4.474E-05	4.550E-05	-0.3	1.4
Tc-99	6.128E-05	6.128E-05	6.183E-05	0.0	0.9
Ru-101	6.651E-05	6.601E-05	6.557E-05	-0.8	-1.4
Rh-103	5.467E-05	5.443E-05	5.299E-05	-0.4	-3.1
Ag-109	1.325E-05	1.333E-05	1.274E-05	0.6	-3.9
Cs-133	6.501E-05	6.469E-05	6.659E-05	-0.5	2.4
Nd-143	4.299E-05	4.304E-05	4.394E-05	0.1	2.2
Nd-145	3.207E-05	3.188E-05	3.244E-05	-0.6	1.2
Sm-147	4.226E-06	4.191E-06	4.246E-06	-0.8	0.5
Sm-149	3.040E-07	3.068E-07	2.768E-07	0.9	-8.9
Sm-150	1.576E-05	1.549E-05	1.673E-05	-1.7	6.2
Sm-151	1.662E-06	1.683E-06	1.546E-06	1.2	-7.0
Sm-152	7.295E-06	7.209E-06	6.997E-06	-1.2	-4.1
Eu-153	8.677E-06	8.497E-06	8.576E-06	-2.1	-1.2
Gd-155	2.445E-08	2.250E-08	2.332E-08	-8.0	-4.6

* APOLLO-2 entry considered as reference

In this context, three WIMS calculation schemes (described in Appendix) were tested and their results are reported in **Table A.V**. It can be noticed that the subgroup scheme, the more general one, is also the scheme that provides the best agreement on the actinides inventory, as compared to APOLLO-2 calculations. This is not so surprising in the sense that the choice of the subgroup scheme makes the calculation more similar to APOLLO-2 and CEA methodology.

Table A.V

Comparisons of the WIMS schemes for the super cell model of BUC IV B benchmark – average MOX assembly inventory

Nuclides	Standard scheme	Fine Scheme	Subgroup Scheme
U –234	3.2	3.1	2.8
U –235	1.1	1.1	1.0
U –236	-0.9	-0.9	-0.7
U –238	0.0	-0.1	0.0
Pu-238	1.0	1.1	0.4
Pu-239	4.3	4.6	3.3
Pu-240	-2.0	-2.2	-1.7
Pu-241	2.9	3.3	0.8
Pu-242	1.1	1.0	0.7
Np-237	-7.4	-7.2	-7.8
Am-241	3.3	3.3	1.3
Am-242m	-8.8	-8.0	-11.0
Am-243	-4.3	-4.3	-4.8
Cm-242	3.3	3.5	2.2
Cm-243	3.6	4.1	2.5
Cm-244	-1.1	-0.9	-1.0
Cm-245	0.7	1.5	0.2

* APOLLO-2 entry considered as reference

In particular, the agreement for Pu239 and Am241 nuclides are respectively about 1 and 2 % better. However,there is a higher disagreement for Am242m.

A.3.4 Conclusions

As a conclusion, trends reported in Table A.IV should be kept in mind for the final inter-comparison of the C/E analysis performed on the basis of different experimental databases, particularly the WIMS trend to overestimate Pu239 build-up by 4 to 5% compared to APOLLO2 and ALEPH.

References for chapter A

1. S. Loubiere, R. Sanchez, M. Coste, A. Hebert, Z. Stankovski, I. Zmijarevic, "APOLLO2 Twelve Years After," Proc. Int. Conf. on Math. and Comp., M&C99, Madrid, Sept. 1999.
2. C. Chabert, A. Santamarina, R. Dorel, D. Biron, C. Poinot, "Qualification of the APOLLO2 assembly code using PWR-UO2 isotopic assays," Proc. Int. Top. Meeting in Reactor Physics and Math. and Comp. into the Next Millennium, PHYSOR 2000, Pittsburgh, USA, May 7-12, 2000.
3. B. Roque, A. Santamarina, C. Mattera, E. Lejeune, "Validation of the new French Criticality-Safety package CRISTAL," Proc. Int. Top. Meet. on Criticality-Safety Challenges in the Next Decade, Chelan, USA, Sept. 7-11, 1997.
4. P. Blanc-Tranchant, A. Santamarina, G. Willermoz, A. Hebert, "Definition and Validation of a 2D Transport Scheme for PWR Control Rod Clusters," Proc. Int. Conf. on Mathematics and Computation, M&C 99, Madrid, Spain, Sept. 27-30, 1999.
5. WIMS, The ANSWERS software package, a general purpose neutronics code, Serco Assurance, 1999
6. D. J. Powney, J. L. Hutton and E. B. Webster, An Investigation into WIMS Condensation Effects for UOX and MOX Pincells, ANSWERS/WIMS/TR06, August 1999
7. W. Haeck and B. Verboomen, ALEPH - A Monte Carlo Burn-up Code, SCK-CEN, BLG n° 1003 (2005)
8. J. F. Briesmeister, MCNP - A General Monte Carlo N-Particle Transport Code, Version 4C, LA-13709-M, Los Alamos National Laboratory, USA (2000)
9. J. S. Hendricks et al., MCNPX, VERSION 2.5.e, LA-UR-04-0569, Los Alamos National Laboratory, USA (2004)
10. A. G. Croff, A User's Manual for the ORIGEN2 Computer Code, ORNL/TM-7175, Oak Ridge National Laboratory, Oak Ridge, USA (1980)
11. R. E. MacFarlane, D. W. Muir, The NJOY Nuclear Data Processing System Version 91, LA-12470-M, Los Alamos National Laboratory, USA (1994)
12. D. L. Poston, H. R. Truelle, User's Manual, Version 2.0 for MONTEBURNS Version 1.0, LA-UR-99-4999, Los Alamos National Laboratory, USA (1999)
13. R. L. Moore, B. G. Schnitzler, C. A. Wemple, R. S. Babcock, D. E. Wessol, MOCUP:MCNP-ORIGEN2 Coupled Utility Program, INEL-95/0523, Idaho National Engineering Laboratory, Idaho Falls, USA (1995)

14. J. Cetnar, W. Gudowski, J. Wallenius, User Manual for Monte-Carl o Continuous Energy Burn-up (MCB) Code Version 1C, KTH, Stockholm, Sweden (2002)
15. J. Oppe and J.C. Kuijper, 'OCTOPUS_TNG Reference Guide', NRG Report 20748/03.54103/C, November 2004
16. I. Lux, L. Koblinger, Monte Carlo Particle Transport Methods: Neutron and Photon Calculations, CRC Press, Boca Raton, USA (1991)
17. P. R. Thorne, G. J. O'Connor and R. L. Boden, OECD/NEA NSC Burnup Credit Benchmark Phase IV-B : Mixed Oxide (MOX) Fuels, February 2002

CHAPTER B

MOX FUEL IRRADIATIONS IN LIGHT WATER REACTORS

Calculations and evaluations made at BN and SCK in Belgium

B.1 Available experimental data

B.1.1 The ARIANE Programme

The ARIANE programme [1] is a vast set of UO2 and MOX fuel irradiations in different LWRs, launched by BN, in charge of programme co-ordination and evaluation, and SCK-CEN in charge of measurements, with the participation of other European laboratories. For this VALMOX project, one has mainly selected in the ARIANE programme a series of irradiations which took place in the Beznau-1 PWR, as they corresponded to the type of MOX fuel used in present power reactors and irradiated up to relatively high burn-up values of 45 to 60 GWd/t. Irradiations of MOX fuel in the BWR reactor of Doodewaard were also considered and are discussed below under section B.7.

While the experimental results themselves are proprietary, calculation-to-experiment ratios for the spent fuel isotopes could be made available, so as to identify the trends in MOX nuclear data.
Radiochemical analysis is made for 49 different isotopes through a common programme in three different laboratories (SCK-CEN, PSI, TUI).
The following isotopic concentrations were determined :
U234, U235, U236, U238, Np237, Pu238, Pu239, Pu240, Pu241, Pu242, Am241, Am242, Am243, Cm242, Cm243, Cm244, Cm245
I129, Cs133, Cs134, Cs135, Cs137, Tc99, Ce144, Nd142, Nd143, Nd145, Nd146, Nd148, Nd150, Sm147, Sm149, Sm150, Sm151, Sm152, Eu153, Eu154, Eu155,
Sr90, Mo95, Ru101, Ru106, Rh103, Ag109, Sb125, Pm147, Gd155.
A detailed power history and the description of core environment is provided for each fuel sample.

B.1.2 Beznau core and fuel samples

The Beznau-1 reactor of NOK, the Nord-Ost Schweizerische Kernkraftwerksgesellschaft, is a PWR of 400 MWe. Its core is made of assemblies of 14*14 rod positions filled with 179 fissile rods, 1 instrumentation tube and 16 guide tubes for control absorber. It was partially loaded with MOX fuel fabricated at the Belgonucléaire MOX fuel plant in Dessel.

The ARIANE programme of MOX fuel irradiation in different reactors has covered irradiations which took place from 1990 to 1996 in the PWR of Beznau-1, and more particularly in the assemblies M109 (10 rods analysed) and M308 (6 rods analysed). Chemical analyses were made by 3 laboratories in parallel, one of which is SCK, from 1997 to 2000.

A typical MOX assembly with well characterised fuel, like M109, is shown on **Fig. B.1**. It contains the usual three concentric zones of different enrichments : a high Pu content zone in the centre, a medium Pu content zone in the periphery, and a low Pu content zone at the assembly corners. The fuel was irradiated during 5 or 6 reactor cycles of approximately 10 GWd/t each before discharge and analysis.

FIG. B.1
LAYOUT OF THE BEZNAU-1 PWR-MOX ASSEMBLIES WITH THE SAMPLE RODS LOCATION

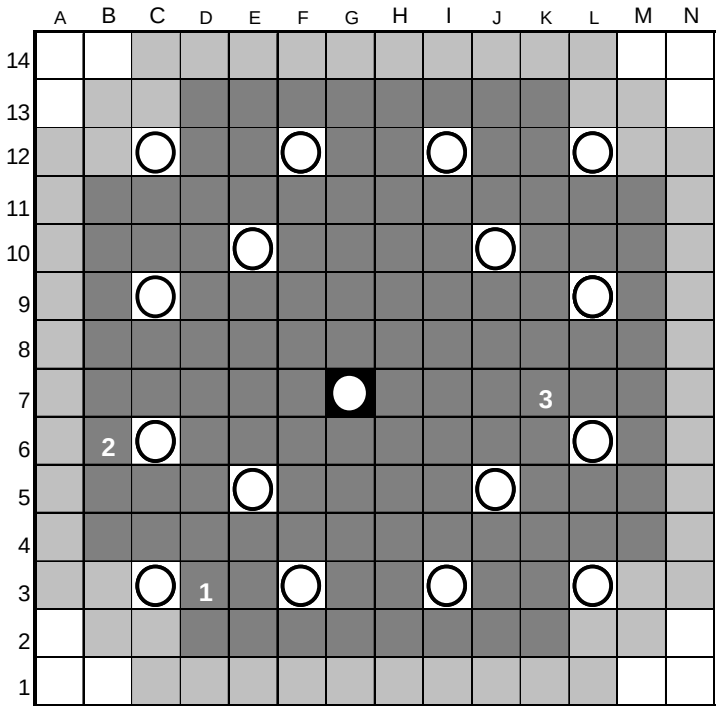

1 Rod D3 (BM1 and BM2 samples) from M109 assembly

2 Rod B6 (BM3 and BM4 samples) from M109 assembly

3 Rod K7 (BM5 and BM6 samples) from M308 assembly

This evaluation has selected two fuel rods placed at locations D3 and B6 in assembly M109 (see Fig. B.1) and one fuel rod K7 in the similar assembly M308. These rods, which all belong to the high Pu content zone, were submitted to post-irradiation examinations ; a central cut near core midplane and an off-centre cut underwent chemical analysis. The evaluation focussed on the central cuts, designated BM1, BM3 and BM5. The analysis of the off-centre cuts BM2, BM4 and BM6 will only shortly be commented.[3]

A large parametric survey was first conducted on the BM1 sample. Its analysis had already started in the preceding FP4 report [2], but a careful re-examination

[3] Actually samples BM2 and 4 are identified BM2D and 4D in report [1], and sample BM5 is named BM5'.

of the experimental results led to recommend slightly changed experimental results ; this recommendation resulted from discussions among the 3 groups of experts engaged in chemical analysis. At the same time, they determined that the experimental values were very accurate for BM1 and BM5, but somewhat less accurate for BM3.

These high Pu content rods had an initial Pu enrichment in the mixed oxide of 5.9% Pu (total) / (U+Pu+Am) in M109 and 5.5% in M308. The uranium was depleted, with 0.24% U235/U.

The initial Pu isotopic vector, typical of a plutonium of first generation, was : Pu238/239/240/241/242/Am241 = 1.00/61.67/25.53/8.83/3.91/1.05 w%.

Fig. B.2 shows the axial locations of the samples.

Fig. B.2
Axial location of the PWR samples analysed by BN and SCK•CEN [4]

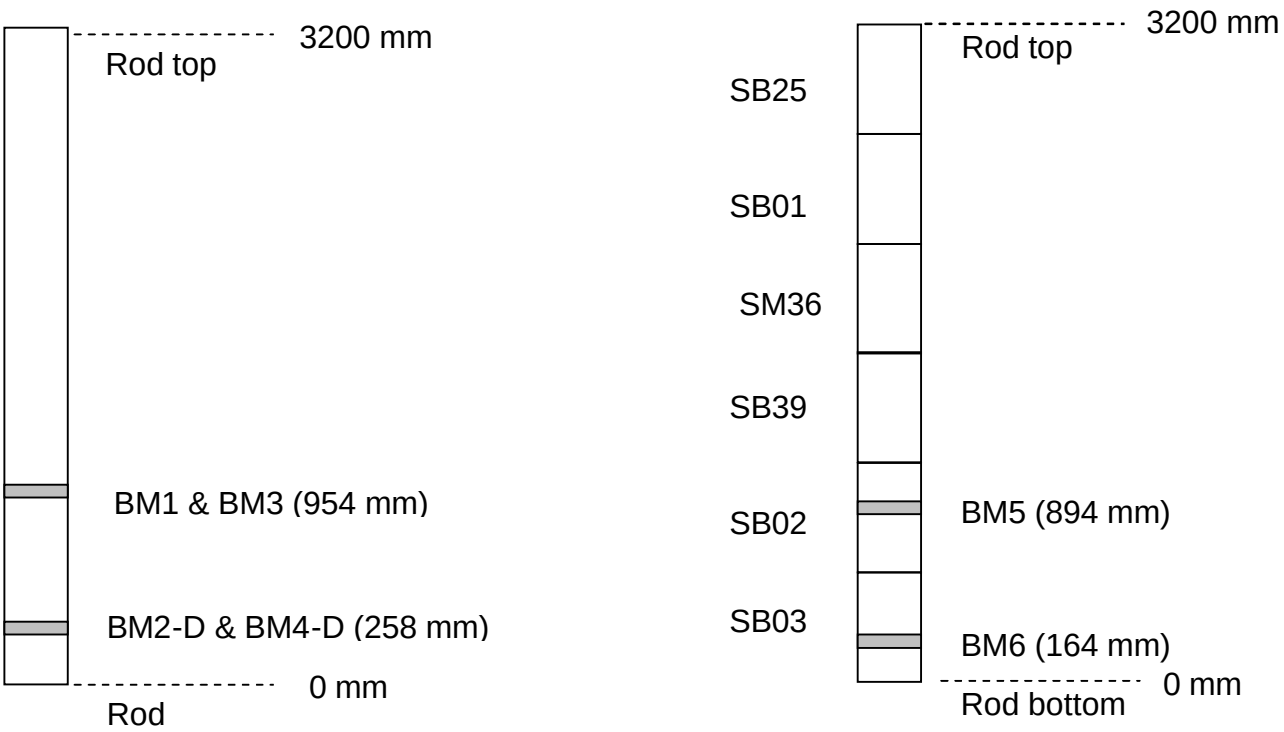

B.1.3 Basis for evaluation

U238 denominator

Prior to C/E analysis, each measured and calculated mass concentration is related to a common denominator U238, thus expressing milligrams of nuclide *i* per gram of U238 nuclide, at the same moment, e.g. 15 mg ^{239}Pu / g ^{238}U.

[4] D7 was a segmented rod, therefore the subdivisions SB01, 02, etc.

This prevents affecting C/E values of any nuclide with the uncertainty of the U238 initial and, to a less extent (since U238 reaction rates are well calculated), final concentration.

Burnup indicator

Since no direct burnup measurement exists, one uses certain fission products that are known to be characterized by a linear behaviour with respect to burnup, whatever the spectrum conditions may be existing nearby the sample during the irradiation. Such fission products are identified as “burnup indicators”. Among them, Cs137 is a well-known gamma emitter that can be measured by a Ge spectrometer. Nd isotopes are broadly recognized as accurate burnup indicators, experimentally determined by radiochemistry. For instance, ORNL and Japanese organizations use Nd148 [3, 4], whereas CEA currently prefers Nd145 and Nd146 due to JEF2 fission yields.
Tests performed on the ARIANE BM-1 sample revealed that Nd145 was best suited, and it was therefore chosen.
Practically, this means that the C/E analysis requires at least 2 depletion calculations:

- in the first calculation, using the power history available in the core follow-up report, C/E value of Nd145 often differs from unity (2 to 10% difference).
- This C/E ratio is then used to correct the power rating uniformly (i.e. same value at each time step) in the BURNUP module. By doing this, one tries to match the measured and the calculated Nd145 concentrations.
- The second WIMS calculation thus provides a Nd145 C/E value close to unity. The analysis for the complete actinides and fission products inventory may be performed as soon as the Nd145 C/E does not differ from unity by more than 1 %. If this agreement is not reached at the second step, a third one is required.

Date of measurement

The experimental values are most useful when they correspond to the End-of-Life (EoL) state, since we are interested in the calculated deviations induced by irradiation inside the reactor. However measurements must often be done later after times of minimum 2 years and sometimes more than 5 years, which is a significant time interval for decaying nuclides, as for instance the β decay of Pu241 to feed Am241 ($T_{1/2}$ = 14.4 y).

The following actinide isotopes are particularly affected, though to different degrees : Pu238, Cm242, Cm244, Pu241 and their respective daughters (U234, Pu238, Pu240, Am241). As Cm242 has a half life of only 6 months, its measurement after some years concerns only a fraction of its EoL quantity, so that the knowledge of its EoL concentration is rather poor. Its daughter Pu238 needs a 15% correction to find its EoL value.

The half life of 18.5 yr of Cm244 leads also to correct significantly its value to correspond to EoL, and Pu240 needs to be corrected accordingly (although for Pu240 the correction is of the order of 1% only).

The decay of Pu241 into Am241 plays an important role in the considered time scale, all the more that Pu241 is about 10 times more abundant than Am241 at EoL. Am241 will be fed through beta decay :

$$Am241(t) = Am241^0 + Pu241^0 \left(1 - \exp(-\lambda t)\right) \quad \text{(B.1)},$$

leading to an Am241 atomic concentration about 3 times higher at the time of measurement.

The decay relation between the parent and daughter products has to be carefully taken into account to deduce the experimental uncertainty, as will be shown hereafter.

Further notes

The C/E analysis has been performed according to the following approach :

- Ø The material inventory has been organized into 4 groups : the actinides, which are of prime interest, the burn-up indicators FP, the lanthanide FP and the metallic FP.
- Ø The C/E are calculated for each nuclide of each sample and comparisons are made with literature when available.

B.1.4 Experimental uncertainties

The experimental uncertainties, ?E/E = $e_{E,}$ have been taken from the ARIANE final report [1] ; they resulted from discussions between the experts in radiochemical measurements. The values are shown in Table B.I below.

Table B.I
Experimental Uncertainties ?E/E in % [5]

Actinides	?E/E	Actinides	?E/E	Actinides	?E/E	Actinides	?E/E
U234	8	Pu238	3	Am241	2.5	Cm243	10
U235	2	Pu239	0.56	Am1(EoL)	9	Cm244	10
U236	4	Pu240	0.56	Am242m	9	Cm245	3
U238	0.5	Pu241	0.56	Am243	3		
Np237	0.7	Pu242	0.56	Cm242	10	+Nd145	0.56

For some of the samples, all 3 laboratories provided measurements and all 3 results were in good agreement. The resulting values were called ‘recommended’. For these samples, the uncertainties of Table B.I are of statistical nature, as systematic uncertainties seem not to exist or are small.

[5] Most of them are for EoL ; the case of Am241 is treated separately (the first value is for the time of measurement, the second for EoL).

The recommended samples were : BM1 and BM5.
For sample BM3 its results were recommended in the first stage, but a discrepancy was observed later between the 3 laboratories. BM3 will still be considered here, but just to observe that the trends for the other samples are confirmed.

For the other samples, either not all 3 laboratories provided measurements, or they did so but their values were somewhat different. It was therefore not recommended to use these results (although in some cases they might be very accurate in fact, but confirmation was missing).

Case of decaying isotopes

The decay relation between the mother and the daughter products has to be taken into account because the experimental uncertainty is time dependent. Let us consider it analytically for the chain Pu241?Am241.

Recalling relation B.1, the absolute uncertainty on Am241 as a function of time is given by :

$$\Delta Am241(t) \;=\; \Delta Am241^0 + \Delta Pu241^0\,\left(1-\exp(-\lambda t)\right) \text{ (B.2)},$$

where the absolute experimental uncertainties at EoL are denoted by the “0” superscript.

Let us introduce relative variables, dividing Eq. [B.2] by Eq. [B.1] and let’s express ε = ?A/A, as the relative experimental uncertainty in Am241 concentration. We also make use of *α(t)* for $\left(1-\exp(-\lambda t)\right)$, and *r* for the EoL ratio $r = Am241^0 / Pu241^0$, which is essentially a function of burn-up, easily obtained by calculation.

This finally leads to the equation :

$$\varepsilon_A(t) \;=\; \frac{r\varepsilon_A^0 + \varepsilon_P^0\alpha(t)}{r+\alpha(t)} \text{ (B.3)},$$

that relates the Am241 relative experimental uncertainty at time *t* to given relative initial uncertainties for the same nuclide and its mother Pu241.

We verify that $\varepsilon_A(0) = \varepsilon_A^0$ at EoL and $\varepsilon_A(\infty) = \frac{r\varepsilon_A^0 + \varepsilon_p^0}{r+1}$.

The case of BM-1 PWR MOX sample has been simulated in **Fig. B.3**. One clearly observes that the e value of Am241 is strongly dependent on the time of measurement : the accuracy of measurement is quite good for long decay times, since the E value tends towards the one of Pu241, which is a rather well computed nuclide. On the other hand, one can observe that the uncertainty on the E value of Am241 at the end of irradiation is rather large and this is an important issue (see final discussion).

Fig. B.3
Experimental accuracy for Am241 versus measurement time
(BM-1 sample)

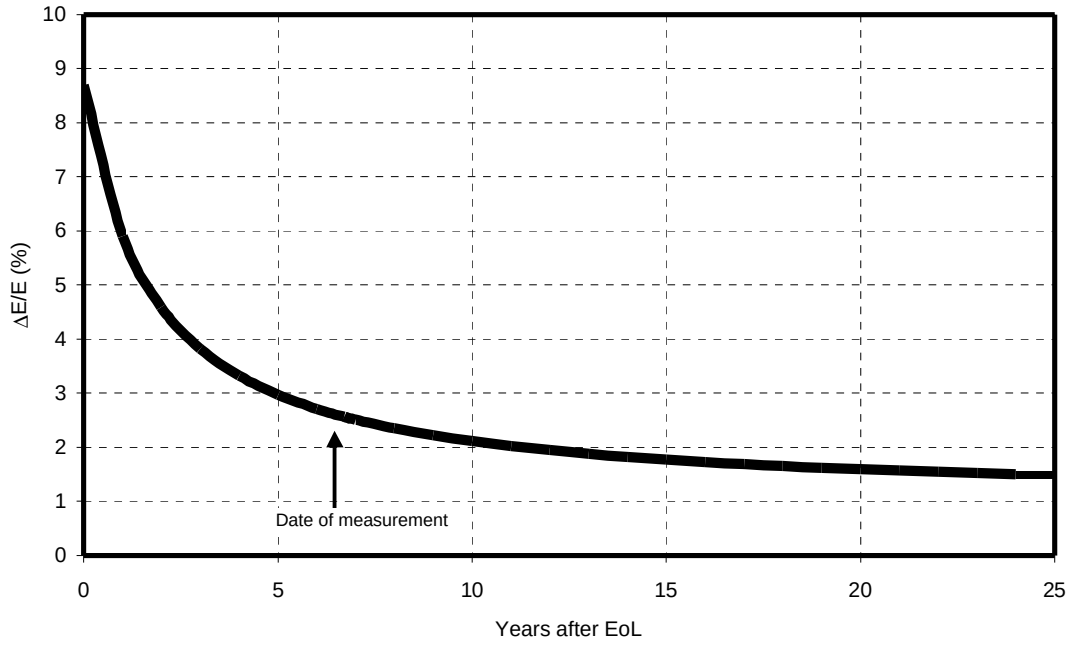

Simulation performed with r = 0.09 (Bu ~ 50 GWd/t), ε_A = 2.5 % et ε_p = 0.56 %

The interpretation is the following : if the uncertainty in the Am241 measurement after 6.7 years cooling is 2.5 %, since at that time about 2/3 of Am241 originates from Pu241 at EoL, it follows that the uncertainty in Am241 at EoL should be ~ 9 %.

B.2 WIMS calculations : modelling

B.2.1 Calculation route

The description of the WIMS package and methods [5] has been given in the preceding Chapter A.

The reference calculation route has been chosen, that consists of the successive steps : HEAD - PERSEUS - PIP - CONDENSATION - DIFF - CACTUS - BURNUP – DIFF, as was explained in Chapter A. The 6-group energy structure was chosen for PWR samples. The 21-group structure was only used for sample BM-1 ; for the other samples the 6-group structure only was used, for CPU reasons. The difference in the results with 6 or 21 groups, already illustrated in Chapter A, can be inferred here from the BM-1 calculations ; it is rather small (1% in general).

B.2.2 Geometrical models

For the PWR samples, the supercell approach was chosen in order to take into account the significant influence of the UO2 neighbouring fuel assemblies : see **Fig. B.4**.

FIG. B.4
VIEW OF THE SUPERCELL MODEL WITH RODS DEFINITION FOR THE PWR MOX SAMPLES.

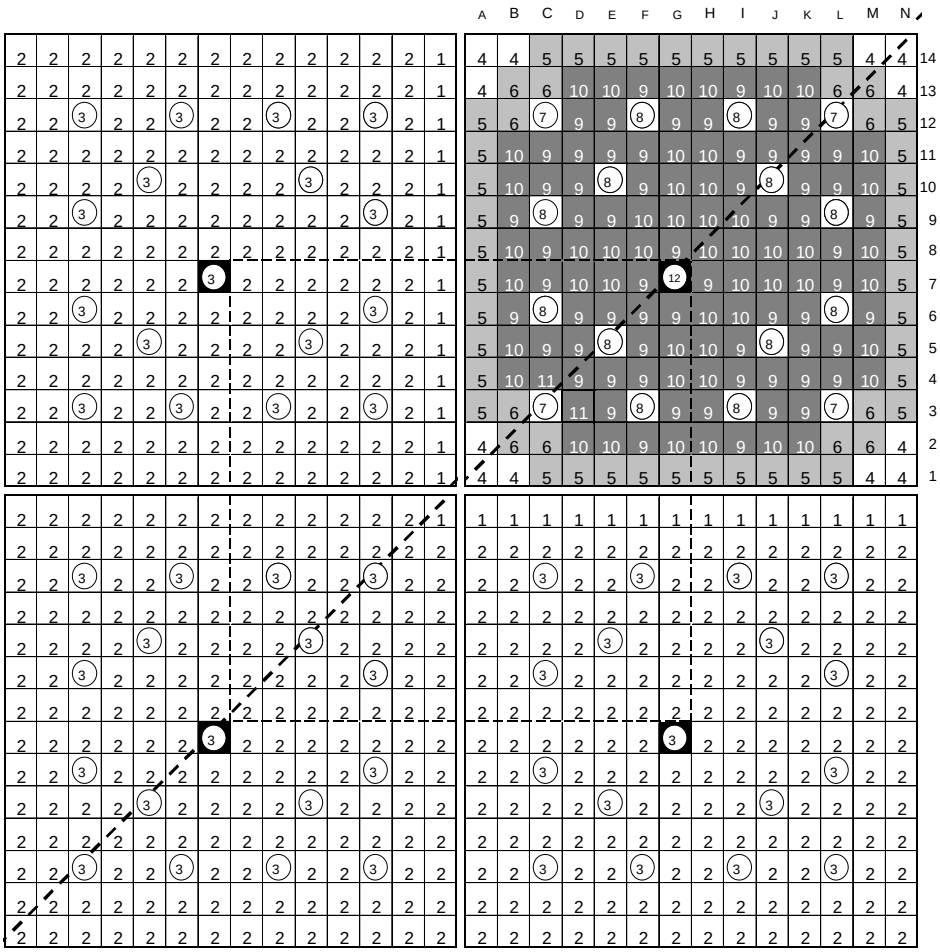

1 - UO_2 fuel rods adjacent to the MOX assembly,
2 - other UO_2 fuel rods,
3 - Instrumented and guide tubes (IT and GT) of the UO_2 assemblies (IT considered identical as GT),
4 - L-MOX fuel rods,
5 - M-MOX fuel rods adjacent to the UO_2 assemblies,
6 - M-MOX fuel rods surrounded by L-MOX and H-MOX fuel rods,
7 - corner GT of the MOX assembly,
8 - other GTs of the MOX assembly,
9 - H-MOX fuel rods in front of GTs,
10 - other H-MOX fuel rods,
11 - analysed H-MOX fuel rod, same as rod type 9 but differentiated for the sake of evaluation,
12 - IT of the MOX fuel assembly.

The small water blade between the PWR assemblies was not simulated. It does not have a great impact on the material inventory for the samples under consideration, but it can affect the pin-wise power distribution.
The boundary conditions were of the translation type, whereas the diagonal symmetry was explicitly used.

B.2.3 Power history

The power history for the PWR samples was defined in great details, each power variation of ± 2 % giving rise to a different time step. The resulting time definition makes the full power history composed of about 50 to more than 100 time steps.

As explained in Chapter A, this leads to a cyclic calculation in which resonance treatment is performed at several time steps, since the composition of the fuel has an important impact on self-shielding.

The two following rules were adopted for the implementation of the power history in WIMS :
- no more than 50 days between two successive WIMS cycles,
- no more than 10 days for the sub-steps used in the burnup equation integration (within each WIMS cycle).

In principle, WIMS allows setting the power rate of individual materials of the geometrical model, but one generally prefers setting the power rate of the whole MOX assembly.

B.2.4 Fuel temperature

As an explicit radial temperature profile in the pellet cannot be dealt with, an effective neutronics fuel temperature (T_{fuel}) is calculated according to the Rowlands formula [6], using the calculated temperature at the surface and at the centre of the pellet. Such calculation is performed at BN using the pin thermo-mechanics COMETHE code [7].

$$T_{fuel}^{eff} = \frac{5}{9} T_{fuel}^{surface} + \frac{4}{9} T_{fuel}^{center} \quad \text{(B.4)}$$

The time definition of the fuel temperature has been investigated. It was found that one representative fuel temperature per core cycle was enough, and a full time discretisation of the fuel temperature (i.e. according to the power history) was not necessary. Such a representative fuel temperature is normally determined by weighted average, as also done for the moderator temperature (see below).

B.2.5 Moderator temperature and composition

One moderator temperature T_{mod} and composition (including boron concentration) per core cycle is also considered enough for the purpose of depletion calculation. However cycle-averaged moderator values must be deduced by weighting individual values by the burn-up of each time step of the cycle, i.e :

$$T_{\mathrm{mod}}^{cycle} = \frac{\sum_i T_{\mathrm{mod},\,i} \times Bu_i}{\sum_i Bu_i} \quad \text{(B.5)},$$

with *i* the index of the various time steps of the cycle.

B.2.6 FA neighbourhood in supercell model

The UO_2 fuel rods surrounding the MOX FA can be considered in two ways :

Ø both UO2 and MOX fuels are fresh at the beginning of the depletion calculation;
ØUO2 fuel is of constant composition, corresponding to the average burnup of the UO_2 fuel assemblies surrounding the MOX FA all along its life.

The second option was preferred for the simulation of the PWR MOX samples.

B.2.7 Calculation uncertainties

Several uncertainties impact the calculated fuel inventory. The WIMS code has been used to assess the sensitivity of nuclides inventory according to the following uncertainties (2σ values, i.e. 95% confidence interval) :

- Ø ± 2 % for the burn-up,
- Ø ± 50 °C for the fuel temperature,
- Ø ± 2 °C for the moderator temperature,
- Ø ± 0.05 mm for the clad diameter (technological uncertainty),
- Ø the methodological uncertainty (see after),
- Ø the initial composition uncertainty, estimated with the sensitivity matrix provided in the previous European Project [5], given the uncertainty on the initial composition (± 0.3 % for U235, ± 0.15% for the other major actinides),
- Ø ± 3 % for the void fraction, only relevant for BWR reactors, not for PWRs.

For the methodological uncertainties, several WIMS calculations have been run, varying the following parameters :

1 Single power rating for the whole irradiation , instead of a detailed power history ;
2 Single value of the fuel temperature for the whole irradiation, instead of a detailed time definition ;
3 Single moderator temperature and composition for the whole irradiation, instead of a detailed time-dependent profile ;
4 Refined XY meshing in the main transport calculation ;
5 Variation of the radial subdivision of the MOX pellets in the resonance treatment and in the multicell collision probability calculation ;
6 Constant burn-up of the neighbouring UO_2 FA (20 → 30 GWd/t).

The impact on the main actinides inventory is hereunder reported (**Table B.II**), in % mass variation.

Table B.II
Sensitivity (%) of the main actinides mass inventory to WIMS modelling

Case Keyword	1 Power	2 T_F	3 T_{MOD}	4 Meshing	5 Rodsub	6 UO_2 Bu
U234	0.2	0	0	0	0	0
U235	0.6	0	0	0.4	0	0
U236	0.4	0	0	0	0	0
Pu238	0	0	0	0.3	0	0
Pu239	0.6	0	0.1	1.3	0	0.6
Pu240	0.1	0.1	0	0.2	0	0
Pu241	0	0	0.1	0.6	0.1	0.3
Pu242	0.4	0	0	0.3	0.1	0
Am241	1.1	0	0.1	0.8	0.1	0.5
Am242m	0.8	0	0.2	1.0	0	0.4
Am243	0.5	0	0.1	0.2	0	0.5

Collecting the sensitivity of the nuclides inventory to the other parameters, the global calculation uncertainty has been evaluated for each nuclide by a quadratic sum :

$$\Delta C/C \quad = \quad \varepsilon_C \quad = \quad \sqrt{\varepsilon_{Bu}^2 + \varepsilon_{TFuel}^2 + \varepsilon_{T\,\mathrm{mod}}^2 + \varepsilon_{Techno}^2 + \varepsilon_{Method}^2 + \varepsilon_{Comp}^2 + \varepsilon_{Void}^2} \quad \text{(B.6)}.$$

B.2.8 Total calculation uncertainties

An example of the determination of the total calculation uncertainties is given in **Table B.III**, along with the breakdown between the various contributions, for a PWR MOX sample at Bu = 50 GWd/t_{HM}.

Table B.III
Calculation uncertainties (2σ values in %) for a PWR MOX sample irradiated up to 50 GWd/t_{HM} (actinides)

Actinides	Bu	Method	T_{fuel}	T_{mod}	Compo	Techno	**?C TOTAL**	***?C TOTAL ex. Bu***
U234	0.4	0.1	0.1	0.1		0.2	0.5	0.4
U235	4.8	0.2	0.3	0.1	0.3	0.0	4.8	0.5
U236	2.7	0.1	0.2	0.2	0.3	0.3	2.7	0.5
U238	0.1	0.0	0.0	0.0	0.0	0.0	0.2	-
Np237	3.7	0.8	0.2	0.5	0.1	0.2	3.9	1.0
Pu238	0.7	0.1	0.1	0.2	0.8	0.1	1.1	0.8
Pu239	4.1	0.5	1.1	0.7	0.6	1.0	4.4	1.8
Pu240	1.7	0.3	0.0	0.0	0.9	0.1	2.0	1.0
Pu241	0.6	0.6	0.5	0.3	1.0	0.3	1.4	1.3
Pu242	2.9	0.1	0.0	0.3	0.8	0.3	3.1	0.9
Am241	2.1	0.5	0.7	0.2	0.9	0.2	2.4	0.9
Am242m	5.5	0.8	0.8	1.0	0.9	1.1	5.9	2.1
Am243	4.0	0.3	0.1	0.1	0.8	0.2	4.1	0.9
Cm242	2.7	0.4	0.1	0.0	0.9	0.0	2.9	0.9
Cm243	5.4	0.3	0.1	0.6	0.9	0.8	5.6	1.4
Cm244	8.4	0.8	0.4	0.6	0.8	0.8	8.5	1.5
Cm245	10.5	0.7	0.4	1.4	0.8	1.9	10.9	2.5

The individual uncertainties are burn-up dependent, so that it is necessary to perform this work for the various samples that are considered in this chapter B.

Uncertainties for the fission products are also available, but they are not shown here ; let us note that for the burn-up indicator Nd145, ?C TOTAL is 2.0% while ?C TOTAL without the burn-up uncertainty contribution is 0.1%.

The uncertainty in burn-up dominates the total calculation uncertainties. However this reasoning is conservative. Indeed the way the calculation is done with iterations to adjust the Nd145 burn-up indicator to measurement means that the burn-up uncertainty has been much reduced and is limited to the uncertainty due to Nd145 fission yields.

B.2.9 Overall uncertainties

The uncertainty affecting the C/E ratio is finally obtained by the following summation :

$$\varepsilon_{C/E} = \sqrt{\varepsilon_C^2 + \varepsilon_E^2} \quad \text{(B.7)}.$$

When comparing the experimental uncertainties ?E/E (par. B.1.4) and the calculation uncertainties ‘except Bu’ (par. B.2.8), one observes that they are in general of comparable and small magnitudes : for the Pu isotopes they are

typically 0.6 and 1%, so that the global uncertainty is less than or equal to about 2%.

The final assessment will make use of all measurements from the ARIANE programme and from many more samples from the French MOX programme described in Chapter C. One may assume that retaining finally the average C/E values for each isotope will make systematic errors (except Nd145 fission yield data) negligible.

C/E versus measurement time for the case of Am241

It was already shown that the decay between the mother and the daughter nuclide had an influence on the experimental uncertainty. Such a decay must obviously be taken into consideration for C/E analyses, especially for the couple Pu241 - Am241.

From the measurements of Am241 (made years after EoL) and Pu241, an experimental value of Am241 at EoL is deduced according to the equations already shown in par. B.1.4. In the presentation of results below, both C/E values at measurement time and at EoL will be given. One will observe that C/E of Am241 at EoL will differ more largely from unity than at measurement time.

B.3 WIMS calculations : results

B.3.1 Major results

Table B.IV below gives the C/E results for the actinides as calculated for the 3 central samples BM1, BM3 and BM5. All values are related to EoL state, except for Am241, for which two values are given (EoL and date of measurement). Most of the experimental values used were recommended (see par. B.1.4) ; some of them were not, and this is indicated. As noted already, only the central samples may give trends which can be used to point out where cross-sections need to be corrected, as these samples lie in regions of constant spectrum conditions.

The results do correspond in general to 6-group calculations, as this was the method of current use. For BM1 21-group results are also given ; they are more accurate, and the comparison with 6-group results provides the bias from using 6 groups only. This bias is relatively small : for the Pu isotopes it is about 1% only.

Table B.V gives the C/E for the actinide elements U, Pu, Am, Cm.

Table B.IV
C/E Ratios for U, Pu, Am and Cm Isotope Masses
MOX Fuel Irradiated in ARIANE/Beznau1 (central samples)

Samples	BM1 21 groups	BM1 6 groups	BM3 [6] 6 groups	BM5 6 groups
Burn-up (GWd/t)		45.5	47.8	56.8
U235	1.03	1.03	(0.83)	1.04
U236	0.88	0.88	-	0.94
U238	-	-		-
Np237	0.69	0.69	N.A.	0.74
Pu238	0.92	0.93	-	0.96
Pu239	1.07	1.08	1.04	1.09
Pu240	1.02	1.00	0.98	1.00
Pu241	1.00	1.02	1.00	1.02
Pu242	0.98	0.98	0.99	0.97
Am241 (m)	1.08	1.08	1.05	1.22
Am241	1.23	1.24	1.20	~ 1.5
Am242m	0.69	0.71	0.60	0.81
Am243	0.95		0.97	1.06
Cm242	0.97	0.97	N.A.	0.95
Cm243	0.77	0.78	0.87	0.96
Cm244	0.86	0.90	0.92	0.87
Cm245	0.86	0.89	0.82	0.87

(m) stands for C/E assessed at date of measurement

Table B.V
C/E results in % with WIMS for the actinide elements
of the PWR MOX samples

Sample	BM-1	BM-3	BM-5
Actinide element	Bu = 45.5 GWd/t	Bu = 47.8 GWd/t	Bu = 56.8 GWd/t
U	0.995		1.01
Pu	0.97	(0.97)	0.97
Am	1.05	(1.09)	1.18
Cm	0.88	(0.93)	0.88

[6] C/E values adapted thanks to the parametric study made for BM1 ; the values in brackets are less reliable.

B.3.2 Major trends

For the major Pu239 fissile isotope, the calculation overestimates the discharged amount. This overestimate of Pu239, 1.07 to 1.08, is rather large.

The prediction is good, close to unity, for Pu240, 241 and 242. For Pu238 there is an underestimation.
Concerning Am241, while its amount at the time of measurement (3 years or more after discharge) is overestimated by about 10%, the overestimate is much higher for the end of irradiation (more than 1.20). Of course the longer the cooling time, the more the contribution of Pu241 decay dominates the Am241 concentration, and this improves the ratio, since Pu241 is well predicted.
Am242 and 243, the Cm isotopes and Np237 are all underestimated, sometimes largely. These trends had already be found in the former FP4 study [2].

It was possible to compare these trends with those found by other groups, not engaged in VALMOX work :
- TRACTEBEL, where WIMS8 was used for complementary investigations [8] ;
- ORNL, using the HELIOS system with ENDF/B-IV data [3].

Their analyses exhibited similar trends for the actinides.

The case of Am241, very sensitive to decay, need further attention. From the direct measurement value, taken some 3 years or more after end of irradiation, a reconstruction by calculation of the situation at End of Irradiation (EoI) is needed, because, even if less accurate, only this situation may lead to a recommendation to correct some cross-sections.
Its C/E ratio at measurement time is better predicted for the simple reason that a large part of the Am241 measured after 3 to 5 years was Pu241 at EoL, and Pu241 is well predicted.
This dual aspect for Am241 will further be considered in this report. For the sake of cross-section corrections, EoL values are to be considered. For helium production which is discussed in a separate Chapter E this is different.

B.3.3 Trends for the off-centre samples

The off-centre samples BM2, BM4 and BM6 were also recalculated, but 2D geometrical models are not adequate to model accurately such locations in the vicinity of the axial reflector. As they lie in the bottom part of the fuel rods, their evaluation is affected by larger uncertainties ; they are placed in a strong gradient and the spectrum is not well described in a 2D model (in spite of the fact that a 3D model was actually used for the core calculations).

The trends observed above were rather similar : in particular, C/E was overestimated for Pu239, but closer to unity for Pu240, 241 and 242, and there was a general underestimation of the americium (except Am241) and curium isotopes.

B.3.4 Further checks

Some calculations were repeated with the WIMS9 version, just made available [9].
As already shown in Chapter A, the C/E values for Pu239 were closer to unity and this should be mainly attributed to resonance treatment, which is improved in WIMS9, since the same JEF 2.2 file is basically used in WIMS9 and in WIMS8a.

B.4 Monte-Carlo Calculations : modelling

B.4.1 Calculation route

The description of ALEPH [11] has been given in the preceding Chapter A. The objective of the Monte Carlo calculations was to follow as closely as possible the BN calculation scheme.

B.4.2 Geometrical models

The MCNPX model is an heterogeneous representation (see Figure B.5) of the macro-assembly, however the nuclide concentrations are considered as uniform in the fuel rod all along the irradiation (the rim effect is not accounted for). Each pin is modelled and followed separately. We use the same[7] 2D macro-assembly model as BN (three UO2 assemblies at average fixed burn-up and one MOX assembly with periodic boundary conditions and diagonal symmetry).

[7] We use a 1/8 model in place of the 1/2 model used by BN to get more statistics. The only cell who break the 1/8 symmetry is the near central instrumentation tube. This simplification has only negligible consequences because the samples calculated (BM1 and BM5) are far away from the instrumentation tube. Of course, ALEPH has no limitation at all concerning geometry and modelling.

FIG. B.5
MCNPX macro-assembly model of Beznau reactor

(reflective boundaries conditions)

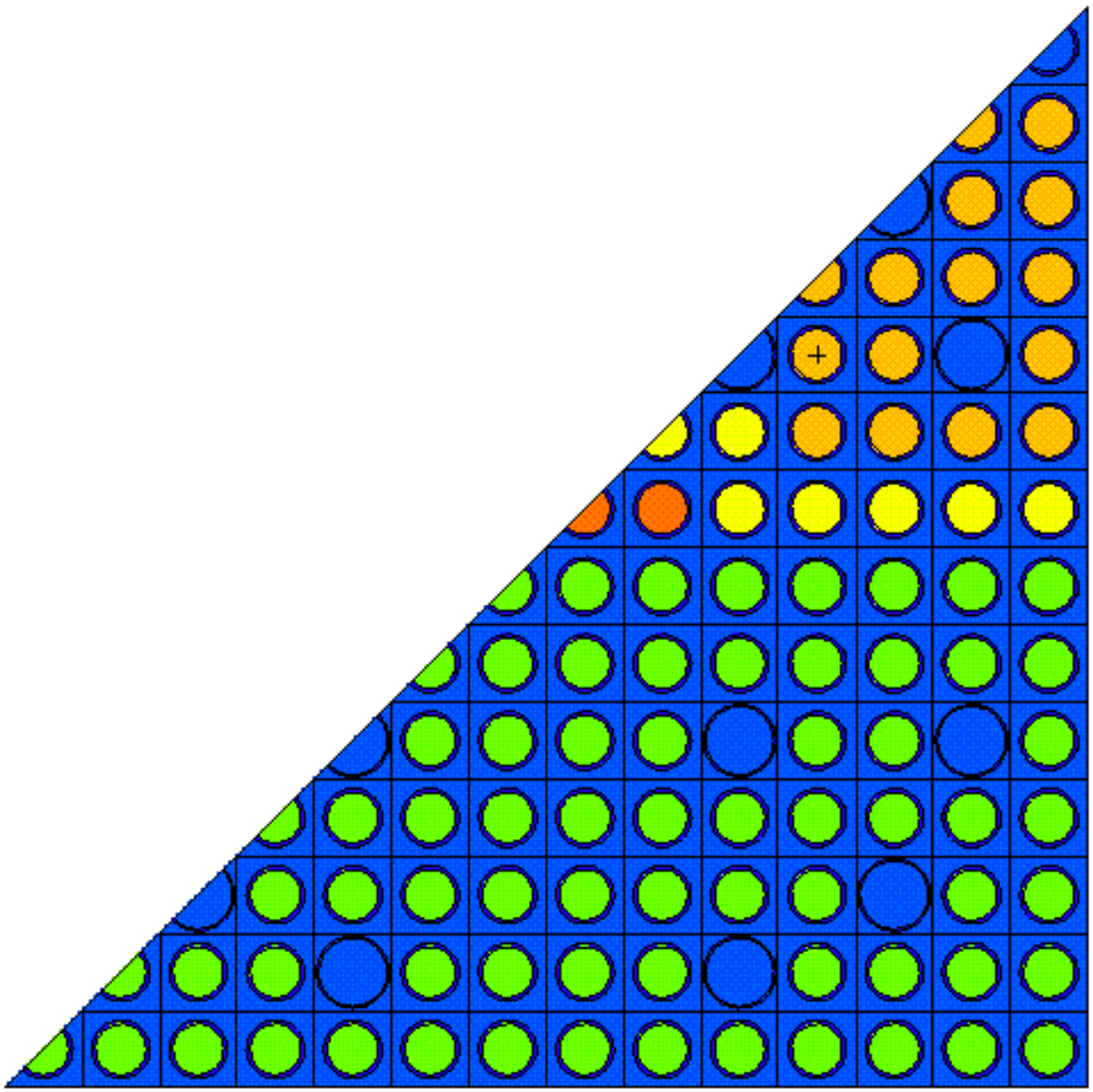

B.4.3 Power history

We follow the BEZNAU reactor power history exactly as given in the ARIANE report [1]. ALEPH recalculates also, for each pin separately, the fuel composition for each burn-up increment of 1 GWd/T HM.

For the fissions products, ALEPH calculates, at each burn-up time step, the total neutron absorption cross section of each fuel pin (actinides, fissions products and other nuclides). ALEPH keeps only, for the transport calculation, the fraction of the fission products contained in each pin (the more absorbing ones) so that the resulting absorption cross section of each pin is only a fraction of the total absorption cross section of the pin[8]. For this study, we used a 99% fraction.

B.4.4 Fuel temperature

All temperatures are kept constant[9] (burn-up averaged quantities - see Section B.2.4) to follow as closely as possible the BN calculation scheme.

B.4.5 Moderator temperature and composition

The moderator temperature, density and boron concentration are also kept constant (burn-up averaged quantities see Section B.2.5) to follow as closely as possible the BN calculation scheme.

B.4.6 FA neighbourhood in supercell model

We follow exactly the BN scheme (see Section B.2.6).

B.5 Monte-Carlo Calculations : results

B.5.1. Major results

Table B.VI below shows the C/E results for the actinides as calculated for the two central reference (see Section B.1.4) samples BM1 and BM5. All values are related to EOL state, except for Am241, for which two values are given (EOL and date of measurement). Most of the experimental values used were recommended (see Section. B.1.4).

Table B.VII shows the C/E for the actinide elements U, Pu, Am, Cm.

[8] Of course, the original nuclide (i.e. composition at BOL) is always kept for the transport calculations.

[9] ALEPH can also automatically change all temperatures, densities and boron concentrations at each power step.

Table B.VI
C/E ratios with ALEPH (JEF-2.2 data) for U, Pu, Am and Cm Isotope Masses MOX Fuel Irradiated in ARIANE/Beznau1 (reference central samples)

Samples	BM1	BM5
Burn-up (GWd/t)		56.4
U235	1.01	1.01
U236	0.89	0.93
U238	-	-
Np237	0.81	0.85
Pu238	0.94	0.93
Pu239	0.99	0.96
Pu240	1.02	1.01
Pu241	0.99	0.97
Pu242	0.98	0.98
Am241 (m)	1.04	1.17
Am241	1.20	1.46
Am242m	0.74	0.81
Am243	1.00	1.09
Cm242	0.94	0.88
Cm243	0.77	0.88
Cm244	0.88	0.86
Cm245	0.92	0.83

(m) stands for C/E assessed at date of measurement

Table B.VI
C/E ratios with ALEPH (JEF-2.2 data) for the actinide elements of the references PWR MOX samples

Sample	BM-1	BM-5
Actinide element	Bu = 45.8 GWd/t	Bu = 56.4 GWd/t
U	1.000	1.000
Pu	1.00	0.98
Am	1.03	1.13
Cm	0.89	0.86

B.5.2. Major trends

ALEPH values are generally better than WIMS values (see section B.3.2). The major improvements are for Pu239 (+8% improvement), Np237 (+12% improvement), Am241 (+4% improvement), Am242m (+5% improvement), Am243 (+5% improvement), and Cm245 (+6% improvement). Exceptions are Pu241 (-1%) and Cm242 (-3%).
The Pu vector is very well predicted (lower than 2% except for Pu238 where there is, like WIMS, an underestimation of 6%). In spite of the large improvement on the Np237 value, the underestimation remains quite large (19%). Am242 and Cm isotopes are all underestimated, sometimes largely.

B.6 Effect of using new JEFF3 data

For the BM1 sample, the same calculation was done with JEFF-3.0 data to check the probable influence of changes introduced in the basic data of U235, U238(n,2n), , Pu241 and Cm245 (as well as for fission products likeEu155).

We have used JEFF-3.0 (325 nuclides) original evaluations to build, with the aid of NJOY99.90, our own linear-linear interpolated continuous (differential) cross sections for MCNPX25e and ALEPH. The fractional reconstruction tolerance used was 0.1% with integral thinning of 5E-8 barns (the only exceptions are Fe 57 and Mo 94 for which a strict fractional reconstruction tolerance of 0.1% was used). All materials were Doppler broadened at their burn-up averaged temperature. We generated also S(a,ß) scattering data for H2O to take into account molecular binding and crystalline effects (coherent scattering) using S(a,ß) functions available in the thermal JEFF-3.0 files.

B.6.1. Major results

Table B.VIII below shows the C/E results and possible improvements for the actinides as calculated for the central reference (see Section B.1.4) samples BM1. All values are related to EOL state, except for Am241, for which two values are given (EOL and date of measurement). Most of the experimental values used were recommended (see Section. B.1.4).

Table B.IX shows the C/E and the possible improvements for the actinide elements U, Pu, Am, Cm.

Table B.VIII
C/E ratios with ALEPH (JEFF-3.0 data) for U, Pu, Am and Cm Isotope Masses MOX Fuel Irradiated in ARIANE/Beznau1 (reference central samples)

Samples	BM1	JEF-2.2 ? JEFF-3.0
Burn-up (GWd/t)		45.8
U235	1.00	+1%
U236	0.93	+4%
U238	-	-
Np237	0.86	+5%
Pu238	0.94	id
Pu239	0.99	id
Pu240	1.03	-1%
Pu241	0.99	id
Pu242	1.01	+1%
Am241 (m)	1.04	id
Am241	1.19	+1%
Am242m	0.74	id
Am243	1.02	-2%
Cm242	0.95	+1%
Cm243	0.74	-3%
Cm244	0.90	+2%
Cm245	0.97	+5%

(m) stands for C/E assessed at date of measurement
+5% means an improvement of 5% using JEFF-3.0 in place of JEF-2.2

Table B.IX
C/E ratios with ALEPH (JEFF-3.0 data) for the actinide elements of the reference PWR MOX samples

Sample	BM-1	JEF-2.2/JEFF-3.0
Actinide element	Bu = 45.8 GWd/t	Bu = 45.8 GWd/t
U	1.000	id
Pu	1.00	id
Am	1.03	id
Cm	0.91	+2%

B.6.2. Major trends

Recalculations with JEFF-3.0 reflect the improvements due to the changes introduced in the basic data of U235 (+1% improvement), U236 (+4% improvement), Np237 (+5% improvement), Pu242 (+1% improvement) and Cm245 (+5% improvement).

B.7 Evaluations for Boiling Water Reactors

B.7.1 Available experimental data

It had originally be planned to recalculate results of fuel irradiation in the large BWR of Gundremmingen, loaded with MOX fuel delivered by Belgonucléaire. However the results of chemical analyses were largely delayed. Therefore it was decided to recalculate instead MOX rods irradiated in the Dodewaard reactor (ARIANE programme), for which experimental results were available.

B.7.2 BWR core and MOX samples

The 3 BWR MOX samples considered by BN were irradiated in the Dodewaard NPP (The Netherlands). This core contained 6 × 6 Fuel Assemblies (FA) of mixed composition UO2 and MOX. In fact the assembly is mainly made of UO2 rods of various U235/U enrichments, plus UGd burnable pins, a water cell and only 2 MOX rods symmetrically set with respect to the diagonal axis.
The Y014 assembly is represented in **Fig. B.6.**
For the BWR samples, the following assembly modelling was chosen. Each BWR fuel assembly is separated from the other by a water blade whose thickness is quite important in comparison with the rod pitch. In this way, BWR assemblies are more independent of each other than PWRs and the assembly modelling is quite relevant, as presented in Fig. B.6.

Fig. B.6
Assembly model with the rods definition for the BWR MOX samples

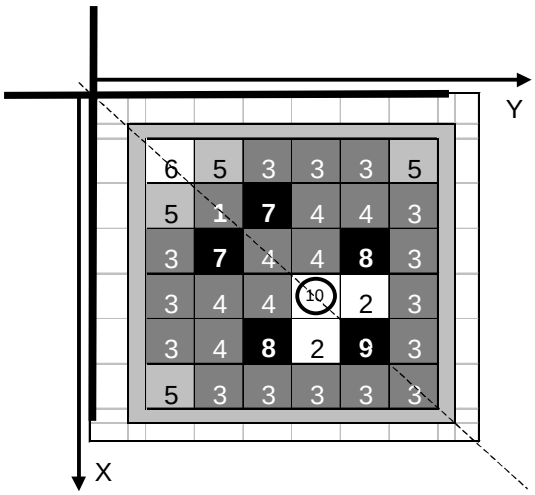

1 - UO_2 fuel rod, U235 enriched 4.9 w%,
2 – analysed MOX fuel rods,
3 – U 3.2 w% fuel rods, adjacent to the water blade,
4 – other U 3.2 w% fuel rods,
5 – U 2.6 w% fuel rods,
6 – U 1.8 w% fuel rod,
7, 8, 9 – UGd burnable rods, Gd 2.7 w% and U235 3.2 w%,
10 – water cell, the control cross blade position is indicated.

The sample DM-1 belongs to this Y014 assembly and is located at axial level 120 cm from the bottom of the active column (of 180 cm), as illustrated in **Fig. B.7.** This sample was irradiated during 5 cycles, reaching a burnup of 61.9 GWd/t (assembly average burnup = 35.3 GWd/t). It was characterized by a local moderator void fraction of 47 vol%.

Fig. B.7 Axial location of the BWR samples studied by BN

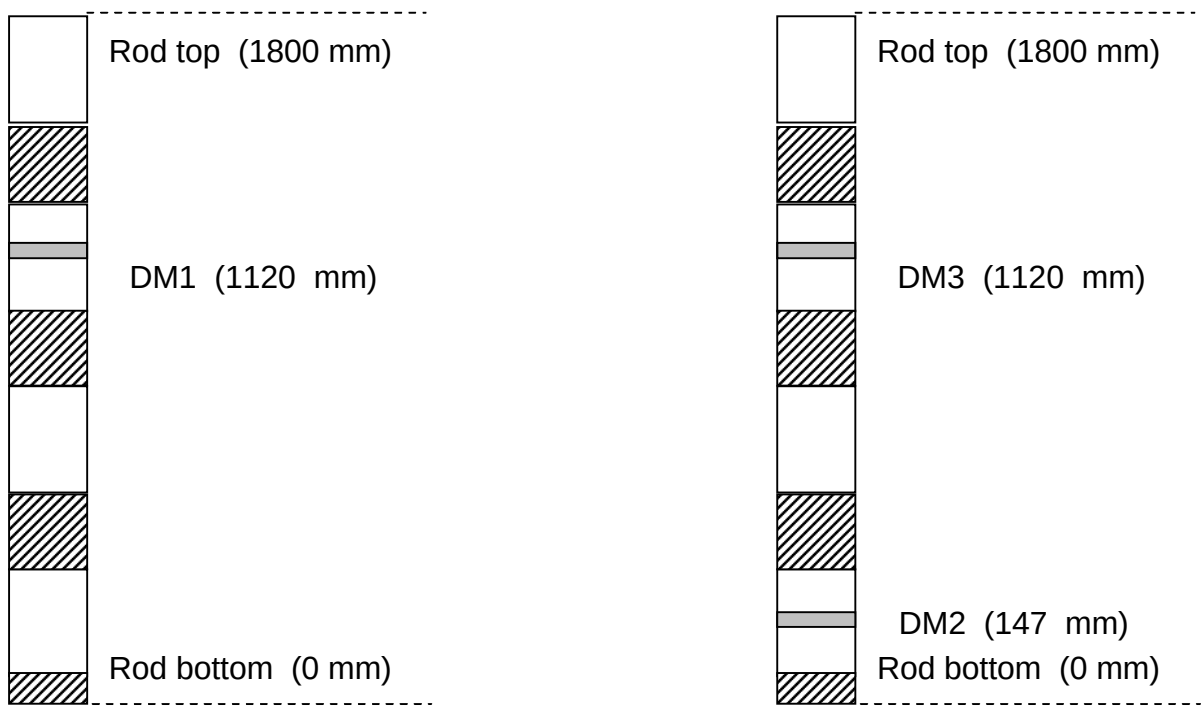

Samples DM-2 and DM-3 belong to the Y012 assembly, located at axial levels 35 and 120 cm from the bottom of the active column. These samples were irradiated during 4 cycles reaching respective burn-ups of 37.8 and 51.4 GWd/t. They were respectively characterized by local moderator void fractions of 4 vol.% and 50 vol.%.

B.7.3 Experimental uncertainties

The experimental uncertainties are similar to those for the PWR MOX samples given in par. B.1.4.

B.7.4 Calculation and overall uncertainties

The calculation uncertainties are similar, for the same burn-up, to those for the PWR MOX samples described in par. B.1.7, with the addition of a term of about 3% for the void fraction, typical of BWRs. This additional term is important as it dominates the other ones, so that (see **Table B.X**) after combination with the experimental uncertainties the global ones are in general close to 4%.

In fact one should also consider the following terms :

- a term linked to the complex geometry of such BWR assemblies of small size, which are much more heterogeneous than the larger PWR assemblies ;
- a term linked to the neutron spectrum, which is softer than in PWRs ; the spectrum is particularly soft in the Dodewaard assemblies, which are essentially UO2 assemblies with small MOX islands.

No accurate assessment of such uncertainties was available. But it seems wise to assign uncertainties of 5 to 8% to the C/E values.

B.7.5 WIMS results

Two **Tables B.X** and **B.XI** below show evaluation results with WIMS for the actinides in BWR MOX samples. It is recalled that the BWR MOX assemblies of Dodewaard are not representative of large current power reactors ; a few MOX pins only are embedded in UO2 fuelled assemblies.
The goal of this evaluation is simply to check that the C/E trends observed on PWR samples are confirmed. To that aim, although 3 samples were recalculated, average results of samples DM-1 and DM-3 only are presented here, as they give a typical set of results.

Table B.X
Typical C/E results obtained with WIMS for the actinides in BWR MOX

Sample	Average DM-1 and DM-3
Actinide isotope	C/E
U235	1.05
U236	0.88
U238	-
Np237	0.77
Pu238	0.98
Pu239	1.20
Pu240	1.02
Pu241	1.07
Pu242	0.96
Am241 (m)	1.15
Am241	˜1.4
Am242m	0.85
Am243	0.97
Cm242	0.99
Cm243	0.96
Cm244	0.90
Cm245	0.99

(m) stands for C/E assessed at date of measurement

Table B.XI
(C-E)/E (%) results obtained with WIMS for the actinide elements in BWR

Sample	Average DM-1 and DM-3
Actinide element	C/E
U	1.00
Pu	1.06
Am	1.06
Cm	0.915

B.7.6 Discussion of these results

The WIMS results for BWR MOX samples do confirm the trends observed for the PWR samples :

- Pu239, the main fissile isotope, is overestimated ; the degree of overestimate (20%) is however much larger (it was 8% in PWRs with the same methods) ; but one should stress again that the neutron spectrum in Dodewaard was much softer than in current PWRs ;
- For the other Pu isotopes the prediction is close to unity (with the exception of the other fissile isotope Pu241, also overestimated : 1.07) ; Pu242 is underestimated ;
- Am241 is overestimated in a similar way ;
- Am242m, Am243 and the Cm isotopes are all underestimated, though to a lesser extent.

These are the conclusions from this first analysis of MOX irradiation in BWRs.
The planned evaluation of Gundremmingen results should lead to more significant conclusions.

References for Chapter B

[1] ARIANE Final Report (Actinides Research in a Nuclear Element), Belgonucléaire report 00253/221 rev. B, by D. Boulanger and M. Lippens, Dec. 2000

[2] Nuclear Data for Advanced MOX Fuels, Final Report of Contract n° FI4I-CT95-0002, by S. Pilate et al., EUR 19126 EN, 2000.

[3] B. D. Murphy and R. T. Primm III : Simulation of Mixed-Oxide and Low-Enriched Uranium Fuel Burn-up in a Pressurized Water Reactor and Validation Against Destructive Analysis Results, Nucl. Sci. & Eng. 142, 258-269 (2002).

[4] Y. Ando *et al*., "Development and verification of Monte carlo Burnup Calculation System", Proceedings ICNC 2003, Japan, Tokai-Mura, Oct. 2003

[5] WIMS, the ANSWERS Software Package, A General Purpose Neutronics Code, AEA Technology, 1999

[6] G. Rowlands, "Resonance absorption and non-uniform temperature distributions", UKAEA, AERE – M 717, Harwell, Berkshire, 1961

[7] S. Shihab, "COMETHE 4D Executive Summary", BN report 9508719/221, 6 Nov. 1995

[8] R. de Wouters (Tractebel, Brussels) : personal communication.

[9] WIMS, a Modular Scheme for Neutronics Calculations, User Guide for Version 9, ANSWERS/WIMS(99)9, ANSWERS Software Service, Serco Assurance, 2004

[10] User's Manual for the ORIGEN2 Computer Code, by A.G. Croff, ORNL-TM-7175, April 1980

[11] W. Haeck and B. Verboomen, ALEPH, a Monte Carlo Burn-up Code, SCK-CEN, BLG n° 1003 (2005)

CHAPTER C

MOX FUEL IRRADIATIONS IN LIGHT WATER REACTORS

Calculations and evaluations made at CEA

C.1 Available experimental data

C.1.1 MOX Programme in France

The French programme of PWR spent fuel analyses has a broad scope and it has been extended to MOX fuels with the analysis of fuel pins from the Saint-Laurent-des-Eaux B1 plant (SLB1) and from the Dampierre 2 plant (DA).

In France 20 PWRs of 900 MWe are loaded with 30% MOX fuel. SLB1 and DA are 2 of them, containing well characterised MOX-AFA assemblies (MIMAS process). MOX assemblies include 3 zones with different plutonium enrichments to flatten the within-assembly power distribution and to attenuate reaction rate discontinuities at the MOX-UOX interface.

So far, while UOX assemblies stay 4 cycles under irradiation and reach about 50 GWd/t, MOX assemblies are allowed to stay 3 cycles only (“Hybrid” fuel management). The next step is to allow the so-called MOX parity, i.e. the same burn-up for MOX as for UOX, up to 52 GWd/t.

C.1.2 MOX loading in SLB1 PWR

In SLB1 the central zone was characterised by a high Pu content of 5.6% and the initial composition was in at % :
U : U234, 0.002 U235, 0.236 U236, 0.002 U238, 99.760
Pu : Pu238, 0.87 Pu239, 66.71 Pu240, 20.61 Pu241, 7.66 Pu242, 2.89 and Am241, 1.27%.

Fig. C.1 shows the MOX assembly as it was loaded in SLB1. The MOX rods of interest belonged to 2 assemblies and were extracted after 1, 2 or 3 reactor cycles, after burn-ups ranging from about 10 to 45 GWd/t.

Analyses have been performed to determine the concentrations in U, Pu, Am, Cm, Np isotopes and Nd and Cs. In general the analytical results were obtained by mass spectrometry. The experimental determination of burn-up was given for each sample through the Nd145, Nd148 and Nd150 ratios to U238. These experimental results are the property of CEA, EDF and FRAMATOME-ANP.

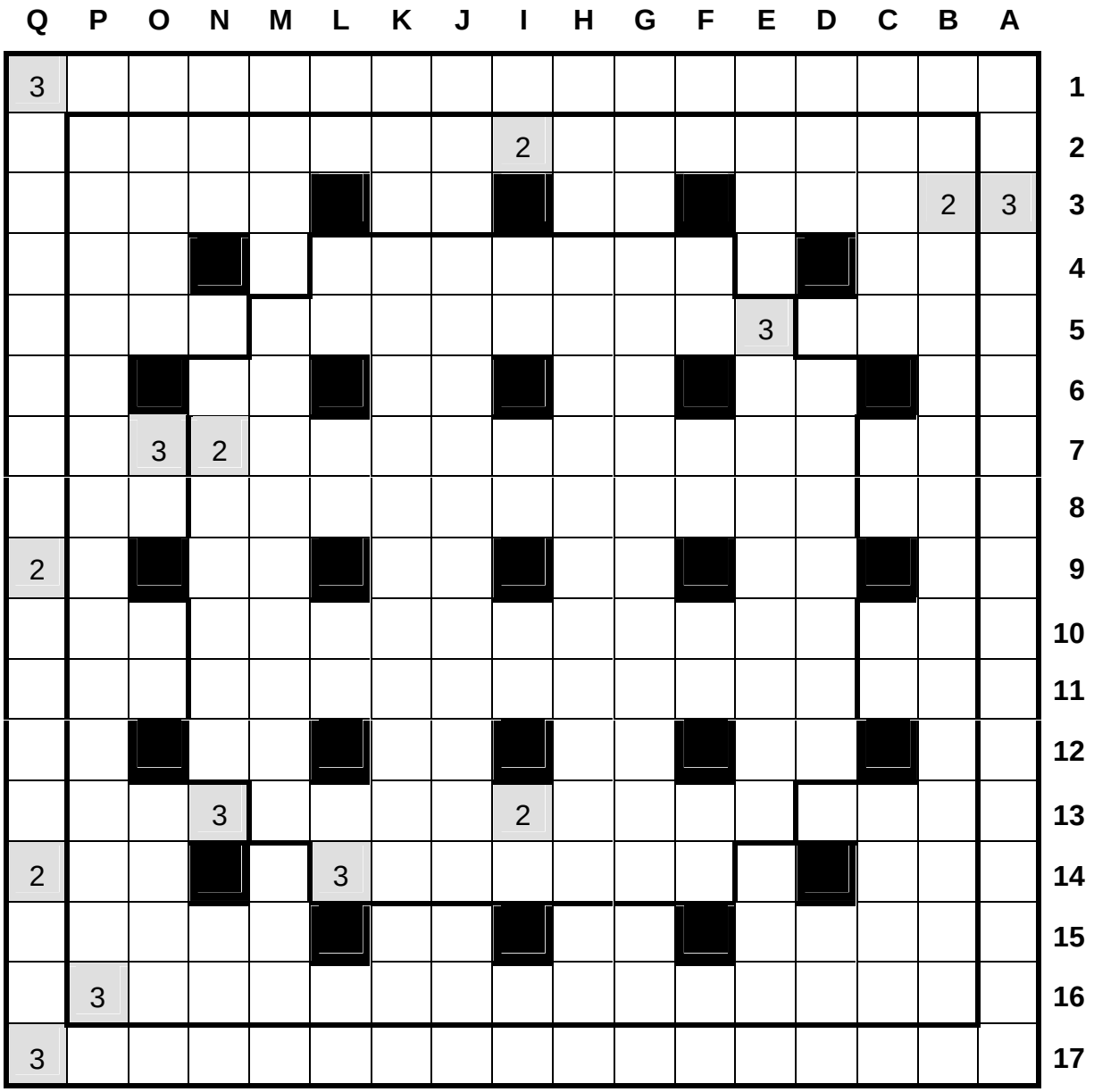

Fig. C.1 : SLB1-FFP00HJX assembly. Pu zoning and experimental pins

C.1.3 MOX loading in Dampierre PWR

The 900-MWe PWR of Dampierre-2 is also characterized by a 30% MOX loading. The central zone of the MOX has a higher Pu content : 6.7%. The intermediate and peripheral zones are characterized respectively by a 5.3% and 3.0%Pu content.
From the MOX assembly FXP0EG, one rod was extracted after 1 irradiation cycle and three rods after 3 cycles.
From the MOX assembly FXP0EH, four rods were extracted after 2 cycles, three rods after 4 cycles and four rods after 5 cycles, reaching about 60 GWd/t at mid-height. As shown in **Fig. C.2**, the four rods extracted after 2 cycles (locations

G04, E13, D05, B02) were replaced with fresh UO2 3.7%^{235}U fuel rods. The three rods extracted after 4 irradiation cycles were replaced by stainless steel rods (P16, M09, E09). The chemical analyses available to Cadarache at the time of VALMOX evaluations concerned 4- and 5-cycle pins (all located in the central or intermediate zone, with initial high Pu content 6.7 % or 5.3%).

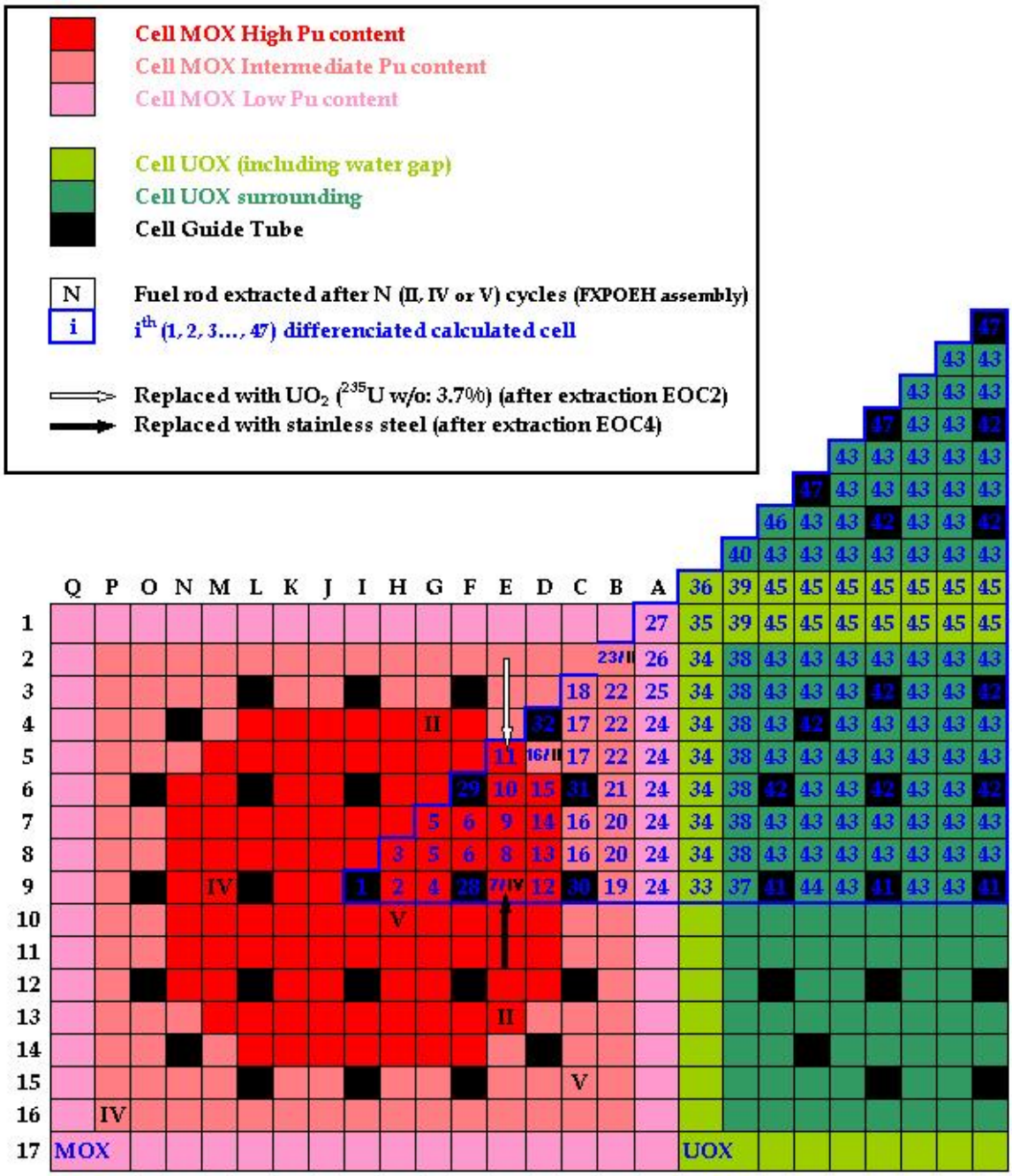

Fig. C.2 : DA2-FXP0EH assembly and MOX calculation pattern

C.1.4 Measurement uncertainties

The measurements are affected by uncertainties of different types [**1**] :

- moderator temperature determination (± 2°C),
- fuel effective temperature determination (± 50°C),

- burn-up determination (Nd_i yields uncertainty ± 2%),
- irradiation history follow-up description,
- chemical assays uncertainties,
- technological uncertainty (% Pu : ± 0.01%, …).

The total uncertainty on C/E was obtained by a quadratic combination of these independent uncertainty components. For the Pu isotopes one arrives at 1s - uncertainties of the order of 1-2% ; for Am isotopes they are close to 3%, and they amount to 4% for the main Cm isotopes (^{244}Cm and ^{245}Cm).

C.2 APOLLO2 calculation modelling

The features of the APOLLO2 code package have been described in Chapter A. The APOLLO2 calculation corresponds to the "*CEA-97* reference scheme", recommended for use to EDF and Framatome-ANP, which implies for MOX fuel [**2**]:

- in the MOX assembly, 23 different pin types individualised for the depletion calculations, and 4 concentric depletion zones per fuel pin (Fig. C.2);
- the surrounding UOX assemblies decomposed into 3 pin types: the outer pin row, the second outer row, and the rest;
- a water gap integrated in the UOX and MOX interface cells (rectangular cells);
- 172-group cross-sections to finely model the resonance region, especially near 1 eV for Pu240, and 0.3 eV for Pu239;
- Isotopes considered for self-shielding are : U238, Pu239, Pu240, Pu241, Pu242, Am241, U235 and U236. The Background Matrix formalism allows space-dependent self-shielding calculation : self-shielding differentiation in the various fuel pins and concentric pellet rings (4 rings) for U238, and 3 different rod types (one for each Pu enrichment zone) for Pu239, Pu240, Pu241 and Pu242. Reference continuous-energy computation pointed out that accurate resonance absorption calculation requires 2D-Pij [**3**] : sophisticated UP1 model is used for U238 and Pu240;
- a burn-up chain with 24 actinides, 85 fission products (i.e. 99% of all fission products absorption is explicitly described);
- use of the thermal-mechanical code METEOR to calculate the fuel temperature profile and to derive an accurate effective temperature [**1**]. Furthermore, an oxide fuel effective temperature is used to account for crystalline bindings in UO2 and MOX pellets [**4**].

The irradiation history was described in 22 steps of which 14 with specific powers (including 4 stretch-out periods) and 8 with inter-cycles cooling. The moderator temperature close to the rod cut is deduced from the axial distribution of fission rate (measured by gamma scanning).

It should be noted that, after extraction, the analysed rods were replaced by UO2 rods (after 2 cycles) or by stainless steel dummies (after 4 cycles). These substitutions were taken into account in the APOLLO2 calculation [**5**].
CEA first performed all calculations using the JEF2.2 data file ; later, for Dampierre evaluations, the calculations were done again with the new JEFF-3.0 file, which gave supplementary useful indications.

C.3 APOLLO2 results for SLB1 assays (JEF2)

The evaluation for MOX fuel loaded into the PWR SLB1 was already largely launched during the preceding VALMOX project [**6**].

The C/E comparison is reported in **Table C.I** for isotopic ratios corresponding to Major Actinides in central rods (asymptotic MOX spectrum). The main observations on these SLB1 results with JEF2.2 are as follows :

- The major plutonium isotopes Pu239, Pu240 and Pu241 are correctly predicted; however a slight Pu239 overestimation is raised with burnup (3% at 40 Gwd/t),
- Pu238 is underestimated by 8% (which probably explains the same trend observed on U234, built mainly from Pu238 decay),
- Pu242 is underestimated by 6% after 3 irradiation cycles, probably due to Pu241(n,γ) epithermal cross-section in JEF2.2 [**7**],
- U236 build-up is underestimated by 7%, due to the low U235 capture resonance integral in JEF2 (and ENDF/B6-release5) [**8**].

Table C.I : C/E biases (in %) on SLB1 asymptotic rods . Major Actinides

	Rods located in Asymptotic neutron spectrum				
Fuel rod position	P14	I13	I02	N13	L14
Cycle	1	2	2	3	3
Zone	Intermediate	Central	Intermediate	Intermediate	Central
Fuel rod burnup (MWd/t)	12 868	28 368	28 453	41 493	45 005
U234/U238	- 4.42	-11.52	- 6.87	- 4.87	- 9.41
U235/U238	1.13	1.89	2.92	4.70	4.28
U236/U238	- 10.13	- 7.10	- 8.24	- 7.84	- 6.45
Pu238/U238	- 8.10	- 9.05	- 8.56	- 6.17	- 8.57
Pu239/U238	0.57	3.98	1.54	4.72	4.13
Pu240/U238	- 0.45	0.62	0.01	1.91	1.28
Pu241/U238	- 2.20	- 1.25	- 3.22	- 1.42	-1.83
Pu242/U238	- 2.19	- 3.37	- 4.60	- 6.21	- 5.64

APOLLO2-JEFF2 prediction for actinide concentrations in peripheral rods is summarized in **Table C.II**. C/E values are consistent with values presented in Table C.I for asymptotic fuel rods : this result means that our MOX reference calculation scheme, with a multi-assembly pattern accounting for surrounding UOX assemblies, is well suited to reproduce the mismatched spectrum at the UOX:MOX interface.

Table C.II : C/E biases (in %) on SLB1 peripheral rods . Major Actinides

	Rods placed in Peripheral zone			
Fuel rod position	A04	Q14	Q17	P16
Cycle	1	2	3	3
Zone	Peripheral	Peripheral	Peripheral	Peripheral
Fuel rod burnup (MWd/t)	9 556	24 664	37 683	42 013
U234/U238	15.75	1.12	2.09	- 3.94
U235/U238	1.20	3.96	5.79	2.04
U236/U238	- 7.76	- 8.00	- 5.63	- 5.18
Pu238/U238	- 9.78	- 8.33	- 7.56	- 6.76
Pu239/U238	2.97	3.40	- 1.28	- 0.23
Pu240/U238	1.05	2.75	4.07	1.14
Pu241/U238	- 6.97	- 2.87	- 3.86	- 3.17
Pu242/U238	- 3.06	- 5.85	- 5.73	- 4.87

Concerning minor actinides, the C/E comparison is presented in **Table C.III** (asymptotic extracted pins) :

- We can notice that Am241 is correctly predicted.
- In agreement with Pu242 underestimation, Am243 is underestimated by 7%.
- Cm244 and its daughter Cm245 are underestimated by 8% to 10%, as a consequence of the low Am243 level.

Table C.III : C/E biases (in %) on SLB1 asymptotic rods . Minor Actinides

	Rods located in Asymptotic neutron spectrum				
Fuel rod position	P14	I13	I02	N13	L14
Cycle	1	2	2	3	3
Zone	Intermediate	Central	Intermediate	Intermediate	Central
Fuel rod burnup (MWd/t)	12 868	28 368	28 453	41 493	45 005
Am241/U238	- 8.28	0.85	- 0.09	1.31	- 1.62
Am242m/U238	- 38.64	- 32.50	- 28.70	- 21.40	- 22.85
Am243/U238	- 15.20	- 6.61	- 7.81	- 7.10	- 6.11
Cm243/U238	- 23.35	- 29.30	- 21.47	- 14.35	- 17.78
Cm244/U238	- 17.99	- 7.90	- 9.69	- 6.40	- 7.08
Cm245/U238	- 16.01	- 7.93	- 13.00	- 6.36	- 8.03

These SLB1 results for Cycles 2 and 3 can be summarized as follow in **Table C.IV** for the MOX pins placed in asymptotic neutron spectrum.

Table C.IV : MOX Fuel Irradiated in SLB1 (central zone)

C/E Ratios for U, Pu, Am and Cm Isotope Masses

Isotopes	C/E in SLB1
U235	1.02 - 1.05
U236	0.92 – 0.93
Pu238	0.91 – 0.94
Pu239	1.01 – 1.05
Pu240	0.99 – 1.02
Pu241	0.97 – 0.99
Pu242	0.94 – 0.98
Am241	0.98 – 1.01
Am242m	0.7 – 0.8
Am243	0.92 – 0.94
Cm243	0.71 – 0.86
Cm244	0.91 – 0.94
Cm245	0.87 – 0.94

These trends of the C/E values are often similar to those observed from BN calculations in Chapter B. However, major exceptions are :

- a lower overestimate for Pu239 : 1.03 in the average versus 1.08 ; however, this is rather conform to the expected WIMS overprediction after the benchmark comparisons of Chapter A ;
- a very good prediction for Am241, close to unity, while BN gets a significant overestimation ; this disagreement between SLB1 and ARIANE results is *not* consistent with the comparison APOLLO2/WIMS8 on Am241 prediction in Benchmark BUC-IVB described in Chapter A.

C.4 APOLLO2 calculations results for Dampierre (JEF2 and JEFF3)

The measurements on Dampierre samples are at least as accurate as those of SLB1. The calculation model was optimised, taking into account all model details : for example, the substitution of the extracted pins by UO2 or steel pins, or the representation of the power stretch-out phases when approaching the end of cycle.

C.4.1 Results with JEF2.2

(C-E)/E ratios for the U, Np, Pu, Am and Cm isotopes calculated for Dampierre with JEF2.2 data are given in **Table C.V**. Five different samples, all placed in the central zone, are considered ; their burn-up ranged from 52 to 60 GWd/t (3 pins were irradiated 4 cycles while 2 pins were extracted after 5 cycles).

Table C.V : C/E biases in % on DAMPIERRE MOX assembly (JEF2)

	(C/E-1) JEF2.2				
	EOC 4			EOC 5	
Irradiation follow-up	E09 (Pu : 6.7%)	M09 (Pu : 6.7%)	P16 (Pu : 5.3%)	H10 (Pu : 6.7%)	C15 (Pu : 5.3%)
$^{234}U/^{238}U$	-1.4	-2.7	+2.7	-1.5	+1.4
$^{235}U/^{238}U$	+1.6	+1.2	-1.3	+1.0	-0.8
$^{236}U/^{238}U$	-6.9	-6.9	-8.0	-7.0	-6.8
$^{237}Np/^{238}U$	-15.0	-12.5	-17.9	-12.6	-10.8
$^{238}Pu/^{238}U$	-3.0	-2.2	-0.9	-0.8	-0.7
$^{239}Pu/^{238}U$	+2.5	+2.0	+2.6	+4.9	+5.5
$^{240}Pu/^{238}U$	+1.1	+0.3	-0.1	+4.1	+1.1
$^{241}Pu/^{238}U$	-0.2	-0.6	+0.3	+1.6	+0.9
$^{242}Pu/^{238}U$	-1.8	-2.0	-1.8	+0.3	-2.9
$^{241}Am/^{238}U$	+4.6	+4.3	+5.0	+7.3	+9.9
$^{241}Am/^{238}U$ EOC	+15.1	+15.7	+17.9	+12.5	+22.0
$^{242m}Am/^{238}U$	-21.3	-22.2	-10.8	-24.1	-15.0
$^{243}Am/^{238}U$	+0.8	+1.5	+1.7	+1.6	+4.2
$^{243}Cm/^{238}U$	-11.5	-10.8	-9.0	-13.7	-8.6
$^{244}Cm/^{238}U$	-5.5	-5.1	-4.4	-4.5	-2.4
$^{245}Cm/^{238}U$	-3.2	-2.1	+0.2	-1.0	+5.3
$^{246}Cm/^{238}U$	-7.6	-6.4	-12.3	-4.7	-6.1
$^{247}Cm/^{238}U$	-13.7	-12.1	-18.9	-10.6	-9.0
$^{143}Nd/^{238}U$	+1.3	+0.4	+0.1	+0.8	+1.2
$^{144}Nd/^{238}U$	-1.7	-2.3	-2.1	-2.0	-1.6
$^{145}Nd/^{238}U$	+0.1	-0.5	-0.6	-0.4	-0.6
$^{146}Nd/^{238}U$	+0.9	+0.5	+0.3	+0.9	+1.3
$^{148}Nd/^{238}U$	+2.2	+1.9	+2.2	+2.1	+2.3
$^{150}Nd/^{238}U$	+0.2	+0.2	+0.6	+0.5	+0.8
$^{133}Cs/^{238}U$	-1.2	nm	+0.0	-0.2	+5.2
$^{134}Cs/^{238}U$	+1.4	nm	+0.3	+16.0	+11.9
$^{135}Cs/^{238}U$	-3.6	nm	-5.7	-2.5	+0.9
$^{137}Cs/^{238}U$	-1.9	nm	-0.7	+0.1	+4.4
Local Burn-up (MWd/t)	52899	52899	51925	57882	59957
Ass. Burn-up (GWd/t)	50.0			59.4	

Compared to SLB1 results of Table C.IV, the trends are generally similar, except for Am241, for which the C/E ratio is no longer close to unity, but would be about 1.15 at end of irradiation, resembling the BN trend observed in Chapter B. In fact, independent measurements [**9**] had also recently suggested that the Am241 capture cross-sections could be too low, which is reflected here in the Am241 overestimate and the corresponding, large underestimate of Am242m. New basic measurements on Am241 are now asked to IRMM Geel.

For Pu239, an observation is that the overestimation grows from 3% to 5% when the burn-up increases from 52 to 60 GWd/t ; **Fig. C.3** illustrates this tendency.

Fig. C.3 : C/E comparison on Pu239 depletion versus Burnup

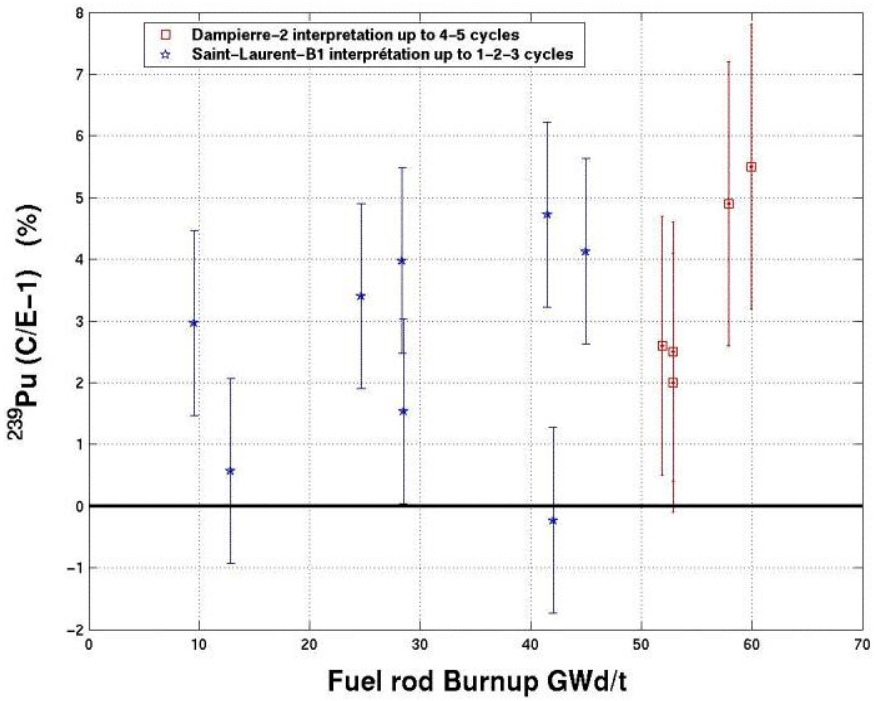

The APOLLO2 results on MOX fuel inventory prediction using JEF2.2 library are summarized in **Table C.VI**.

Table C.VI : APOLLO2-JEF2 results of DA2 MOX P.I.E (C/E-1 in %)

APOLLO2.5 CEA-97	(C/E-1)±δE/E in % (1σ) EOC 4	 EOC 5
	JEF2.2	JEF2.2
$^{234}U/^{238}U$	-0.5 ± 2.0	-0.1 ± 2.2
$^{235}U/^{238}U$	+0.5 ± 2.3	+0.1 ± 2.5
$^{236}U/^{238}U$	-7.2 ± 1.3	-6.9 ± 1.3
$^{237}Np/^{238}U$	-15.2 ± 2.6	-11.7 ± 2.5
$^{238}Pu/^{238}U$	-2.0 ± 1.4	-0.8 ± 1.9
$^{239}Pu/^{238}U$	+2.4 ± 2.2	+5.2 ± 2.2
$^{240}Pu/^{238}U$	+0.4 ± 0.9	+2.6 ± 1.0
$^{241}Pu/^{238}U$	-0.2 ± 0.9	+1.3 ± 1.3
$^{242}Pu/^{238}U$	-1.8 ± 1.3	-1.3 ± 1.3
$^{241}Am/^{238}U$	+16.2 ± 3.8	+17.2 ± 3.7
$^{242m}Am/^{238}U$	-18.1 ± 2.6	-19.6 ± 3.5
$^{243}Am/^{238}U$	+1.3 ± 2.0	+2.9 ± 1.7
$^{243}Cm/^{238}U$	-10.4 ± 1.8	-11.2 ± 2.3
$^{244}Cm/^{238}U$	-5.0 ± 3.8	-3.4 ± 3.4
$^{245}Cm/^{238}U$	-1.7 ± 4.2	+2.1 ± 3.7
$^{246}Cm/^{238}U$	-8.7 ± 7.5	-5.4 ± 6.9
$^{247}Cm/^{238}U$	-14.9 ± 9.2	-9.8 ± 8.5
$^{143}Nd/^{238}U$	+0.6 ± 1.5	+1.0 ± 1.6
$^{144}Nd/^{238}U$	-2.0 ± 3.0	-1.8 ± 2.2
$^{145}Nd/^{238}U$	-0.3 ± 0.5	-0.5 ± 0.5
$^{146}Nd/^{238}U$	+0.5 ± 2.5	+1.1 ± 2.4
$^{148}Nd/^{238}U$	+2.1 ± 2.2	+2.2 ± 2.1
$^{150}Nd/^{238}U$	+0.3 ± 0.6	+0.6 ± 0.6
$^{133}Cs/^{238}U$	-0.6 ± 1.7	+2.5 ± 1.7
$^{134}Cs/^{238}U$	+0.9 ± 3.7	+13.9 ± 5.0
$^{135}Cs/^{238}U$	-4.7 ± 2.5	-0.8 ± 2.5
$^{137}Cs/^{238}U$	-1.3 ± 2.1	+2.3 ± 2.1
Local Burn-up (GWd/t)	52	60

C.4.2 Results with JEFF3.0

JEFF3.0 is the new European Data File, not yet released to users at the beginning of the VALMOX contract but available to CEA for tests. It incorporates several modifications of cross-sections including :

- U235 resonant capture increase [**8**];
- Pu241 epithermal capture increase [**10**];
- U238 (n,2n) increase by +10% [**11**]

Table C.VII compares Dampierre P.I.E analysis using JEF2.2 and JEFF3.0 evaluations (respectively CEA93 and CEA2003 libraries in APOLLO2).

Table C.VII : Fuel inventory prediction in DA2 MOX spent fuel using JEF2.2 and JEFF3.0

C/E-1 in %

	C/E-1 ± ? E/E (% 1σ)			
	CYCLE 4		CYCLE 5	
	JEF2.2	JEFF3.0	JEF2.2	JEFF3.0
$^{234}U/^{238}U$	-0.5±2.0	-1.1±2.0	-0.1±2.2	-0.7±2.2
$^{235}U/^{238}U$	0.5±2.3	-0.2±2.3	0.1±2.5	-0.8±2.5
$^{236}U/^{238}U$	-7.2±1.3	-3.1±1.3	-6.9±1.3	-2.7±1.3
$^{237}Np/^{238}U$	-15.2±2.6	-2.2±2.6	-11.7±2.5	-1.7±2.5
$^{238}Pu/^{238}U$	-2.0±1.4	-2.7±1.4	-0.8±1.9	-1.4±1.9
$^{239}Pu/^{238}U$	2.4±2.2	1.7±2.2	5.2±2.2	4.8±2.2
$^{240}Pu/^{238}U$	0.4±0.9	1.1±0.9	2.6±1.0	3.3±1.0
$^{241}Pu/^{238}U$	-0.2±0.9	0.0±0.9	1.3±1.3	1.6±1.3
$^{242}Pu/^{238}U$	-1.8±1.3	2.1±1.3	-1.3±1.3	3.0±1.3
$^{241}Am/^{238}U$ EOC	16.2±3.9	15.2±3.9	17.2±3.7	16.5±3.7
$^{242M}Am/^{238}U$	-18.1±2.6	-18.9±2.6	-19.6±3.5	-20.2±3.5
$^{243}Am/^{238}U$	1.3±2.0	3.8±2.0	2.9±1.7	5.7±1.7
$^{243}Cm/^{238}U$	-10.4±1.8	-15.2±1.8	-11.2±2.3	-15.8±2.3
$^{244}Cm/^{238}U$	-5.0±3.8	-2.8±3.8	-3.4±3.4	-1.0±3.4
$^{245}Cm/^{238}U$	-1.7±4.2	4.8±4.2	2.1±3.7	10.0±3.7
$^{246}Cm/^{238}U$	-8.7±7.5	-12.5±7.5	-5.4±6.9	-8.7±6.9
$^{247}Cm/^{238}U$	-14.9±9.2	-4.2±9.2	-9.8±8.5	2.7±8.5
$^{143}Nd/^{238}U$	0.6±1.5	-0.2±1.5	1.0±1.6	0.0±1.6
$^{144}Nd/^{238}U$	-2.0±3.0	-1.5±3.0	-1.8±2.2	-1.2±2.2
$^{145}Nd/^{238}U$	-0.3±0.5	-0.5±0.5	-0.5±0.5	-0.7±0.5
$^{146}Nd/^{238}U$	0.5±2.5	0.5±2.5	1.1±2.4	1.1±2.4
$^{148}Nd/^{238}U$	2.1±2.2	2.0±2.2	2.2±2.1	2.1±2.1
$^{150}Nd/^{238}U$	0.3±0.6	0.2±0.6	0.6±0.6	0.5±0.6
$^{133}Cs/^{238}U$	-0.6±1.7	-0.1±1.7	2.5±1.7	3.1±1.7
$^{134}Cs/^{238}U$	0.9±3.7	-1.6±3.7	13.9±5.0	11.3±5.0
$^{135}Cs/^{238}U$	-4.7±2.5	-5.2±2.5	-0.8±2.5	-1.3±2.5
$^{137}Cs/^{238}U$	-1.3±2.1	-1.4±2.1	2.3±2.1	2.3±2.1
BU (GWd/tHM)	52.6	52.6	58.9	58.9

Clear improvements are obtained on the actinide prediction at the End Of irradiation Cycle (EOC) from JEF2.2 to JEFF3.0 for the 5 MOX high burned fuel pins.

Owing to ^{235}U resonance integral $I_?$ increase (by about 6%) [**8**], the predicted ^{236}U concentration is improved using JEFF3.0. Moreover, the ^{237}Np and ^{238}Pu are increased in agreement with measured isotopic contents. In MOX spent fuel, the ^{237}Np concentration is very well calculated using JEFF3.0, due to the $^{238}U(n,2n)$ increase in this new JEFF3.0 evaluation.

Thanks to the increase of the capture integral in the large E_0=0.26eV of ^{241}Pu [**10**], the longstanding ^{242}Pu underprediction in JEF2-based calculation is cancelled using the JEFF3.0 file.

C.4.3 Changes from JEF2.2 to JEFF3.0

Table C.VIII shows the effect of changing from JEF2.2 to JEFF3.0 on the deviations (C-E)/E for MOX spent isotopic mass concentrations at EoL.

Table C.VIII : Changes on (C-E)/E values from JEF2.2 to JEFF3.0

Isotopes	Changes (%)	Improvement
U235 U236	-0.8 +4	- YES
Np237	+10	YES
Pu238 Pu239, 240, 241 Pu242	-0.7 not significant +4	- - YES[10]
Am241 Am242m Am243	not significant not significant +3	- - YES[11]
Cm243 Cm244	-5 +2	No YES

The improvement on U235 is small. The one on U236 is more important, as a logical consequence of the increase in U235 capture resonance integral brought in the JEFF3.0 data file. Np237 build-up is dramatically improved thanks to the modification of U238(n,2n). One would also expect an improvement for Pu238, but contrary to UOX fuel [**12**] this is not significant in MOX fuels; of course the content of Pu238 at EoL not only depends on Pu238 formation from the chain U235-236-Np237 and U238(n,2n), but also on Cm242 decay.

The changes in data files concerning Pu239 and Pu240 are slight in LWR spectra and do not impact significantly their depletion.

[10] Clear improvement in SLB1 (and UOX fuels), not significant in Dampierre
[11] Clear improvement in SLB1, but not in Dampierre

The change brought to the resonant capture of Pu241 does not influence Pu241 itself due to the preservation of the whole absorption cross section in JEFF3.0; it results in an increase in Pu242, Am243 and Cm244. The large underprediction observed in SLB1 experiment is strongly reduced.

The improvement for Am241 is marginal, because the JEF2.2 evaluation of Am241 nuclear data was kept unchanged in JEFF3.0.

On the whole for MOX fuels, the benefits mainly concern U236 and Np237.
The major plutonium isotopes Pu239, Pu240 and Pu241, as well as Am241, are not significantly affected.

C.4.4 Practical conclusions

One retains from this analysis that 2 actions on cross-sections deserve primarily to be undertaken, in order to improve the prediction of :

- Pu239, the major fissile isotope, which is overestimated by +3±2% (40Gwd/t) up to +5%±2% (60Gwd/t), which is larger than the target accuracy. Complementary analysis, based on Conversion ratio and U238 capture measurements in Eole reactor at Cadarache, has pointed out the main explanation [**11**] : U238 resonant capture in JEF2 and JEFF3.0 is too high by 1%. This trend was accounted for in the new ^{238}U evaluation performed for JEFF3.1 [**13**].
- Am241, which is overestimated by 15% ± 4% at End of Life. This P.I.E information, combined with consistent results on Pu ageing in Eole MOX cores, was reported to JEFF Group and a new Am241 evaluation for JEFF3.1 is in preparation [**14**].

In summary, the CEA results confirm the major trends from the BN and SCK results presented in Chapter B.
With WIMS8 as employed at BN, Pu239 was overestimated by 7%, and Am241 by more than 20%, it was clear from Chapter A that WIMS9 results would improve the C/E agreement. The Monte-Carlo results obtained at SCK with ALEPH give trends which are very close to those found at CEA with APOLLO2.

References for chapter C

1. C. Chabert, A. Santamarina, R. Dorel, D. Biron, C. Poinot, "Qualification of the APOLLO2 assembly code using PWR-UO2 isotopic assays. The importance of irradiation history and thermo-mechanics on fuel inventory prediction," Proc. Int. Top. Meeting in Reactor Physics and Math. and Comp. into the Next Millennium, PHYSOR 2000, Pittsburgh, USA, May 7-12, 2000.
2. C. Chabert, A. Santamarina, P. Bioux, "Elaboration and experimental validation of the APOLLO2 depletion trans port route for PWR Pu recycling," Proc. Int. Meeting PHYSOR 2000, Pittsburgh, USA, May 7-12, 2000.

3. B. Roque, A. Santamarina, “Burnup Credit in LWR-MOX Assemblies”, Proc. of Int. Conf. On Nuclear Criticality Safety ICNC’99, Versailles, Sept 20-24, 1999
4. A. Meister, A. Santamarina, ” The Effective Temperature for Doppler Broadening of Neutron Resonances in UO_2,” International Conference on the Physics of Nuclear Science and Technology PHYSOR-98, Long Island (NY), USA, October 5-8, 1998.
5. D. Bernard, A. Santamarina, "Experimental Validation of the APOLLO2 code for High Burnup MOX fuel. JEF2.2 Results and JEFF3.0 Improvements," Proc. Int. Conf. PHYSOR 2004 – The physics of fuel cycles and advanced nuclear systems, Chicago, USA, April 25-29, 2004.
6. Nuclear Data for Advanced MOX Fuels, Final Report of Contract n° FI4I-CT95-0002, by S. Pilate, R. Jacqmin et al., EUR 19126 EN, 2000
7. A. Courcelle, A. Santamarina, H. Derrien, L. Leal, "Pu241 capture cross-section. Recommendations for JEFF3”, JEFDOC-884, Paris, November 19-21, 2001
8. A. Courcelle, A. Santamarina, C. Chabert, O. Litaize, "Experimental Validation of U235 evaluations. Recommendations for JEFF3”, JEFDOC-862
9. C. Chabert, A. Santamarina, P. Bioux, "Trends in nuclear data derived from integral experiments in thermal and epithermal reactors," Proc. Int. Conf. Nuclear Data ND2001, Tsukuba, Japan, October 7-12, 2001.
10. A. Courcelle, A. Santamarina, H. Derrien, L. Leal, "Reevaluation and validation of ^{241}Pu resonance parameters,” JEFDOC-916 and Nuclear Science and Engineering, **150**, (2005)
11. A. Courcelle, A. Santamarina, C. Chabert, O. Litaize, "Experimental Validation of U238 evaluations. Recommendations for JEFF3”, JEFDOC-883, Paris, November 19-21, 2001
12. A. Courcelle, A. Santamarina, S. Mengelle, "Improvements of isotopic ratios prediction through Takahama-3 chemical assays with the JEFF3.0 nuclear data library," Proc. Int. Conf. PHYSOR 2004 – The physics of fuel cycles and advanced nuclear systems, Chicago, USA, April 25-29, 2004.
13. H, Derrien, A. Courcelle, L. Leal, A. Santamarina, "Evaluation of 238U resonance parameters from 0 to 20 KeV," Proc. Int. Conf. On Nuclear Data ND2004, Santa Fe, USA, 26 Sept – 2 oct, 2004.
14. D. Bernard, A. Santamarina, O. Litaize, " JEF2.2/JEFF3.0 iprovements on spent fuel inventory prediction in LWRs. Trends from integral experiments and proposals for JEFF3.1”, JEFDOC-1043, Paris, November 24-26, 2004

CHAPTER D

SENSITIVITY AND UNCERTAINTY CALCULATIONS

D.1 Statistical adjustment and trends on nuclear data obtained at CEA

Integral data measured in critical experiments and spent fuel chemical assays provide relevant information regarding the quality of neutron interaction data. The so-called statistical adjustment method has been extensively used to produce multi-group libraries and improve prediction for the design of reactors. The purpose of the adjustment procedure is to determine optimal modifications of nuclear data (usually group averaged cross-sections and neutron multiplicities) through a rigorous mathematical framework in order to minimize the discrepancies between calculated and measured integral parameters. The present methodology is based on a non-linear regression method using an iterative technique, which is implemented in the automated code RDN (Re-estimation of Nuclear Data) [1].

The primary objective of this work is not to produce an adjusted library but, on one hand to check the consistency between integral measurements and JEF2.2 evaluations, and on the other hand to suggest some nuclear data modifications to be introduced in JEFF3 new evaluations.

Measured isotopic ratios in irradiated MOX assemblies were used ; however, critical experiments (k_{eff} and Buckling values), as well as PWR-UOX spent fuels, are included in the adjustment to improve the reliability of the obtained nuclear data trends.

D.1.1 Overview of integral experiments data base

Traditional adjustment studies are often based on reactivity experiments and central reaction rate ratio measurements of specific isotopes. The originality of the present study is not only to take into account k_{eff} measurements in LWR-type lattices, as well as highly enriched uranium solution experiments, but also to include isotopic ratios measured in PWR Post-Irradiation Experiments [1]. These measurements provide isotopic ratios N_i / N_{U238} of the isotope *i* for several burn-up values. Each experimental value can be considered as an individual integral measurement : about 400 C/E values from UOX [2] and MOX assemblies [3] have been included in the RDN code. Measured actinides are: U234, U235, U236, Np237, Pu238, Pu239, Pu240, Pu241, Pu242, Am241, Am243, Cm244 and Cm245. **Table D.I** summarizes the P.I.E measurements included in the statistical adjustment.

Table D.I : Spent Fuel measurements used in the present adjustment

Fuel **UOX** PWR name	U enrich^{t} U235 wt %	Number of samples	Burn-up range
Bugey-3	3.10%	7	20 - 38 GWd/t
Fessenheim-2	3.14%	8	49 - 58 GWd/t
Gravelines	4.50%	8	26 - 60 GWd/t
Fuel **MOX** PWR name	Pu enrich^{t} Pu wt %	Number of samples	Burn-up range
Saint-Laurent B1	2.91%	3	10 - 38 GWd/t
	4.42%	4	13 - 42 GWd/t
	5.64%	2	28 – 45 GWd/t

The selected k_{eff} and Buckling measurements in Low-Enriched UO_2 lattice experiments cover a wide range of moderation ratios [4]. Most of them are LWR-type and have been carried out in the Eole and Minerve zero-power reactors at CEA-Cadarache. VVER and HCPWR critical experiments are taken from the International Criticality Safety Database ICSBEP handbook.

Experiments using highly-enriched uranium solutions (UO_2F_2+H_2O or $UO_2(NO_3)_2$+HNO_2) are widely used in criticality-safety to check the accuracy of nuclear data. Therefore, we investigated experiments from various international laboratories involving uranium concentration ranging from 20 g/l (corresponding to softer neutron spectrum) up to 700 g/l (intermediate neutron spectrum) [5].

D.1.2 Calculation methods. C/E determination and sensitivity coefficients

To minimize errors in the Keff calculation of UO_2 lattices and highly enriched systems, the Monte-Carlo Code TRIPOLI4 (resonance self-shielding in the unresolved range is accounted for using probability tables) is used with JEF2.2 pointwise cross-sections.

Isotopic ratios predictions are based on the APOLLO2.5 and its 172-group library CEA93.V6 also based on JEF2.2. The accurate calculation route, already described in Chapters A and C, follows the main recommendations defined in previous UOX and MOX PIE analyses [3].

K_{eff} sensitivity profiles to nuclear data have been easily obtained from the First Order Perturbation Theory implemented in APOLLO2; sensitivity coefficients to the cross sections and multiplicities of the main isotopes were derived on the European JEF 15-group structure.

For isotopic ratios, sensitivity coefficients have to be assessed as a function of the burn-up. Despite the large number of calculations needed, direct APOLLO2 calculations have been carried out.

D.1.3 Microscopic parameters and data covariance

JEF2.2 broad group adjustment was performed on the 15-group structure, whose energy boundaries are reported in **Table D.II**.

Using reliable nuclear data uncertainties and correlations is of importance for the quality of the results. Correlations between energy groups, cross-sections and isotopes should be in principle considered; however, in the most recent libraries, obtaining a reliable error information on cross-section is still difficult especially in resonance range which is of primary importance in our work. Consequently, uncertainties have been estimated using crude techniques (comparison between evaluated files, quick review of cross-section measurements, information given by the standard cross-section committee and nuclear data compilations). A special attention was paid to set realistic values to the nuclear data variances in the thermal and epithermal range below 500 eV (see some a-priori uncertainty values in Table D.II).

D.1.4 Statistical adjustment results and trend analysis

The quantitative results obtained by the RDN code are summarized for uranium and Pu isotopes respectively in **Tables D.II and D.III**. In these tables, nuclear data modifications in bold are considered to be significant : the uncertainty after adjustment is significantly reduced and lower than the data modification.

The present results on nuclear data are consistent with previous qualitative analyses [6] and demonstrate the reliability of the adjustment process.

- **Uranium :** The need for increasing JEF2 U235 capture resonance integral is quantified : +12%±3%, and is accounted for in the JEFF3 evaluation [7]. The thermal value ν_t^{U235} = 2.437 is confirmed within 0.2% accuracy.

  Concerning U238, a strong reduction of the (n,2n) cross section is proposed : this trend is introduced in the JEFF3.0 evaluation [8]. A reduction of 0.7% of the U238 shielded capture cross-section in the resolved range is suggested but this small modification is in the uncertainty of this data (a posteriori standard deviation ±1.6%); however, considering the importance of this data for Keff and Pu239 build-up calculations, this result supported our work for an improved U238 evaluation in JEFF3.1 [9].
- **Plutonium :** The most significant trend deduced for Pu239 is an increase by 3.7% of the JEF2.2 capture cross-section in the large resonance at 0.3 eV and a decrease by 1.8% of the fission cross-section. An accurate trend is shown for the epithermal capture of Pu241 : the capture integral of the 0.26 eV resonance in JEF2.2 needs to be increased by 7.4% ± 2.6%(1σ). This correction, arising from the underestimation of the Pu242 build-up, was investigated in the framework of a CEA-ORNL collaboration and corrected in JEFF3.0 with a new evaluation [10].
- **Minor actinides :** It was pointed out that Am241(n,γ) cross section should be increased by 15% in the [0 – 4eV] energy range [11]. An increase by 3.0% ± 2.3% of the Am243 epithermal capture (three first

large resonances) was also highlighted. Modifications proposed by the adjustment for other minor actinides lie within the a posteriori nuclear data uncertainty.

Table D.II; Adjustment results in % for uranium nuclear data

Energy range	Change in %	Std. Dev. After adj	Std. Dev. Before adj
U235	**capture**		
12.03 keV – 454 eV	+6.3	8.8	10.0
454 eV – 22.6 eV	**+12.9**	**3.1**	**10.0**
22.6 eV – 4.0 eV	**+12.8**	**3.6**	**10.0**
4.0 eV – 0.54 eV	**+12.4**	**3.7**	**10.0**
0.54 eV – 0.1 eV	+0.7	1.6	2.0
< 0.1 eV	+0.4	0.8	1.0
U235	**fission**		
22.6 eV – 4.0 eV	+1.6	2.3	3.0
4.0 eV – 0.54 eV	+1.3	2.4	3.0
0.54 eV – 0.1 eV	-0.4	0.8	1.0
< 0.1 eV	-0.2	0.3	0.4
U235	ν_t		
22.6 eV – 4.0 eV	+0.1	0.7	0.7
4.0 eV – 0.54 eV	+0.2	0.7	0.7
0.54 eV – 0.1 eV	+0.3	0.5	0.7
< 0.1 eV	+0.1	0.2	0.4
U236	**capture**		
12.03 keV – 454 eV	+0.2	10.0	10.0
454 eV – 22.6 eV	+1.8	8.0	10.0
22.6 eV – 4.0 eV	+0.9	3.4	5.0
U238	**capture**		
12.03 keV – 454 eV	-0.1	2.2	2.2
454 eV – 22.6 eV	-0.5	1.6	2.0
22.6 eV – 4.0 eV	-0.7	1.7	2.0
4.0 eV – 0.54 eV	0.0	1.0	1.0
U238	**n,2n**		
19.6 MeV – 6.07 MeV	**+6.3**	**2.1**	**10.0**

Table D.III; Adjustment results in % for plutonium nuclear data

	Change in %	Std. Dev. after adj	Std. Dev. before adj
Energy range		**Capture**	
22.6 eV – 4.0 eV	+3.0	6.5	7.0
4.0 eV – 0.54 eV	+0.3	4.0	4.0
0.54 eV – 0.1 eV	**+3.7**	**1.3**	**3.0**
< 0.1 eV	+0.1	1.2	1.2
Pu239		**Fission**	
4.0 eV – 0.54 eV	-0.4	2.5	2.5
0.54 eV – 0.1 eV	-1.8	1.3	1.5
< 0.1 eV	-0.1	0.5	0.5
Pu240		**Capture**	
22.6 eV – 4.0 eV	+0.4	4.0	4.0
4.0 eV – 0.54 eV	+5.6	2.0	3.0
0.54 eV – 0.1 eV	+0.3	1.0	1.0
Pu241		**Capture**	
454 eV – 22.6 eV	+4.9	10.0	10.0
22.6 eV – 4.0 eV	+11.2	9.8	10.0
4.0 eV – 0.54 eV	+0.8	7.0	7.0
0.54 eV – 0.1 eV	**+7.4**	**2.6**	**5.0**
< 0.1 eV	+0.4	1.5	1.5
Pu241		**Fission**	
454 eV – 22.6 eV	+1.3	3.9	4.0
22.6 eV – 4.0 eV	-1.5	2.9	3.0
4.0 eV – 0.54 eV	-0.3	3.0	3.0
0.54 eV – 0.1 eV	-0.3	1.8	2.0
< 0.1 eV	-0.0	1.0	1.0

D.1.5 Conclusions

Combination of integral and differential information is an efficient way to improve neutron interaction data. The RDN statistical adjustment method gives a rigorous framework for such objective. The high reliability of the obtained data trends is linked to the quality of French integral measurements and our ability to model them without significant calculation biases.

This work takes advantage of the high sensitivity of spent fuel isotopic ratios to a small number of isotopes and cross-sections so that a discrepancy between the calculated and the measured value gives information that could not be obtained by using only integral quantities such as critical mass or k_{eff}.

Valuable results have been obtained for thermal and resolved range data in JEF2.2 :

- they confirmed the overall quality of JEF2.2 cross-sections and multiplicities for thermal reactors,
- they gave the guidelines for modifications of the resolved resonances for U235 and Pu241, and of U238(n,2n) and FPs cross sections in JEFF3.0 [12],
- they support the work for new evaluations of U238 and Am241 in JEFF3.1.

D.2 Sensitivity and uncertainty calculations at NRG

D.2.1 Introduction

The main task of NRG within the VALMOX project, work package 3, is the analysis of the sensitivity (with respect to uncertainties in cross sections) and uncertainty of the calculation of the isotope composition of the discharged fuels, at the end of irradiation, but also after 10,000 years in final repository. The studies are focussed on the analysis of the PWR MOX fuel irradiation experiments, and the OECD/NEANSC Burn-up Credit Benchmark, already described in previous sections.

This section covers the following topics:

- Calculational procedure for sensitivity and uncertainty calculation. This can also be regarded as "error propagation" in burn-up calculations (subsection D.2.2).
- Cross section uncertainty data (subsection D.2.3).
- Uncertainty and sensitivity calculation for the OECD/NEANSC Burn-up Credit Benchmark Phase IV-B ("BUC IV-B") (subsection D.2.4)
- Uncertainty and sensitivity calculation for the Dampierre E09/M09 pin (subsection D.2.5)
- Uncertainty and sensitivity calculation for the Beznau ARIANE BM1 pin (subsection D.2.6). Additional analyses concerning sensitivity and uncertainty of helium production in this particular sample are presented in Chapter E.

D.2.2 Calculational procedure

At NRG the studies are performed using the spectrum code WIMS8A [1] in combination with the codes CASEMATE (formerly called CSS1SMAT) and MAMAMEA [2]. ***CASEMATE*** ("***CA***lculate ***SE***nsitivity ***MAT***ric***E***s"), the new version of the CSS1SMAT code offers more flexibility, allowing the user to choose by him/herself the neutron induced reaction types and decay reaction types. These changes were essential for the determination of the total helium build up by alpha decay of actinides.
The calculation scheme includes two main scripts that have as main tasks:

1. spectrum calculation in 172 energy groups for each burnup step, and
2. calculation of relative sensitivity matrices (with respect to initial densities, one-group microscopic cross-sections and decay constants) for each burnup step.

The first task is performed by the spectrum code WIMS8A using its own nuclear data library based on JEF2.2 data. The second task is carried out with the NRG code CASEMATE. Reference [2] describes in detail the method used in this code together with its applications. The sensitivity matrices calculated for each burnup step are combined into a matrix for the entire burnup scheme using the matrix manipulation code MAMAMEA, following the procedure described in [2].

CASEMATE has as main input files containing the initial number densities for each isotope, one-group flux, and one-group cross-sections. The data required by CASEMATE is extracted from the WIMS interface files using auxiliary codes as summarised in **Table D.IV**.

Table D.IV : Auxiliary codes used in the sensitivity/uncertainty analyses.

	Code	Task
1	WIFLUX	Extract flux from the WIMS interface files
2	WIENBO	Extract energy boundaries for the energy group scheme used represent the neutron spectrum
3	WIXSEC	Extract microscopic cross-sections for each nuclide
4	WINUDE	Extract number density for each nuclide

The calculation of the uncertainties in the final nuclide densities requires as input the relative uncertainties in the one-group cross-sections. These are calculated with the code COLONE [3] that collapses the multi-group cross sections and uncertainties from the EAF-based FISPACT library [4], using the spectrum in 172 groups calculated in the first phase for each burn-up step.

D.2.3 Cross-section uncertainty data

The results are given for the calculations performed using EAF-based uncertainty data [4] complemented with uncertainty data provided by CEA for some actinides, viz. ^{235}U, ^{238}U, ^{237}Np, ^{238}Pu, ^{239}Pu, ^{240}Pu, ^{241}Pu, ^{242}Pu, ^{243}Pu, ^{241}Am, ^{243}Am, ^{244}Cm and ^{245}Cm [5].

Concerning the differences between the cross section uncertainty data from the EAF uncertainty file (FISPACT library) and the data supplied by CEA (more adequate for core calculations) the following should be noted:

- The relative cross section uncertainty values are generally a factor of 2 to 10 smaller than the corresponding values from the EAF-based FISPACT lbrary.
- The cross section uncertainty data in the EAF-based FISPACT library are generally given for 3 energy groups in the range from 0 eV up to 20 MeV, whereas the CEA data are given in 15 energy groups covering the same range. In the collapse to a single energy group by the COLONE code, as required for CASEMATE, it is assumed that the uncertainties in different energy groups (of the cross section uncertainty files) are uncorrelated [3]. This leads to 1-group cross section uncertainties based on CEA data, which are considerably smaller (by a factor of 2 to 10) than the corresponding ones originating from EAF-based data [8], with the exception of the ^{238}U (n,2n) reaction. Depending upon the case-specific “one-group cross section-to-density” sensitivity coefficients, this leads to correspondingly smaller uncertainties in final densities.

D.2.4 Uncertainty and sensitivity calculation for the BUC IV-B pin cell benchmark

Results have first been obtained for a simple test case (MOX pin-cell as defined in the OECD/NEANSC Burnup Credit Benchmark Phase IV-B - case #5) [6], chosen as "proof of principle". The calculation scheme as presently set up can be easily modified for more complicated and realistic cases.

As defined in the benchmark specification, the MOX fuel is irradiated over three operating cycles, with a downtime of 30 days between cycles. After discharge at the end of the third cycle a cooling period of 5 years is applied. This cooling period should be kept in mind when analysing the results. Two sets of calculations were performed: one set using 3-group cross section uncertainties from EAF [4], and one set using 15-group cross section uncertainty data from CEA [5] instead, for those reactions for which these data are available.

The following results are available in refs. 7 and 8:

- Relative "density-to-density" sensitivity coefficients, together with the initial and final number densities.
- Relative "one-group cross section-to-density" sensitivity coefficients.
- Relative covariance matrix of the calculated final nuclear density vectors.
- Relative uncertainties in final nuclide densities. It should be noted that the relative uncertainties in the final nuclide densities are equal to the square root of the corresponding diagonal elements of the relative covariance matrix of the calculated final nuclide density vectors. Also it should be noted that the presented uncertainties (covariances) of the final densities are assumed to be caused by uncertainties in cross sections ***ONLY***. The uncertainties in initial densitities, as well as uncertainties or deviations caused by the modelling are assumed to be zero. The effect of uncertainties in initial densities can, however, be taken into account using the “density-to-density” sensitivity coefficients.

As mentioned earlier, the use of cross section uncertainty data from CEA for some of the nuclides may have considerable influence on the calculated uncertainties in the final densities. This is mainly the case for fission products, such as the Nd-isotopes, and for a number of actinides. A more detailed investigation of these differences could be carried out on the basis of the actual values of the cross section uncertainties and the “one-group cross section-to-density” sensitivity matrix. As the “one-group cross section-to-density” sensitivity matrix is virtually independent of the choice of the source of the cross section uncertainty data, the main sources of differences are expected to be the actual library values of the cross section uncertainties, and the assumption that the uncertainties of different energy groups (in the 3-group or 15-group structure) are uncorrelated.

D.2.5 Uncertainty and sensitivity calculation for the Dampierre E09/M09 pin

D.2.5.1 Assembly model

The experiment in the Dampierre reactor has been performed for one MOX assembly surrounded by UOX assemblies. Several pins at different positions in

the assembly and two different enrichments have been analysed by the CEA. The samples have been extracted from the reactor after different number of irradiation cycles, consequently with different final burn-up values.

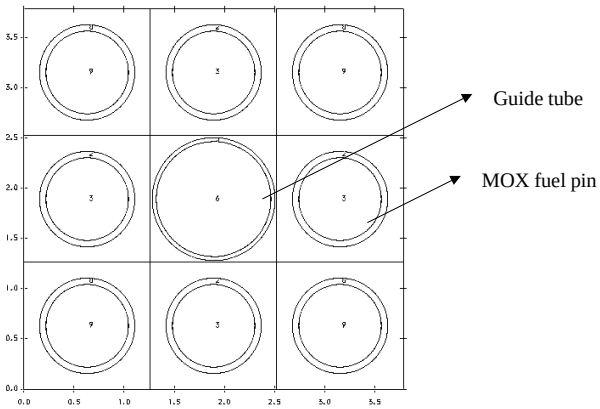

Fig. D.1. Model used for the Dampierre experiment (approximate)

The model implemented in our study approximates the conditions set up for MOX samples with enrichment 6.7%, positioned halway to the edge of the assembly (pins E09 and M09) and extracted from the reactor after four irradiation cycles. The maximum burnup achieved by this sample is about 52 GWd/tHM.

The full supercell model of the MOX assembly and its “environment” was not available to NRG, so a simplified model as pictured in **Fig. D.1**, a 3x3 model with identical fuel pins and a guide tube at the center, has been used. However, this model is considered to be sufficiently accurate for the purpose of error propagation calculations to obtain the uncertainties in final nuclide densities, caused by uncertainties in cross sections. In the model reflective boundary conditions have been assumed.
As mentioned in subsection D.2.3, the calculations are based on EAF uncertainty data [4] complemented with uncertainty data provided by CEA for some reactions of some actinides [5].

D.2.5.2 Results of uncertainty/sensitivity analysis

Detailed results of the calculations for this experiment are given in **Tables D.V to D.VIII** and **Fig. D.2**. The uncertainties in the final nuclide densities, as well as the initial and final vectors are shown in **Table D.V**. We assume that these uncertainties are only attributed to uncertainties in the cross sections. Possible uncertainties in the initial densities were not considered. **Fig. D.2** shows the results in a bar chart. For most of the nuclides the uncertainties are below 10%. The nuclides with the largest uncertainties are U^{233}, Am^{242m} and Cm^{243}. Although the uncertainty for U^{233} is larger than 40 %, its contribution to the final vector is negligible. The uncertainty for Am^{242m} and Cm^{243} is about 20%.

Table D.V. Uncertainties in the final nuclide densities for the Dampierre experiment.

	Nd-initial	Nd-final	dNd-final	∆Nd-final
	[at.m^{-3}]	[at.m^{-3}]	[--]	[at.m^{-3}]
ND146FP		3.670E+25	6.30E-03	2.311E+23
ND148FP		2.175E+25	8.81E-03	1.915E+23
ND150FP		1.264E+25	7.67E-03	9.692E+22
U233		1.283E+19	4.10E-01	5.259E+18
U234	8.067E+23	9.686E+23	1.10E-01	1.065E+23
U235	5.205E+25	2.174E+25	9.35E-03	2.033E+23
U236	4.654E+22	6.126E+24	3.42E-02	2.092E+23
U237		4.485E+22	7.13E-02	3.199E+21
U238	2.127E+28	2.046E+28	4.70E-04	9.608E+24
NP237	4.755E+22	3.426E+24	7.87E-02	2.698E+23
NP239		1.900E+24	1.32E-02	2.517E+22
PU238	1.747E+25	3.106E+25	1.74E-02	5.405E+23
PU239	9.068E+26	3.925E+26	1.40E-02	5.478E+24
PU240	3.656E+26	3.150E+26	1.80E-02	5.659E+24
PU241	1.283E+26	1.884E+26	1.42E-02	2.679E+24
PU242	7.122E+25	1.144E+26	2.36E-02	2.699E+24
AM241	2.841E+25	1.732E+25	2.10E-02	3.637E+23
AM242M		3.339E+23	1.88E-01	6.279E+22
AM243		3.064E+25	3.71E-02	1.137E+24
CM242		5.092E+24	1.10E-02	5.582E+22
CM243		2.744E+23	2.11E-01	5.783E+22
CM244		2.093E+25	4.10E-02	8.571E+23
CM245		2.693E+24	5.60E-02	1.509E+23

Table D.VI shows relative "density-to-density" sensitivity coefficients for all nuclides considered in the analysis. Also mentioned in this table are the initial and final nuclide densities (in atoms per m^3). For each row the values sum up to one.

As an example we can select the case of Cm^{243}, a nuclide absent at the start of the irradiation. For this nuclide, Am^{241} and Pu^{240} give the largest contribution to the uncertainty in the final concentration: about 75% of the total. One notices that a change of 10% in concentration of Am^{241} will result in a 10% $\times$ 0.498 = 4.98% increase in the final concentration of Cm^{243}.
Table D.VII shows the major contributors for the main nuclides of interest.

A Table which is not attached here gives the relative "one-group cross section-to-density" sensitivity coefficients. From this table one can deduce which reactions contribute the most to the uncertainty in the final density of each nuclide. For Am^{243}, for example, the largest contribution is from radiative capture of Pu^{242}, from which the short-lived Pu^{243} ($t_{1/2}$ = 4.956 h) is produced. The isotope Pu^{243} is not modelled explicitly in CASEMATE, and is assumed to decay instantaneously to Am^{243}. The positive coefficient indicates that an increase in this cross section gives rise to an increase in the Am^{243} density.

A closer analysis in conjunction with the uncertainties in cross sections (see **Table D.VIII**) can identify which reactions should be tackled in order to improve the predictions of the final density:

- In the case of **Am^{242m}**, the largest contributions to final uncertainty are from the $Am^{242m}(n,\gamma)$ and $Am^{242m}(n,f)$ reactions. For these reactions no CEA uncertainty data is available.
- In the case of **Cm^{243}**, the $Cm^{242}(n,\gamma)$, $Cm^{243}(n,f)$, and $Cm^{243}(n,\gamma)$ reactions give the largest contributions. Also for these reactions no CEA data is available.

The covariance matrix was established for the final nuclide densities, but it is not attached here. The diagonal terms represent the variance for each nuclide, and the off-diagonal terms the covariance between two nuclides. As this matrix is symmetric,
the elements above the main diagonal have been omitted.

Table D.VII. Relative "density-to-density" sensitivity coefficients for the main nuclides of interest, for the Dampierre experiment.

		Initial					
		U^{238}	Pu^{239}	Pu^{240}	Pu^{241}	Pu^{242}	Am^{241}
Final	Pu^{238}	0.04	-	0.11	0.10		0.38
	Pu^{239}	0.71	0.28	-	-	-	-
	Am^{241}	0.06	0.20	0.36	0.15	-	0.22
	Am^{242m}	0.05	0.18	0.35	0.17	-	0.26
	Cm^{243}	0.17	0.08	0.23	0.18	-	0.50
	Cm^{244}	-	0.04	0.14	0.15	0.64	0.03

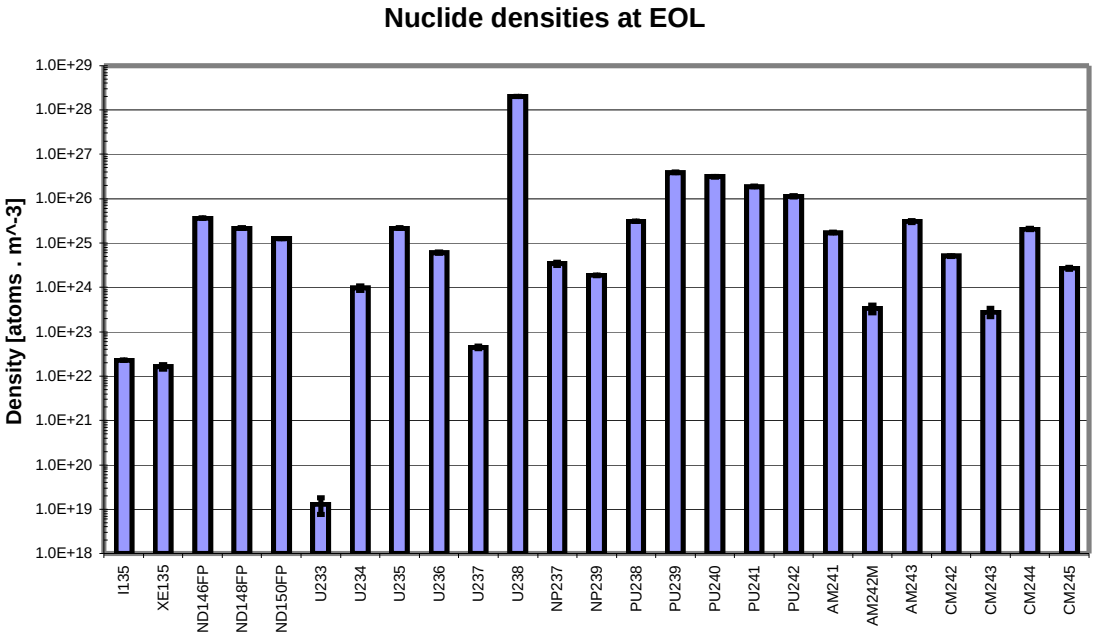

Fig. D.2. Final nuclide densities at the end of irradiation in the Dampierre experiment. Error bars indicate the calculated uncertainties.

Table D.VI. Relative "density-to-density" sensitivity coefficients for the Dampierre experiment. Values smaller than 10^{-4} have been omitted.

	Initial	U234	U235	U236	U238	NP237	PU238	PU239	PU240	PU241	PU242	AM241
Final	Density	8.067E+23	5.205E+25	4.654E+22	2.127E+28	4.755E+22	1.747E+25	9.068E+26	3.656E+26	1.283E+26	7.122E+25	2.841E+25
I135	2.286E+22	1.60E-04	1.45E-02		5.24E-01		4.35E-03	2.75E-01	1.47E-01	2.50E-02	5.07E-03	4.73E-03
XE135	1.626E+22	1.52E-04	1.37E-02		5.34E-01		4.63E-03	2.76E-01	1.38E-01	2.36E-02	5.02E-03	5.08E-03
ND146FP	3.670E+25	1.07E-04	2.22E-02		3.25E-01		2.61E-03	4.61E-01	1.13E-01	7.00E-02	2.45E-03	3.44E-03
ND148FP	2.175E+25		1.82E-02		3.29E-01		2.59E-03	4.53E-01	1.20E-01	7.05E-02	2.84E-03	3.51E-03
ND150FP	1.264E+25		1.20E-02		3.27E-01		2.27E-03	4.51E-01	1.27E-01	7.39E-02	3.21E-03	3.59E-03
U233	1.283E+19	6.31E-01	4.65E-03		4.92E-03	1.83E-04	2.38E-01	2.31E-03	9.57E-03	1.48E-02		9.43E-02
U234	9.686E+23	4.45E-01	6.66E-03		1.19E-02	3.16E-04	2.96E-01	7.25E-03	2.64E-02	3.34E-02		1.73E-01
U235	2.174E+25	1.03E-02	9.82E-01		7.34E-04		3.60E-03	1.16E-03	1.35E-04	2.12E-04		1.37E-03
U236	6.126E+24	4.57E-03	9.68E-01	5.52E-03	2.50E-03		1.05E-03	6.99E-03	1.08E-02			2.75E-04
U237	4.485E+22	1.37E-03	2.93E-01	1.68E-03	6.98E-01		3.12E-04	2.11E-03	3.28E-03			
U238	2.046E+28				1.00E+00							
NP237	3.426E+24	7.14E-04	2.20E-01	2.19E-03	7.68E-01	5.39E-03	1.25E-04	1.26E-03	2.73E-03			
NP239	1.900E+24				1.00E+00							
PU238	3.106E+25		7.78E-03	1.16E-04	4.44E-02	6.58E-04	3.18E-01	3.77E-02	1.11E-01	1.03E-01		3.77E-01
PU239	3.925E+26				7.05E-01		5.83E-03	2.82E-01	8.62E-04	9.88E-04		4.57E-03
PU240	3.150E+26				3.05E-01		2.69E-03	3.99E-01	2.90E-01	5.78E-04	1.78E-03	1.43E-03
PU241	1.884E+26				1.66E-01		1.51E-03	3.51E-01	4.14E-01	6.57E-02	8.51E-04	5.95E-04
PU242	1.144E+26				4.42E-02		4.14E-04	1.52E-01	3.02E-01	1.58E-01	3.21E-01	2.22E-02
AM241	1.732E+25				6.32E-02		5.89E-04	2.02E-01	3.63E-01	1.54E-01	2.86E-04	2.17E-01
AM242M	3.339E+23				4.89E-02		4.59E-04	1.76E-01	3.48E-01	1.67E-01	2.11E-04	2.60E-01
AM243	3.064E+25				1.77E-02		1.68E-04	8.17E-02	2.12E-01	1.63E-01	4.96E-01	2.86E-02
CM242	5.092E+24				3.92E-02		3.70E-04	1.52E-01	3.24E-01	1.75E-01	1.65E-04	3.09E-01
CM243	2.744E+23				1.66E-02		1.58E-04	8.29E-02	2.25E-01	1.77E-01	9.70E-04	4.98E-01
CM244	2.093E+25				6.84E-03			4.07E-02	1.35E-01	1.45E-01	6.42E-01	2.95E-02
CM245	2.693E+24				3.70E-03			2.61E-02	1.01E-01	1.32E-01	7.09E-01	2.84E-02

Table D.VIII. Relative uncertainties (one group) for each of the reactions used, collapsed using the reference spectrum (start of irradiation), for the Dampierre experiment. The data for reactions in red/bold/underlined character are based on CEA uncertainty data.

U233	N,GAMMA	1.17E-01	PU238	N,GAMMA	**1.80E-02**	CM242	N,GAMMA	1.96E-01
U233	FISSION	1.03E-01	PU238	FISSION	3.17E-01	CM242	FISSION	5.03E-01
U233	N,2N	4.00E-01	PU238	N,2N	5.95E-01	CM242	N,2N	4.00E-01
U234	N,GAMMA	2.78E-01	PU239	N,GAMMA	**1.98E-02**	CM243	N,GAMMA	2.45E-01
U234	FISSION	4.81E-01	PU239	FISSION	**8.23E-03**	CM243	FISSION	1.57E-01
U234	N,2N	4.00E-01	PU239	N,2N	1.00E-01	CM243	N,2N	4.00E-01
U235	N,GAMMA	**3.90E-02**	PU240	N,GAMMA	**1.48E-02**	CM244	N,GAMMA	**4.32E-02**
U235	FISSION	**7.09E-03**	PU240	FISSION	4.78E-01	CM244	FISSION	4.12E-01
U235	N,2N	5.00E-02	PU240	N,2N	4.00E-01	CM244	N,2N	4.00E-01
U236	N,GAMMA	**4.18E-02**	PU241	N,GAMMA	**2.75E-02**	CM245	N,GAMMA	**3.34E-02**
U236	FISSION	3.60E-01	PU241	FISSION	**1.04E-02**	CM245	FISSION	**1.98E-02**
U236	N,2N	5.95E-01	PU241	N,2N	4.00E-01	CM245	N,2N	4.00E-01
U237	N,GAMMA	5.59E-01	PU242	N,GAMMA	**4.42E-02**			
U237	FISSION	1.16E+00	PU242	FISSION	4.84E-01			
U237	N,2N	4.00E-01	PU242	N,2N	4.00E-01			
U238	N,GAMMA	**1.37E-02**	AM241	N,GAMMA	**1.97E-02**			
U238	FISSION	**1.77E-02**	AM241	FISSION	3.34E-01			
U238	N,2N	**1.00E-01**	AM241	N,2N	5.00E-02			
NP237	N,GAMMA	**3.38E-02**	AM242M	N,GAMMA	6.54E-01			
NP237	FISSION	4.97E-01	AM242M	FISSION	1.59E-01			
NP237	N,2N	4.94E-01	AM242M	N,2N	4.00E-01			
NP239	N,GAMMA	6.10E-01	AM243	N,GAMMA	**2.99E-02**			
NP239	FISSION	9.64E-01	AM243	FISSION	4.63E-01			
NP239	N,2N	4.00E-01	AM243	N,2N	5.24E-01			

D.2.6 Uncertainty and sensitivity calculation for the Beznau Ariane BM1 pin

D.2.6.1 Assembly model

Within the ARIANE program several MOX samples have been irradiated in the Beznau PWR. For the uncertainty/sensitivity analysis here described the so-called BM1 sample has been selected. The macro assembly model used is pictured in **Fig. D.3**, and is composed of ¾ UOX with 3.4% enrichment and ¼ MOX with 6.01% enrichment. Reflective boundary conditions have been considered. The BM1 sample is located adjacent to a guide tube, and is irradiated to a maximum burn-up of 47 GWd/tHM. The detailed irradiation history of the sample has been taken into account.

The uncertainty/sensitivity analysis has been performed for two points in time: at the end of irradiation (EOL) and after 10000 years of storage in a repository ("Long Storage" - LS). The helium production as result of alpha decay of actinides has also been considered. These results are presented in chapter E.

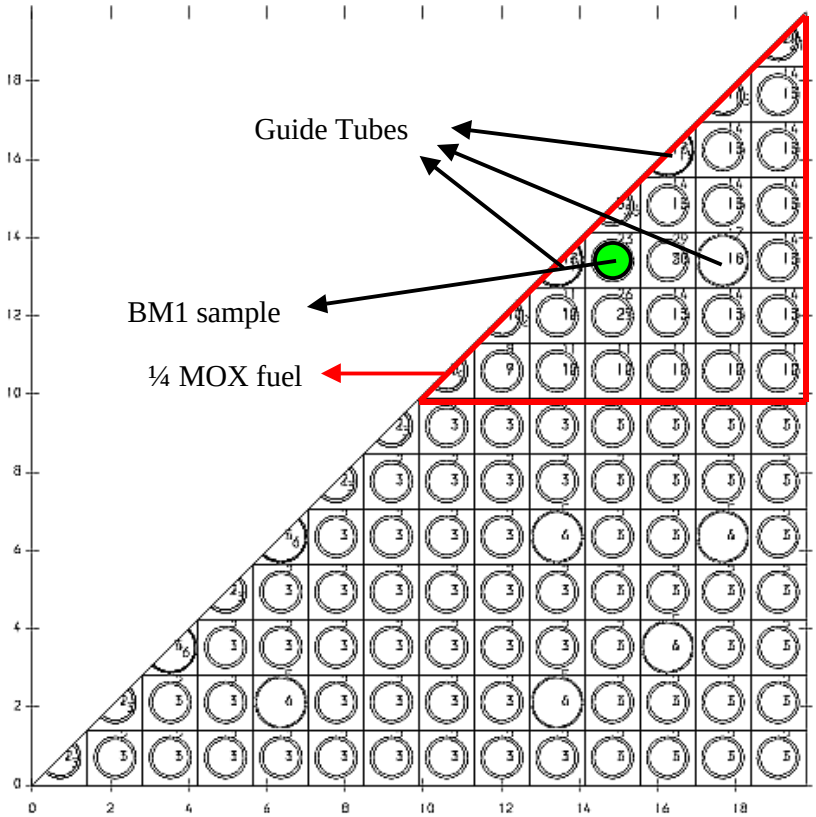

Fig. D.3. Macro assembly model of the Beznau experiment, with ¾ UOX and ¼ MOX fuel.

D.2.6.2 Results of uncertainty/sensitivity analysis at end of irradiation (EoL)

Fig. D.4 shows the nuclide densities (with uncertainties) calculated at the end of irradiation. The results have been compared with those obtained for the Dampierre experiment. Although the maximum burn-up, initial enrichment, and initial vector differ for the two experiments, the results are very similar. In **Table D.IX** the relative density-to-density sensitivity coefficients are shown for the main nuclides of interest.

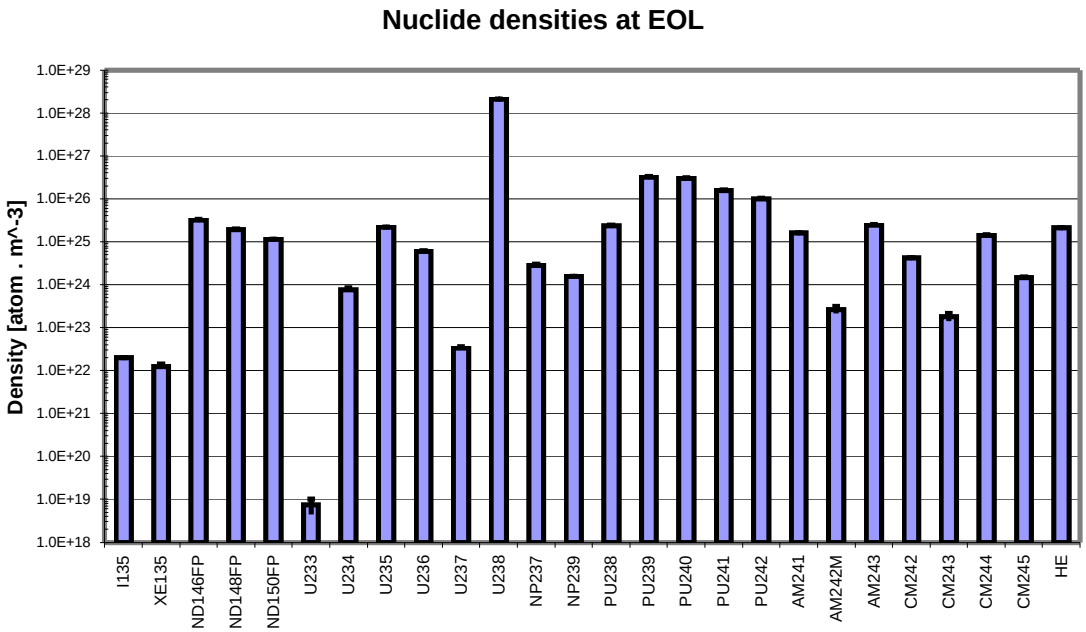

Fig. D.4 Final nuclide densities at the end of irradiation (EOL) for the Beznau Ariane BM1 sample. Error bars indicate the calculated uncertainties.

Table D.IX. Relative "density-to-density" sensitivity coefficients for the main nuclides of interest, for the Beznau Ariane BM1 sample at EOL.

		Initial					
		U^{238}	Pu^{239}	Pu^{240}	Pu^{241}	Pu^{242}	Am^{241}
Final	Pu^{238}	0.04	0.05	0.16	0.18	-	0.24
	Pu^{239}	0.69	0.30	-	-	-	-
	Am^{241}	0.06	0.22	0.39	0.20	-	0.13
	Am^{242m}	0.05	0.19	0.38	0.22	-	0.15
	Cm^{243}	0.02	0.10	0.29	0.28	-	0.30
	Cm^{244}	-	0.04	0.14	0.17	0.62	0.02

Comparison of these results with Table D.VII shows that the main contributors to each of the nuclides are practically the same, although there are some differences in the values. For example the sensitivity coefficients of Cm^{243} and Am^{242m} to the initial concentration of Am^{241} are larger for the Dampierre experiment. The difference can be attributed to the difference in Am^{241} initial concentration of a factor of two.

More detailed information for this experiment can be obtained from the following tables (all available, see [8], but most of which not included here):

- Relative uncertainties in the final nuclide densities (**Table D.X**).
- Relative "density-to-density" sensitivity coefficients, together with the initial and final nuclide densities.
- Relative "one group cross section-to-density" sensitivity coefficients.

The collapsed (one-group) uncertainties for each of the reactions and the relative covariance matrix of the calculated final nuclide densities are quite similar to those found for the Dampierre experiment, and therefore not presented here. The conclusion taken in the previous section regarding the cross sections that most contribute to the uncertainty in the final density of Cm^{243} and Am^{242m} also applies for the BM1 sample. This is because the relative one-group cross section-to-density sensitivity coefficients do not differ much from those for the Dampierre experiment, as well as the collapsed uncertainties.

Table D.X Uncertainties in the final nuclide densities for the Beznau Ariane BM1 sample at EOL.

	Nd-initial	**Nd-final**	**dNd-final**	**∆Nd-final**
	[at.m^{-3}]	[at.m^{-3}]	[--]	[at.m^{-3}]
ND146FP		3.233E+25	5.74E-03	1.856E+23
ND148FP		1.935E+25	7.55E-03	1.461E+23
ND150FP		1.124E+25	6.72E-03	7.557E+22
U233		7.389E+18	4.00E-01	2.953E+18
U234	4.388E+23	7.656E+23	8.55E-02	6.543E+22
U235	5.178E+25	2.167E+25	7.48E-03	1.622E+23
U236	2.175E+23	6.014E+24	2.89E-02	1.739E+23
U237		3.411E+22	7.00E-02	2.387E+21
U238	2.152E+28	2.086E+28	3.72E-04	7.766E+24
NP237		2.801E+24	7.46E-02	2.089E+23
NP239		1.553E+24	1.32E-02	2.055E+22
PU238	1.385E+25	2.379E+25	1.42E-02	3.389E+23
PU239	8.479E+26	3.226E+26	1.38E-02	4.444E+24
PU240	3.221E+26	2.993E+26	1.60E-02	4.780E+24
PU241	1.204E+26	1.574E+26	1.34E-02	2.101E+24
PU242	5.303E+25	9.908E+25	2.13E-02	2.114E+24
AM241	1.438E+25	1.604E+25	1.83E-02	2.937E+23
AM242M		2.624E+23	1.93E-01	5.060E+22
AM243		2.440E+25	3.71E-02	9.054E+23
CM242		4.147E+24	1.01E-02	4.188E+22
CM243		1.775E+23	1.97E-01	3.493E+22
CM244		1.413E+25	4.13E-02	5.838E+23
CM245		1.439E+24	5.66E-02	8.142E+22
HE		2.131E+25	9.89E-03	2.108E+23

D.2.6.3 Results of uncertainty/sensitivity analysis after long storage (LS)

During storage of the discharged fuel the neutron flux is virtually zero, and therefore the only source of error for the determination of the final vector after 10000 years ("Long Storage" - LS) are the uncertainties (covariances) in the initial nuclide densities (i.e. the nuclide densities at the *end* of irradiation). So, the uncertainties/covariances calculated in the previous section are considered here. Uncertainties in the decay constants could also contribute to the final uncertainty, but in our study we assumed that they are negligible.

For the final nuclide densities after long storage, for most nuclides the relative uncertainties remain below or around 5%. Nuclides that show a larger uncertainty are the ones that are short-lived (Pu^{238}, Am^{242m}, Cm^{242}, and Cm^{243}) and therefore have a negligible concentration in the final vector. More detailed information for this calculation can be obtained from the following tables, which are available (see [8]) but have not all been included here:

- Relative uncertainties in the final nuclide densities (**Table D.XI**)
- Relative "density-to-density" sensitivity coefficients, together with the initial (EOL) and final (LS) nuclide densities
- Relative covariance matrix of the calculated final nuclear density vector.

Table D.XI Uncertainties in the final nuclide densities after long storage, for the Beznau Ariane BM1 sample.

	Nd-initial	**Nd-final**	**dNd-final**	**∆Nd-final**
	[at.m^{-3}]	[at.m^{-3}]	[--]	[at.m^{-3}]
ND146FP	3.233E+25	3.233E+25	5.74E-03	1.856E+23
ND148FP	1.935E+25	1.935E+25	7.55E-03	1.461E+23
ND150FP	1.124E+25	1.124E+25	6.72E-03	7.557E+22
U233	7.389E+18	7.072E+18	4.00E-01	2.827E+18
U234	7.656E+23	2.813E+25	1.28E-02	3.599E+23
U235	2.167E+25	1.049E+26	1.07E-02	1.126E+24
U236	6.014E+24	2.103E+26	1.49E-02	3.142E+24
U237	3.411E+22	1.392E-01	1.41E-02	1.958E-03
U238	2.086E+28	2.086E+28	3.72E-04	7.765E+24
NP237	2.801E+24	1.765E+26	1.28E-02	2.257E+24
NP239	1.553E+24	8.341E+18	3.71E-02	3.095E+17
PU238	2.379E+25	6.686E+03	1.38E-01	9.251E+02
PU239	3.226E+26	2.560E+26	1.32E-02	3.368E+24
PU240	2.993E+26	1.091E+26	1.53E-02	1.674E+24
PU241	1.574E+26	1.079E+21	5.66E-02	6.107E+19
PU242	9.908E+25	9.731E+25	2.13E-02	2.075E+24
AM241	1.604E+25	3.415E+22	5.65E-02	1.931E+21
AM242M	2.624E+23	4.248E+03	1.93E-01	8.191E+02
AM243	2.440E+25	9.527E+24	3.71E-02	3.535E+23
CM242	4.147E+24	1.031E+01	1.93E-01	1.988E+00
CM243	1.775E+23	5.689E-24	1.93E-01	1.095E-24
CM244	1.413E+25	3.179E+01	3.71E-02	1.180E+00
CM245	1.439E+24	6.367E+23	5.66E-02	3.602E+22
HE	2.131E+25	5.488E+26	8.30E-03	4.554E+24

D.2.7 General remarks and conclusions

Further details of the calculations presented in the previous subsections are contained in refs. 7 and 8. A comparison of the 1-group uncertainties in the reactions used obtained, for the "BUC IV-B" benchmark, with EAF- and CEA-based data, shows that the values are much smaller for the CEA-based data. The values are obtained under the assumption that the multi-group (3- or 15-group, respectively) uncertainty data are uncorrelated. This explains why the collapsed uncertainties are sometimes smaller than one would expect, based on the 15-groups values of the cross section uncertainties. Especially the uncertainty in the Am^{241} (n,g) cross section is considered to be too small (by at least a factor of two), considering the disagreement found between results of integral and differential measurements [9,10].

According to Santamarina, CEA Cadarache [9], the uncertainty in this reaction in the thermal-energy range (groups 13 up to 15) should be increased to about 5% for all three groups with full correlation between them. Moreover, the uncertainty in capture branching ratio for the production of Am^{242g} and Am^{242m} is substantial (about 30%) and should also be taken into account. These two effects will give rise to an increase in the uncertainty on the nuclide densities for the higher actinides like Cm^{242} and Cm^{243}. Both effects have not been considered so far in our study. On the other hand, the *sensitivity coefficients are independent of the uncertainties,* and therefore they will not be affected by a change in the uncertainties in the cross sections.

A better estimate of the uncertainty can be obtained once full covariance information will be available for the 15-groups uncertainty data, and once a suitable code is operational to perform the collapse of these covariance data to a single energy group, as required for the CASEMATE methodology. This extension of the work should be considered in a follow-up study.

References for Chapter D

Section D.1

1) A. Courcelle, A. Santamarina, F. Bocquet, G. Combes, C. Mounier, G. Willermoz, "JEF2.2 nuclear data adjustment using Post-Irradiation Experiments," International Conference on the Physics of Fuel Cycles and Advanced Nuclear Systems PHYSOR-2004, Chicago, USA, April 25-29 (2004).
2) C. Chabert, A. Santamarina, R. Dorel, D. Biron, C. Poinot, "Qualification of the APOLLO2 assembly code using PWR-UO2 isotopic assays. The importance of irradiation history and thermo-mechanics on fuel inventory prediction," PHYSOR-2000 International Topical Meeting on Advances in Reactor Physics and Mathematics and Computation in the Next Millennium, Pittsburg, USA, May 7-11 (2000).

3) C. Chabert, A. Santamarina, P. Bioux, "Elaboration and experimental validation of the APOLLO2 depletion transport route for PWR Pu Recycling," PHYSOR-2000 International Topical Meeting on Advances in Reactor Physics and Mathematics and Computation, Pittsburg, USA, May 7-11 (2000).
4) A.Santamarina, C. Chabert, A. Courcelle, O. Litaize, G. Willermoz, D. Biron, L. Daudin, "Qualification of the APOLLO2.5/CEA93.V6 code for UOX and MOX fuelled PWRs," Int. Conf. on the Physics of Reactor PHYSOR2002, Seoul, Korea, October 7-10, 2002.
5) A. Courcelle, A. Santamarina, C. Chabert, O. Litaize, "Experimental Validation of U235 evaluations. Recommendations for JEFF3", JEFDOC-862.
6) C. Chabert, A. Santamarina, "Trends in Nuclear Data derived from Integral Experiments in Thermal and Epithermal Reactors," ND2001 International Conference on Nuclear Data, Tsukuba, Japan, September (2001).
7) L.C. Leal, H. Derrien, N.M. Larson, R.Q. Wright, "R-Matrix analysis of U235 neutron transmission and cross section measurements in the 0 to 2.25 keV Range", Nucl. Sci. and Eng. **131**, pp. 230-253 (1999)
8) A. Courcelle, A. Santamarina, O. Litaize, "Experimental Validation of U238 evaluations. Recommendations for JEFF3", JEFDOC-883, Paris, November 19-21, 2001
9) H, Derrien, A. Courcelle, L. Leal, A. Santamarina, "Evaluation of 238U resonance parameters from 0 to 20 KeV," Proc. Int. Conf. On Nuclear Data ND2004, Santa Fe, USA, 26 Sept – 2 oct, 2004.
10) H. Derrien, L.C. Leal and A. Courcelle, A. Santamarina, "Reevaluation and Validation of the ^{241}Pu resonance parameters in the Energy Range Thermal to 20 eV," Nucl. Sci. and Eng., **150**, (2005)
11) D. Bernard, A. Santamarina, O. Litaize, " JEF2.2/JEFF3.0 improvements on spent fuel inventory prediction in LWRs. Trends from integral experiments and proposals for JEFF3.1", JEFDOC-1043, Paris, November 24-26, 2004
12) A. Courcelle, C. Chabert, O. Litaize, B. Roque, A. Santamarina, O. Serot, "Experimental validation of main fission product and actinide nuclear data. Improvements for JEFF," PHYSOR-2002, International Conference on the New Frontiers of Nuclear Technology : Reactor Physics, Safety and High-Performance Comp., Seoul, Korea, October 7-10 (2002).

Section D.2

[1] "WIMS - A Modular Scheme for Neutronics Calculations - User Guide for Version 8", AEA Technology, ANSWERS Software Service, UK, 1999.
[2] J.C. Kuijper *et al*., "Sensitivity and uncertainty assessment associated to burnup calculations", Proc. PHYSOR 2000, Pittsburgh, PA, USA, May 7-12 2000.
[3] R. Klein Meulekamp, note to J.C. Kuijper, "1-groeps FISPACT cross-secties", March 2004, NRG document 20748/04.58291 FAI/RKM/AK, March 2004.
[4] J-Ch. Sublet, J. Kopecky and R.A. Forrest, "The European Activation File: EAF-97 – Cross section library", Report **UKAEA FUS 351**, 1997.
[5] J.C. Kuijper, note to R.P.C. Schram *et al*., "Cross section uncertainty data (1-sigma) from CEA - 28 Oct. 2003", NRG document 20748/04.60349 FAI/JCK/AK, June 2004
[6] P.R. Thorne, G.J. O'Connor & R.L. Bowden, "Problem Specification for the OECD/NEANSC Burnup Credit Benchmark Phase IV-B: Mixed Oxide (MOX) Fuels", Report BNFL Safety & Environmental Risk Management BNFL Risley, Warrington, Cheshire WA3 6AS, United Kingdom, February 2002.

[7] D.F. da Cruz, note to J.C. Kuijper, “VALMOX - uncertainty analysis calculation scheme / Revision 1”, NRG document 20748/04.60352 FAI/DdC/AK, June 2004.
[8] D.F. da Cruz, note to J.C. Kuijper, “VALMOX - uncertainty/sensitivity analysis for Beznau and Dampierre experiments”, NRG document 20748/04.62677 FAI/DdC/AK, September 2004; also contains results of additional calculations on the BUC IV-B” benchmark.
[9] A. Santamarina, CEA Cadarache, private communication.
[10] O. Bouland, “Motivation for new measurements on ^{241,242,243}Am isotopes”, Proc. International Conference on Nuclear Data for Science and Technology "ND2004", September 26 - October 1, 2004.

CHAPTER E

HELIUM PRODUCTION IN MOX FUELS

E.1 Position of the problem

The production of helium is much higher, by an order of magnitude, in spent MOX fuels than in UOX fuels, because of alpha emission from actinide decay. Part of this helium is released from the bulk of oxide fuel in gaseous form, which enhances the pin inner pressure. Such a release occurs during irradiation but may also continue long after the irradiation, during cooling and storage periods. Helium release could thus potentially be a concern with respect to the safe storage of MOX fuels.

On the other hand, the production of gaseous fission products like Xe and Kr isotopes is about the same for MOX and UOX fuels at the same burn-up.

Helium migration, absorption and release are not considered here. They are complex processes, depending on fuel characteristics, temperature, microscopic structure, porosity, irradiation history, etc. The relationship between helium production and helium release is studied elsewhere. The VALMOX project focuses only on helium source terms. One of the objectives of the project was to determine the accuracy of calculated helium production in spent MOX fuels as a function of storage time after irradiation.

E.2 Calculation of helium production

The helium production was calculated at BN using a coupling of the code packages WIMS8 [12]and ORIGEN2 [1] and the JEF2.2 data file. After each burn-up step, one-group actinides cross-sections were transferred from WIMS8 to ORIGEN2, which has the advantage of a larger set of actinides than WIMS, with explicit chains and a number of fission products ; it also easily treats periods of non-irradiation like cooling and storage, during which unstable isotopes decay.This coupling allows one to calculate the helium build-up for different storage times after irradiation.

At CEA, the helium production is calculated by the fuel cycle code CESAR [2].

At End of Life (Bu=50 Gwd/t) of a MOX assembly the Helium production corresponds to 2.9 10^{24} atoms by Ton of initial Heavy Metal in a ORIGEN2 calculation, and 3.1 10^{24} atoms/THMi in a CESAR calculation.
This code calculations supply the 3 components of Helium production :

- 65% from α decay of transactinides
- 25% from (n, α) reactions in the oxygen of the fuel
- 10% from ternary fissions

[12] See reference to WIMS8 in Chapters A and B

Fig. E.1 shows a typical evolution of helium build-up during assembly cooling.

Fig . E.1 also shows the evolution over 10,000 years of the major contributors to the helium production along the following a-decay chains :
Cm242 ? Pu238, half-life : 163 days
Cm244 ? Pu240, half-life : 18.5 years
Pu238 ? U234, half-life : 84 years
Am241 ? Np237, half-life : 433 years
Pu240 ? U236, half-life : 6563 years.

Other less important chains are :
Cm243 ? Pu239, half-life : 29.1 years
Pu239 ? U235, half-life : 24,110 years.

The role of the ß-emitter Pu241 which decays to Am241 is also important with its half-life of 14.4 years.

Fig. E.1
Typical helium build-up with identification of the concentration of the major precursors

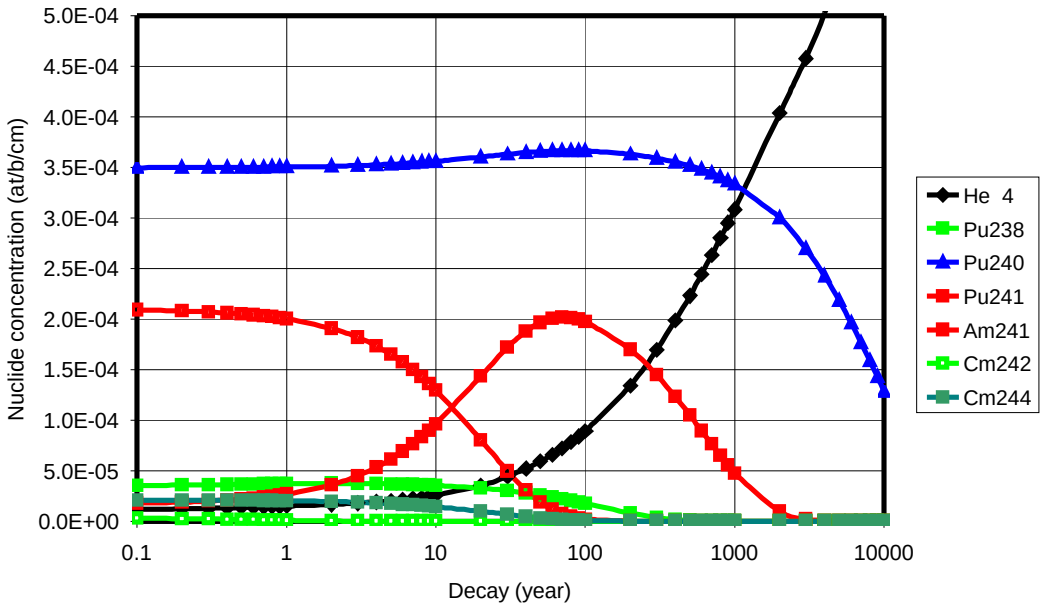

While periods of 1,000 to 100,000 years and more are of concern for underground waste repositories, periods of 1 to 100 years will rather be considered here, as they correspond to possible intermediate storage times.

Fig. E.2 shows the evolution of helium build-up over this time range, for a typical MOX sample irradiated up to 50 GWd/t. The major contributions are explicitly indicated. For the decay chains, a distinction is made between the mother and the daughter isotope at EoL. For example, Pu238 existing at EoL is considered separately from Pu238 progressively formed from decaying Cm242. This is also

done for Pu240 and for Am241. One will see below that the ß-decaying Pu241 will play an important role as it forms much Am241.

Fig. E.2
Typical helium build-up with major contributions during cooling

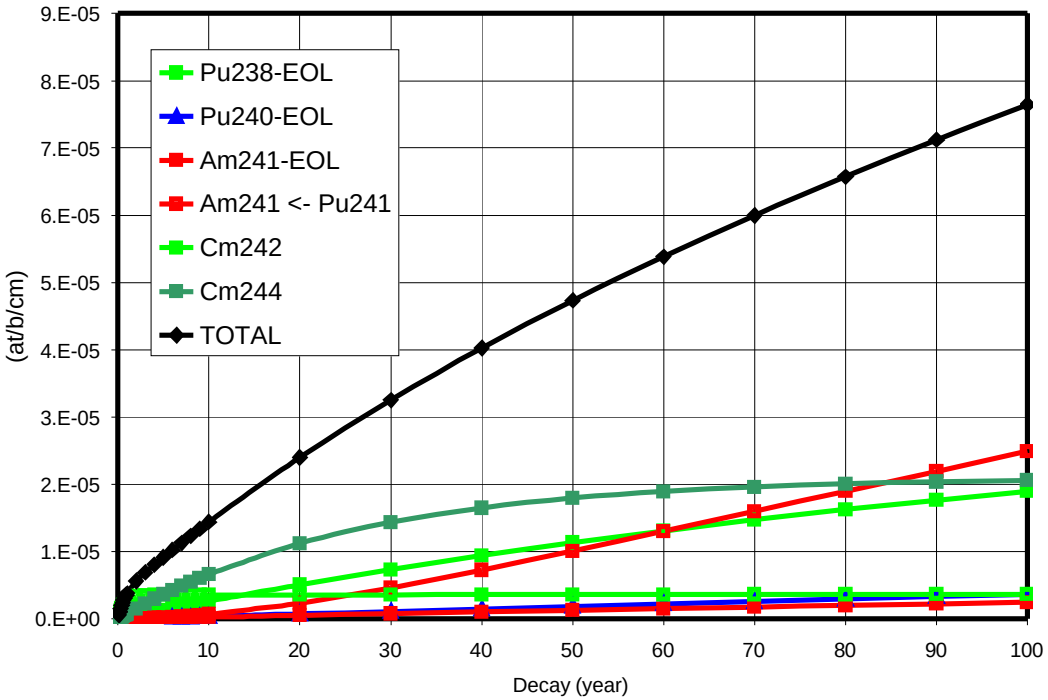

The list and ranking of the main contributors to this helium build-up changes considerably as time passes. **Table E-I** gives the contributions in % for different storage times.

Table E-I
Sources of Helium Production [13] for Storage Times of 1 to 1000 Years

Sources	Contributions in % after storage times in years :				
	0 (EoL)	1	10	100	1000
Cm242	80.0	49.8	0.2	-	-
Cm244	14.0	33.8	41.3	0.1	-
Pu238 – EoL	4.8	12.0	26.0	15.1	-
Pu238 ← Cm242	-	0.9	2.6	1.7	-
Pu240 – EoL	0.6	1.6	4.1	9.7	63.3
Pu240 ← Cm244	-	-	0.1	0.6	3.8
Am241 – EoL	0.5	1.2	2.9	5.2	2.3
Am241 ← Pu241	-	0.7	22.7	67.4	30.2

[13] instantaneous production rate

One may already infer from the values of this Table that the accuracy of prediction of helium depends primarily of that of :

Cm242 at EoL
Cm242 and Cm244, 1 year later
Cm244 and Pu238, 10 years later
Pu241 after 100 years
Pu240 after 1000 years.

Table E-II gives the major contributions in % to the build-up of helium during assembly cooling, i.e. the integration over time of the helium production rates.

Table E-II
Sources of Helium Build-up for Storage Times of 1 to 1000 Years

Sources	Contributions in % after storage times in years :				
	0 (EoL)	1	10	100	1000
Cm242	80.0	70.1	14.9	3.1	1.1
Cm244	14.0	20.5	46.8	17.8	6.0
Pu238 – EoL	4.8	7.1	21.1	23.2	9.8
Pu238 ← Cm242	-	0.4	2.0	2.4	1.1
Pu240 – EoL	0.6	1.0	3.1	6.1	18.5
Pu240 ← Cm244	-	-	0.1	0.3	1.1
Am241 – EoL	0.5	0.7	2.2	3.8	4.6
Am241 ← Pu241	-	0.2	9.8	43.3	57.8

E.3 A priori uncertainty in helium production from propagation of nuclear data uncertainties

Before using any results of the evaluations of high burn-up MOX fuels described in Chapters B and C, one may deduce the uncertainty of helium production from that of the basic cross-sections of actinides as follows. Employing the NRG methodology, described in section D.2 based on WIMS8-CASEMATE, the helium build-up has been calculated, for the Beznau BM1 sample, during fuel irradiation and during fuel storage in a repository (for 10,000 years), as well as the uncertainty in its final concentration. In fact, this information was generated as part of the calculations on the Beznau sample, as described in subsection D.2.6 and the corresponding tables. In the remainder of this section the specific results concerning helium (α-decay component) will be discussed.

Table E.III presents the build-up of helium at the end of irradiation ("EOL") and after long (10,000 years) storage ("LS"), calculated as result of alpha decay of actinides, as well as its uncertainty.[14] Since the burnup module of WIMS does not keep track of the helium production, the procedure has been set up entirely in CASEMATE.

The major contributors to the helium production can be seen from **Fig. E.3**, which shows in a pie chart the "density-to-density" sensitivity coefficients for He at both points in time. Although the major contributors are practically the same both during irradiation and during storage, their relative contributions are different, especially for Am^{241}. During the fuel irradiation relative short-lived curium isotopes are produced by radiative neutron capture of Am^{241}.

From these charts one can conclude that plutonium represents the largest source of helium, especially in the spent fuel. The evolution of the nuclide density of helium and the most important nuclides during cooling was depicted above in Fig. E.1.

Table E.III. Helium build-up (and relative uncertainty) at the end of irradiation (EOL) and at the end of 10000 years storage (LS).

	$N\ [b^{-1}cm^{-1}]$	ΔN
EOL	2.131E-05	1.0%
LS	5.488E-04	0.8%

One notices that uncertainty in the final helium concentration is quite small, and for the 'long storage" case even smaller than the uncertainty in the initial concentrations (at EOL) of the most relevant nuclides for helium production. This peculiarity can be attributed to the covariance data, which is automatically taken into account in the calculations: negative correlations between uncertainties in densities at EOC lead to smaller uncertainties after long storage.

[14] Units in at/b.cm equivalent to 10^{24} at/cm^3

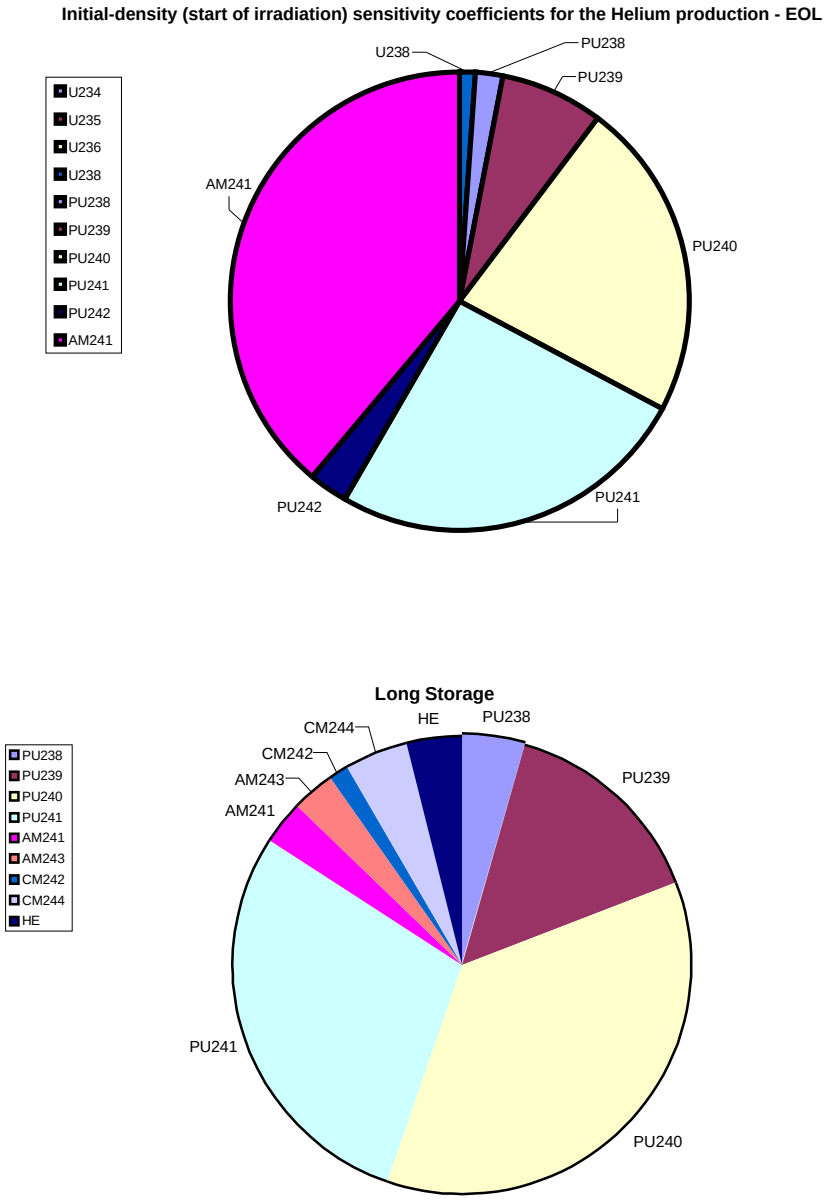

Fig. E.3. "Density-to-density" sensitivity coefficients for He production at the end of irradiation (EOL) and after 10,000 year of storage (LS) :
Above: influence of irradiation - Below: influence of 10,000-year storage.

In these calculations the helium production during irradiation as result of (n,α)-reactions or ternary fissions was not covered. Therefore, the calculated 1% uncertainty corresponds to the α-decay component only ; but this component becomes dominant for the total helium build-up after 30 years cooling.

E.4 Accuracy of the JEF2 prediction of helium production and build-up (α-decay component)

As illustrated in Fig. E.2 and Table E.I, the accuracy of helium production calculations is given by a combination of the errors in the prediction of its main sources.

E.4.1 Accuracy of WIM8 prediction

From Chapter B one may retain the following source uncertainties, see **Table E.IV** below.

Table E.IV
Helium sources : bias factors and uncertainties (WIMS8/JEF2.2 basis)

Sources	Bias factors	Uncertainties (1s in %)
Cm242	0.97	5
Cm244	0.86	5
Pu238	0.92	4
Pu240	1.02	1
Am241	1.20	4
Pu241	1.00	1

For storage times of 0 (EoL), 1 yr, 10 yr, 100 yr and 1000 yr, the combination of the information from Tables E.I, E.II and E.IV allows to deduce the bias factors and uncertainties for helium production and build-up in MOX fuels : see **Table E.V** below.

Table E.V
Helium production and build-up :
bias factors and uncertainties (1s) for different storage times

Storage times (years)	1	10	100	1000
Production	0.93 ± 0.04	0.94 ± 0.03	1.00 ± 0.02	1.01± 0.01
Build-up	0.94 ± 0.04	0.94 ± 0.04	0.96 ± 0.03	1.00 ± 0.02

One observes the following :

- after short storage times of 1 to 10 years, as the helium production is dominated by the curium isotopes Cm242 and 244, and Pu238, which are all underestimated by WIMS calculations, the helium production itself is obviously

underestimated too, and its uncertainty is of the order of 4% ; the same trend affects helium build-up ;

- after longer storage times, like 100 and 1000 years, the helium production is dominated by the sources Pu240 and 241 and is very well predicted in the same manner as these isotopes.

Therefore, the helium build-up is underestimated by 6% at EoL and up to 10 yr cooling, and is very well predicted at longer term.

E.4.2 Accuracy of APOLLO2 prediction

The same type of calculations was done using the APOLLO2 code package at CEA.[15]
The major sources of helium production were exactly the same. Their relative importance varied much with storage time, too.

Table E.VI shows the bias factors and uncertainties obtained by APOLLO2 calculations and the JEF2.2 data file in Chapter C, for samples irradiated up to 53 GWd/t.

Table E.VI
Main helium sources : bias factors and uncertainties (APOLLO2/JEF2.2 basis)

Sources	Bias factors	Uncertainties (1s in %)
Cm242	0.96	4
Cm244	0.95	3
Pu238	0.98	2
Pu240	1.01	1
Am241	1.16	4
Pu241	1.00	1

Again, from the information collected in the above Tables it is easy to deduce the bias factors and uncertainties for the helium production and the helium build-up calculated after different storage times. This is given in the following **Table E.VII**.

[15] See reference in Chapter A or Chapter C.

Table E.VII
Helium production and build-up:
bias factors and uncertainties (1s) for different storage times

Storage times (years)	1	10	100	1000
Production Build-up	0.96 ± 0.04 0.96 ± 0.04	0.97 ± 0.03 0.97 ± 0.03	1.00 ± 0.02 0.99 ± 0.02	1.00± 0.01 1.00 ± 0.01

The observations are similar to those made for the WIMS8 results :

- after short storage times of 1 to 10 years, the helium production is dominated by the curium isotopes Cm242 and 244, and Pu238, which are all underestimated, and the helium production itself is underestimated by 3 to 4%;
- after longer storage times, like 100 and 1000 years, the helium production is dominated by the Pu240 and 241 sources and is very well predicted in the same manner as these isotopes.

One notes that the uncertainty is 4% (1 sigma) at EoL, significantly more than the 1% deduced from cross-section sensitivity analyses of Section E.3 above. The small, theoretical 1% value is to be understood as a target. The values of this Table VII are to be retained as they result from the PIE work presented in this report. For long storage times, these values precisely tend to 1%.

E.5 JEF2 bias and associated uncertainty on the total helium build-up

Concerning the α-decay component of helium build-up, which is the major one (65% at EoL, 90% after 10 yr, 98% after 100 yr), the previous section has pointed out similar trends in WIMS8-Beznau and APOLLO2-Dampierre2 analyses. For APOLLO2/Dampierre it was predicted within : -4% ± 4% (1s) at EoL, -3% ± 3% for cooling time T≈10 years, -1% ± 2% for cooling time T≈100 years and 0 ± 2% for T˜1000 years.

Concerning the (n,α) component linked to assembly irradiation, the main contribution is due to the ^{16}O isotope in the oxide fuel : the average value in a MOX spectrum amounts to $s_{n,\alpha}$ = 6.07 mb (to compare to $s_{n,\alpha}$ = 0.02 mb for ^{17}O, i.e a 10^{-6} negligible contribution). Therefore, the uncertainty in the (n,α) component is essentially determined by the uncertainty in the O^{16} $s_{n,\alpha}$ cross section : ±20% (1s) deduced from the comparison of various evaluations (JEF2.2, ENDFB/VI, JENDL3.2,…) [3].

In the fission process, the two heavy fragments are accompanied by a light charged particle, about three to four times every thousand events. Therefore, ternary fission constitutes a source of helium and tritium gas production during reactor operation : 10% of the helium build-up at the MOX assembly EoL. A recent study [4], performed

in the JEFF3 framework, proposed the following ternary ^{4}He yields for adoption in JEFF3.1 (compared to the UKFY3.4 English one) :

$^{239}Pu(n_{th},f)$ (in 10^{-3})	2.19 ± 0.09 (JEFF3.1)	2.08 ± 0.10 (UKFY3.4)
$^{241}Pu(n_{th},f)$ (in 10^{-3})	1.86 ± 0.07 (JEFF3.1)	2.01 ± 0.29 (UKFY3.4)

These values show that the uncertainty in ternary fission rate in plutonium amounts to ±5% (1s).

Accounting each component of the helium build-up (i.e 65% α-decay 25% (n,α) and 10% ternary fission at Eol), we obtain the biases and associated uncertainties (1s) to apply to JEF2 calculations of total helium build-up as given in the following **Table E.VIII.**

The two components from (n,a) reactions and ternary fissions which are important at EoL become less and less important as the storage time increases : after 100 years they just represent 1.3% of the total.
It is not possible to infer from the PIE analyses discussed in this report whether there is a bias between calculation and reality; therefore the more probable value C/E=1. was used.

These values correspond to APOLLO2 calculations. For WIMS8 results the trends are similar, as already shown in Table E.V above ; the degree of underestimation is more pronounced, however.

Table E.VIII
Total helium build-up : bias factors and uncertainties (1s)

Storage times (years)	0 (EoL)	10	100	1000
Build-up	-3 ± 6 %	-2 ± 4 %	-1 ± 2 %	0 ± 1 %

E.6 JEFF3.0 trends on helium production and build-up

Chapter C has showed the effects of using the working library JEFF3.0 instead of JEF2.2. According to the results found, one may note that there was practically no influence for what concerns Pu238, Pu240 and Pu241, thus the prediction of helium production after 100 or 1000 years (or more) is not changed : it remains excellent.

The prediction of Cm244 was improved : the bias for samples irradiated at 53 GWd/t changed from 0.95 to 0.97 (for samples irradiated up to 60 GWd/t it was even 0.99 ± .04). This improvement, due to the changes brought to the capture cross-section of Pu241, also affects the prediction of helium production after 10 or 20 years storage and improves it.

E.7 Note on helium release

Ref. [5] gives some information on the fraction of helium released, mentioned here. Measurements on BWR rods are interesting in the sense that these rods had been only weakly pressurised with helium at fabrication ; while the fraction of fission gas Xe and Kr released was about 15%, the fraction of helium released varied from 45 to 60%, i.e. that it was 3 to 4 times larger. In absolute terms the total fission gas volume after 45 GWd/t is about 10 times larger than the helium gas volume produced, and the Kr+Xe gas release amounts to 3-4 times the helium volume.
Helium release depends on a lot of factors like fuel temperature and rod inner pressure. In fact, helium is more easily released than fission gas (6), owing to higher solubility and diffusion rate. But the net helium balance at EoL is also depending on the initial pin pre-pressurisation, as this pre-pressurisation promotes helium infusion and diminishes the net pin innner pressure increase.
A series of pins irradiated in the SLB1 PWR were punctured about 2 years after end of irradiation. These pins were the same as those considered in Chapter C. Initially, at fabrication and before closing the cladding tubes, they had been filled with helium gas at 26 bar. No helium release could be observed [7].
This conclusion was confirmed by the recent CEA studies on MOX-MIMAS fuels made at Belgonucléaire : for fuel pins irradiated 1, 2, 3 or 4 cycles, the measured helium volume at EoL was lower than the initial volume ; for 5-cycle fuel pins a slight increase of helium volume was observed (within the experimental uncertainty bar) [8].

REFERENCES

[1] User's Manual for the ORIGEN2 Computer Code, by A.G. Croff, ORNL-TM-7175, April 1980

[2] M. Samson and al., "CESAR : A simplified evolution code for reprocessing applications", RECOD' 98, 25-28 October 1998, Nice (France)

[3] A. Courcelle, A. Santamarina, C. Chabert, O. Litaize, JEFDOC-883, JEFF Meeting, 19-21 November 2001, Paris

[4] O. Serot, C. Wagemans, J. Heyse, "New results on Helium and Tritium Gas Production from Ternary Fission", Int. Conf. On Nuclear Data ND2004, Santa Fe (USA)

[5] La production et le relâchement d'hélium dans un crayon combustible de type MOX, Belgonucléaire report 9601480/220 A, by D. Freson and M. Lippens, July 1996

[6] C. Ronchi, J.P. Hiernaut, "Helium diffusion in uranium and plutonium oxides", Journal of Nuclear Materials, 325, p 1 (2004)

[7] P. Blanpain, X. Thibault, J.P. Pages, "Recent studies from the in reactor MOX fuel performance in France", Int. Top. Meeting on LWR Fuel Performance, Portland (USA), 1997

[8] Y. Guerrin, C. Struzik, "Synthèse sur le comportement en réacteur du combustible MOX", CEA Report NT DEC SESC/LIPA 02-011.

CHAPTER F

FINAL ASSESSMENT AND CONCLUSIONS

F.1 Main results with JEF2.2

The main results from the evaluations of MOX fuel irradiation in LWRs made at BN, SCK and CEA using JEF2.2 basic data are shown in Table F.I.

Table F.I

MOX Fuel Irradiated in LWRs (central zone)
Main results obtained with JEF2.2 data
C/E Ratios for Pu, Am and Cm Isotope Masses

Isotopes	Beznau-BM1[16] WIMS8	Beznau-BM1[17] ALEPH	SLB1[18] APOLLO2	Dampierre[19] APOLLO2
Pu238	0.92	0.94	0.93	0.99 ± 0.02[20]
Pu239	1.07	0.99	1.03	1.05 ± 0.02
Pu240	1.02	1.02	1.01	1.02 ± 0.01
Pu241	1.00	0.99	0.98	1.01 ± 0.01
Pu242	0.98	0.98	0.96	0.99 ± 0.01
Am241 EoL	1.23	1.20	1.00	1.17 ± 0.04
Am242m	0.69	0.74	0.75	0.81 ± 0.03
Am243	0.95	1.00	0.93	1.02 ± 0.02
Cm243	0.77	0.77	0.78	0.89 ± 0.02
Cm244	0.86	0.88	0.93	0.96 ± 0.03
Cm245	0.86	0.92	0.91	1.01 ± 0.04

[16] BM-1 sample, 45 GWd/t, 21 groups, see Table B.IV
[17] BM-1 sample, 45 GWd/t, see Table B.VI
[18] SLB1, average values, 45 GWd/t, see Table C.IV
[19] Dampierre, 60 GWd/t, see Table C.VII
[20] Experimental uncertainty in one standard deviation

The results corresponding to 45 GWd/t obtained with 3 code packages can directly be compared with one another, taking also into account the basic methods comparison made in Chapter A for the benchmark case (48 GWd/t).

There is a generally good consistency, except for Am241 in SLB1 : the C/E values, practically unity, are not in line with the overestimation pointed out in other results. Part of this discrepancy is associated with the Pu241 underestimation observed in SLB1. Parallel investigations suggest that the SLB1 result for Am241 should be discarded.

The general consistency was already shown on the benchmark case in Chapter A, which aimed at the validation of the methods. APOLLO2 was shown to be an excellent basis for design calculations, as its results were well confirmed by the ALEPH Monte Carlo method. WIMS8 also provides a good design basis but because of some approximations Pu239 is less accurate.

It is therefore not surprising that in Table F.I ALEPH and APOLLO2 results are in good agreement for all quoted isotopes, except for Pu239 (observed bias between Beznau and SLB1 : 4% $\pm$ 3%), for Am243 and Cm244.
WIMS8 results are also generally close to APOLLO2, except for Pu239 which is calculated systematically higher by 4%. This deviation seems to be attributable to slight deficiencies in resonance treatment of U238 captures in WIMS8. Differences do also exist for Am242m, Cm244 and Cm245, all being largely underestimated by WIMS8.

The effect of increasing the burn-up from about 50 to 60 GWd/t was commented in Chapter C. It is small for most isotopes, with the important exception of Pu239, for which the C/E ratio becomes slightly larger : from 1.03 to 1.05. The C/E ratio for Pu241 also increases by 1%.

F.2 Main results with JEFF3.0

Results for the same cases were also obtained with ALEPH and APOLLO2 using the newly available JEFF3.0 library.
The main changes in actinide cross-sections made from JEF2.2 to JEFF3.0 were :

- U235 resonant capture increase;
- Pu241 epithermal capture increase;
- U238 (n,2n) increase by +10%.

Table F.II shows the main results with JEFF3.0. Only APOLLO2 results are shown here, which is sufficient as APOLLO2 results were checked to be reliable, well backed by the Monte Carlo code ALEPH.[21] They correspond to the high burn-up value of 60 GWd/t.

[21] Except for Pu239

Table F.II

MOX Fuel Irradiated in LWRs (central zone)
Main results obtained with JEFF3.0 data
C/E Ratios for Pu, Am and Cm Isotope Masses

Isotopes	Dampierre APOLLO2[22]
Pu238	0.99 ± 0.02
Pu239	1.05 ± 0.02
Pu240	1.03 ± 0.01
Pu241	1.02 ± 0.01
Pu242	1.03 ± 0.01
Am241 EoL	1.17 ± 0.04
Am242m	0.80 ± 0.03
Am243	1.05 ± 0.02
Cm243	0.84 ± 0.02
Cm244	0.99 ± 0.03
Cm245	1.10 ± 0.04

As commented in Chapter C, the changes from using JEF2.2 to JEFF3.0 are logical as they are a consequence of the changes brought to the basic cross-sections : for example, the prediction in Pu242, Am243 and Cm244 contents was affected by the increase of Pu241 capture cross-sections. The changes brought to the nuclear data of Pu239 and Pu240 were small, hence little difference is seen in the code predictions for these nuclides.

F.3 Recommendations of changes in the JEFF3 file

Mainly two actions on cross-sections deserve to be undertaken, in order to improve the prediction of Pu239 and Am241 concentrations, which are still largely overestimated in JEFF3.0 calculations.

[22] Dampierre, 60 GWd/t, see Table C.VII

The precise recommendations for the JEFF3.1 evaluations are the following :

- To decrease by 1% the ^{238}U resonance integral, in order to lower by 1% the Pu239 content at 45 Gwd/t.
- To increase by +15% the $^{241}Am(n,\gamma)$ capture cross-section in the [0 – 1.5 eV] thermal and epithermal range.

In addition, the prediction of the build-up in Cm245 and Cm246 would be improved by the adoption of the recent JENDL3.3 evaluation of ^{245}Cm.

F.4 Conclusions concerning the helium build-up

Chapter E was devoted to the prediction of helium build-up during the storage time which follows the irradiation. The various sources of this build-up were evaluated.

At fuel discharge (EoL) and in the 10 following years, the dominant sources are the a-decay of Cm242, Cm244 and Pu238, and the (n,a) reactions in oxygen ; as the 3 quoted isotopes are underestimated by calculation, the helium build-up is also underestimated by calculation ; the uncertainty in the prediction reaches ± 6% (1s) at EoL and ± 4% for 10 years storage.

For longer storage times, the prediction progressively improves and becomes excellent : after 100 years, the helium build-up is rightly predicted with an uncertainty of ± 2% (1s), which tends to ±1% at longer term (1000, 10000 years).
This is due to the fact that the dominant sources of a-radiations are then the decay of the plutonium isotopes Pu240 and Pu241, and these isotopes are well predicted.

When the corrections to cross-sections recommended here for the JEFF3.1 data file will be done, the underestimation of the helium build-up prediction at short term will be reduced and the prediction will remain excellent at long term.

APPENDIX to CHAPTER A

Validation of Computer Codes for MOX Calculations

Codes and calculation schemes

1. APOLLO2

1.1 APOLLO2 methodology

The APOLLO2 code performs direct or adjoint transport calculations with a fixed source or for a critical parameter. External iterations on the spatial distribution source and the eigenvalue are accelerated by Chebyshev method. Upscattering is accounted for by thermal iterations, which are accelerated through group-constant rebalancing factors together with a rest minimization technique.

A first solver corresponding to the solution of the integral transport equation by the Collision Probability method is implemented. 1D and 2D geometries are available; the XY solver works on a basic regular mesh, but allows for several levels of local mesh refinement and for elementary square or rectangular cells with sectorized internal circles. A recent improvement was brought by the TDT module which performs interface-current transport calculations of unstructured XY geometries [**1**]. The TDT module has been generalized to treat 3D geometries generated by axial translation of a 2D unstructured motif. The GUI Silene is used to create TDT geometries that are made out of homogeneous cells whose perimeters are composed by straight segments, arcs or circles.

The double-heterogeneity problem, encountered in HTR bundles and LWR Gd fuel rods, is handled through an independent treatment of each type of grain and the replacement of the stochastic medium by a homogeneous medium.

Recently, a Method Of Characteristics was developed with an efficient synthetic acceleration.
From the beginning, the integro-differential equation can be solved using a 1D or 2D discrete-ordinates module accelerated by the DSA technique. A 2D linear-linear nodal S_N method, with Boundary Projection Acceleration, was added to this module. The multidimensional discrete ordinates code IDT, that uses nodal and characteristics methods for the discretization of the spatial variable on regular 2D and 3D Cartesian meshes, was developed and recently implemented in APOLLO2 [**2**].

Concerning resonance reaction rate calculation, a powerful space-dependent self-shielding based on the French “Background Matrix” method [**3**] is implemented; in Version 5 of APOLLO2, a more efficient quadrature technique for the homogeneous/heterogeneous equivalence is available, based on Probability Tables. Furthermore, a model based on the subgroup method is also available.
The development of the APOLLO2.5 industrial code was achieved within Quality Assurance process. Therefore, a rigorous methodology of Verification–Validation–Qualification was developed and applied [**4**].

1.2 The Verification/Validation/Qualification process

The first step of this process verifies that numerical models and programming of each module are correct; this Verification is also based on the Test Machine which avoids non-regression in the new APOLLO2 Version.

The second step corresponds to the Validation of the APOLLO2 functionalities (Pij, resonance self-shielding, fine flux, depletion, accurate SPH homogenization, Sn, etc.) as well as the 'CEA-97' reference calculation route. This Validation is based on the comparison of APOLLO2.5/CEA-97 calculation results against continuous-energy Monte Carlo TRIPOLI4 reference calculation. Both calculations use the same nuclear data JEF2.2. This Validation enables also the "calibration" of the recommended CEA-97 Reference route : the calculation bias is determined for each LWR design parameter. This validation process is automated through the MACH2 Machine.

The Qualification is the third step, corresponding to the comparison of the results of the global package (code + ref. Calc. route + data library, i.e APOLLO2.5/CEA-97/CEA93.V6) against experimental results from integral measurements : see **Table App.A.I.**

1.3 The MACH2 Validation Machine

The Validation process is based on the benchmark concept. A simplified geometry, representative of the LWR calculation challenge, is defined in order to check the APOLLO2 deterministic route against reference calculation results, generally obtained from the TRIPOLI4 [**5**] 3D continuous-energy Monte Carlo code.

Table App.A.I The PWR benchmarks in MACH2 for APOLLO2 validation

Benchmarks	Functionalities	Main Reaction rates	PWR parameters
UOX lattice (fresh fuel)	Pij, self-shielding	U235, U238	Keff
UOX lattice 40GWj/t	Pij, self-shielding	U235, U236, Np237, Pu, Am	Keff, reactivity loss with burnup
MOX 7%Pu lattice	Pij, self-shielding	U, Pu, Am241	Keff
URE reprocessed-U lattice	Pij, self-shielding	U236, U234	Keff
Evolution UOX	Evolution	Actinide concentrations vs Bu	fuel inventory, cycle length
UOX 17x17 assembly	Pij, self-shielding, Sn	abs.+fission radial distribution	pin-by-pin power map
MOX assembly + Mixed core	Pij, self-shielding, Sn	abs.+fission radial distribution	UOX/MOX interface, zoning, power
UO2-Gd2O3 burnable poison	Evolution	Concentration Gd, U235, Pu239	poison worth and reactivity loss vs Bu
B4C isolated absorber	Pij, Equivalence, Sn	absorber capt. rates, fission map	absorber worth, pin-by-pin power map
Stainless-steel rod	Pij, self-shielding, Sn	$\Delta\rho$, Fe56, Ni58, Cr52, Mn55	absorber worth, pin-by-pin power map
UOX assembly - 24 B4C cluster	Pij, Equivalence, Sn	abs.+fission radial distribution	CRC worth, pin-by-pin power map
MOX assembly -24 B4C cluster	Pij, Equivalence, Sn	abs.+fission radial distribution	CRC worth, pin-by-pin power map

Main capture and fission rates (Table App.A.I - 3rd column) are validated on a 13-macrogroup output. This validation is automatically repeated in MACH2 for the various options of the APOLLO2 modules (main functionalities given in 2nd column), including the "CEA-97" scheme. Furthermore, phenomenological neutron balance is also carried out through a "six factor" breakdown of the K_8 and printed out on the validation report, as shown in **Table App.A.II**.

Table App.A.II APOLLO2.5 Validation Report issued by MACH2 (UOX lattice benchmark)

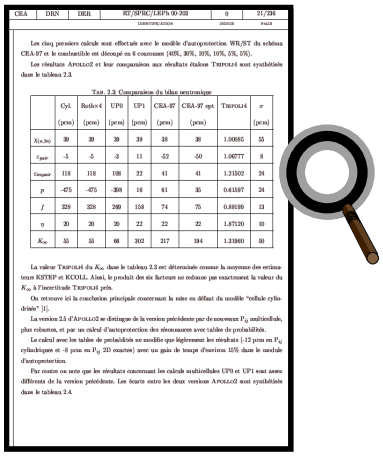

TAB. 2.3: Comparaison du bilan neutronique

	Cyl. (pcm)	Roth×4 (pcm)	UP0 (pcm)	UP1 (pcm)	CEA-97 (pcm)	CEA-97 opt (pcm)	TRIPOLI4	σ (pcm)
$\chi_{(n,2n)}$	39	39	39	39	38	38	1.00085	55
ε_{pair}	-5	-5	-3	11	-52	-50	1.06777	8
ε_{impair}	118	118	108	22	41	41	1.21502	24
p	-475	-475	-398	16	61	35	0.61597	24
f	328	328	269	158	74	75	0.88199	13
η	20	20	20	22	22	22	1.87120	10
K_∞	55	55	66	302	217	194	1.31960	50

1.4 The APOLLO2 Qualification

The calculation errors and their confidence intervals, reported in the APOLLO2.5 Qualification Report [**4**], are used by CEA and its industrial Partners to define the Safety Factor to be adopted in PWR and Mixed-core design studies.

The average of the C/E errors among the various integral experiments, mainly from EOLE critical mock-ups, allowed the “calibration” of the APOLLO2.5/CEA93/CEA-97 product, as well as the associated uncertainty, for the main PWR parameters (**Table App.A.III**). The qualification range extends up to 4.8% w/o U235 for UOX fuels, and up to 13%Pu for MOX fuels.

Table App.A.III Average error and uncertainty (1σ) of the APOLLO2.5/CEA93 tool

PWR Parameter	UOX	MOX
Keff	+ 270 ± 150 pcm	+ 100 ± 250 pcm
Power Peak	- 0.4 ± 0.7 %	+ 1.3 ± 1.5 %
$\Delta\rho$ ^{cycle}	+ 0.5 ± 2 %	-
dK/dT_{fuel} (Doppler)	+2 ± 4 %	+11 ± 4 %
dK/dT_{mod} T = 20°C-80°C	- 0.0 ± 0.3 pcm/°C	- 1.5 ± 0.3 pcm/°C
dK/dT_{mod} T ≅ 300°C	- 0.9 ± 1.0 pcm/°C	+ 3.0 ± 2.2 pcm/°C
dK/dC_B (boron coeff)	+ 3 ± 5 %	+ 0 ± 3 %
$\Delta K/\Delta V_{mod}$ (void coeff)	+ 0 ± 3 %	+ 2.0 ± 2 % (40-60% void) + 1.3 ± 1 % (100% void)
βeff	+ 2.4 ± 1.6 %	+ 0.1 ± 1.6 %
Neutron Lifetime Λ	+ 4 ± 3%	+ 6 ± 3%
$\rho^{Cluster}$ (24 B_4C or Ag-In-Cd)	+ 1 ± 1 %	+ 5 ± 3%
24 SiO_2-B_2O_3 $\rho_{initial}$	+ 2.7 ± 1.5 %	-
UO_2-Gd_2O_3 $\rho_{initial}$	+ 0.2 ± 0.6 %	+ 1 ± 4 %
UO_2-Gd_2O_3 ρ(BU)	+ 0 ± 2 %	-
Reflector Saving	- 1.4 ± 2 %	+3.5 ± 2 %

2. WIMS8

2.1 Resonance treatment in WIMS8

There are two methods of calculating resonance shielding effects in WIMS : equivalence theory and subgroup theory. Equivalence theory for both homogeneous and heterogeneous geometries is implemented in the HEAD module. Sub-group theory is implemented by following the calculation of HEAD by the module PRES, a collision probability theory module and then the module RES. Optionally, the collision probability module can be replaced by a run of the CACTUS flux module. This option is automatically detected and the CACTUS flux is used in place of the flux solution performed by RES using the calculated collision probabilities

Within the HEAD module itself, additional slowing down calculations, known as 'fine group' calculations, are performed. These fine group calculations are used for 3 purposes:

- Ø To evaluate current weighted broad group transport cross sections.
- Ø To calculate an interaction factor which describes how resonances in one nuclide affect the resonance shielding in another nuclide. This model of resonance interaction is used in the lower energy portion of the resonance range between 55.5 eV and 4 eV; a statistical model of resonance interference is used between 55.5 eV and up to 9.11 KeV or 183 KeV according to the version of WIMS.
- Ø To calculate a correction to the broad group removal cross sections due to the effect of the resonances; this correction is related to the resonance escape probability and is therefore known as the f(p) treatment.

• Homogeneous Resonance Theory

By equating the neutron reaction rate at a given energy to the rate of slowing down to that energy , effective cross sections can be generated which reproduce the reaction rates predicted by the NJOY calculations.

The theory is derived from two methods of solving the neutron slowing down equations: The narrow resonance approximation where the energy width of the resonance is assumed to be much smaller than the neutron energy loss per collision, and the wide resonance approximation where the energy width of the resonance is assumed to be much greater than the neutron energy loss per collision.

The detailed theory employs the intermediate resonance treatment which is an interpolation between the two extreme conditions. The interpolation parameter, known in WIMS as λ, is a measure of the effectiveness of a scatterer with respect to hydrogen, with hydrogen itself being assigned the value λ=1. Resonance scatter is considered in the slowing down source. The resonance shielding process for homogeneous geometries involves reading from tables of resonance integrals with the look up parameter being the background scattering cross section σ_p.

• Equivalence Theory

The purpose of the equivalence treatment is to form a relationship between heterogeneous geometry and homogeneous geometry problems. The heterogeneous problem can then be solved by the solution of one or more homogeneous problems. The effect of the heterogeneous geometry is to provide additional paths for neutrons, outside the fuel, to avoid collisions in the fuel resonances and thereby act as an effective increase in the neutron scattering cross-section relative to a homogeneous geometry. The heterogeneous system is approximated by a two region system consisting of a region containing resonance nuclides and a region containing moderator.

It can be shown that if the fuel self collision probability can be represented by a rational approximation, the heterogeneous problem can be represented by a homogeneous problem where the σ_p value has been augmented by a term derived from the geometry of the problem.

The important points to note for equivalence theory are :

Ø A complex problem is related to homogeneous resonance integrals tabulated on the library.
Ø The value of the background scatter cross section σ_p, is adjusted to take account of the problem geometry and the other resonance nuclides in the problem.
Ø The method is only applicable for simple geometries for which rational approximations to the fuel self collision probability can be determined.
Ø The fuel pellet is treated as a single region and therefore even if the fuel region is subdivided into a number of sub-regions by the user the same microscopic cross sections will be assigned to each sub region.
Ø Resonance overlap is calculated by a fine group slowing down calculation at lower energies.
Ø Corrections are made to the outscatter cross section, either based on a calculation of resonance escape probability or the fine group calculation.

• Subgroup Method

The subgroup method can be considered to be intermediate between the equivalence treatment and a continuous energy treatment and has many of the features of the continuous energy treatment including :

Ø General geometry.
Ø Resonance shielding not restricted to fuel.

In the subgroup method the generation of broad group averaged cross sections is performed by transforming the resonance integrals from energy to cross section space. This is a good approximation as the cross sections for non resonant nuclides only vary slowly with energy. The generation of shielded cross sections is carried out by evaluating weighted summations over a number of subgroups :

$$\bar{\sigma}_x = \frac{\sum_i w_i \sigma_{x,i} \phi_i}{\sum_i w_i \phi_i} \quad (1)$$

where i is the subgroup index and x is the reaction under consideration (absorption, fission etc). The subgroup cross sections ($\sigma_{x,i}$) and weighting factors (w_i) are determined by fitting to the homogeneous resonance integrals on the library. The form of the slowing down operator is the same as for equivalence theory except that resonance scatter is not considered.

As a subgroup flux can be determined for each of the regions in the problem, spatial variation in resonance shielding can be modelled.

The f(p) correction is calculated from the factors determined in HEAD.

The resonance interaction model employs the same assumptions as in HEAD. For the higher energy part of the resonance range, a statistical interactions of the resonances is assumed. In subgroup theory this requires solving the flux equations for combinations of subgroups. For the lower energy part of the resonance range, the interaction factors calculated in HEAD using the fine group calculation are used.

The important points to note for subgroup theory are :

- Ø As for equivalence theory, a complex problem is related to homogeneous resonance integrals tabulated on the library.
- Ø Subgroup cross sections and weights are derived which when used in the slowing down equations reproduce the homogeneous resonance integrals tabulated on the library.
- Ø The method can be applied to any geometry which can be modelled by collision probability methods or CACTUS.
- Ø Resonance scatter is not included in the slowing down calculation.
- Ø The cross section variation across a fuel pellet is modelled correctly.
- Ø Resonance overlap is calculated by random interaction or by a fine group slowing down calculation at lower energies.
- Ø Corrections are made to the outscatter cross section, based on factors calculated in the HEAD module.

2.2 Differences between WIMS8 and WIMS9 resonance treatment

The resonance treatment implemented in WIMS9 is described in the previous sections. The major differences between WIMS9 and WIMS8 are as follows:

- Ø The upper energy boundary of the resonance range is 183 keV in WIMS9 and 9.11 kev in WIMS8.
- Ø Transport cross sections are formed by current weighting in WIMS9 and by flux weighting in WIMS8.
- Ø The f(p) corrections factors are generated by a fine group calculation in WIMS9 but are determined from the resonance integrals in WIMS8.

- Ø In WIMS9, the resonance interactions factors are calculated from a statistical model at higher energies and from the fine group calculation at lower energies; in WIMS8 a statistical model is always used.
- Ø In WIMS9 equivalence theory resonance scatter is treated in the slowing down equations, in WIMS8 it is not.

2.3 Definition of the calculation routes

Due to the modular nature of WIMS, several calculation routes can be considered for depletion calculation. These routes are defined in **Fig. App.A.1.**

The **coarse scheme** is a FA depletion calculation well suited to get reactivity values and fuel material inventory after irradiation. In a certain sense, this calculation is similar to the simpler pin cell calculation (see benchmark description section), as it can provide the same information, being unable to assess correctly the pin wise power distribution.

The **fine scheme** is a limit methodology wherein each pin of the assembly has been defined as a separate WIMS rod type, the resonance treatment being performed on every rod type filling the geometrical model. This way of doing is not a standard one, as the computation time and the input data are longer, although it can facilitate the data post processing.

The **reference schemes** for UO2 and MOX fuel are similar as they both request the use of the DIFF option, differing only by the number of groups in the energy condensation process, prior to transport CACTUS calculation.

Finally we call the **subgroup scheme** the WIMS scheme using PRES – RES sequence for resonance subgroup cross sections treatment. The latter scheme is the more general one, since it can be applied in a wide range of situations. For instance, the PRES – RES should be considered as soon as one is interested in radial dependence of the material inventory ; the reference scheme does not compute correctly the outer region of the pellet since the same cross sections are used for the whole pellet.

In the frame of the VALMOX project, only results obtained with the reference schemes are given in detail.

A typical super cell calculation requires ~ 1-2 hour of CPU time (Sun Blade 1000, 600 MHz, 1GB RAM). The equivalent cell calculation takes only 2-3 minutes. The calculation time depends mainly on the number of meshes (size of the geometrical model) and the number of condensed groups.

Fig. App.A.1
WIMS depletion calculation routes,
as defined in the BELGONUCLEAIRE methodology

Coarse scheme	Fine scheme	Reference UOX scheme	Reference MOX scheme	Subgroup scheme
HEAD - 1 wims rod per rod type - 1 annulus* for the pellet	HEAD - 1 wims rod per rod in the model - 1 annulus* for the pellet	HEAD - 1 wims rod per rod type - 1 annulus* for the pellet	HEAD - 1 wims rod per rod type - 1 annulus* for the pellet	HEAD -1 wims rod per rod type -4 annuli for the pellet
				PRES
				CACTUS
				RES
PERSEUS	PERSEUS	PERSEUS	PERSEUS	PERSEUS
PIP	PIP	PIP	PIP	PIP
CONDENSE 6 groups PWR 8 groups BWR	CONDENSE 6 groups PWR 8 groups BWR	CONDENSE 6 groups PWR 8 groups BWR	CONDENSE 21 groups	CONDENSE 6 groups PWR 8 groups BWR
		DIFF Add & copy materials	DIFF Add & copy materials	DIFF Add & copy materials
CACTUS	CACTUS	CACTUS - with “diff” keyword	CACTUS - with “diff” keyword	CACTUS - with “diff” keyword
		DIFF Make a material from “diff” materials	DIFF Make a material from “diff” materials	DIFF Make a material from “diff” materials
BURNUP	BURNUP	BURNUP	BURNUP	BURNUP

* Excepted for UGd pins for which 7 annular regions of equal surface are defined in the pellet

3. ALEPH

3.1 Multigroup approach in ALEPH

In the multi group ALEPH approach, we calculate the reaction rate s_{ijk} as:

$$\sigma_{ijk} = \frac{\sum_g \sigma_{ijk}^g \Phi_k^g}{\sum_g \Phi_k^g} \quad (2)$$

in which s^g_{ijk} and $?^g_k$ are the cross section and spectrum of energy group g with boundaries $[E_{g-1},E_g]$. Only the multi group spectrum has now to be calculated by the MC code. The group structure has been chosen so that the reaction rates calculated by equation are within one standard deviation of the values calculated by MCNP(X).

The resulting group structure is quite large (of the order of 1E+4 groups) and can be assumed to be practically continuous (see Fig. A.2 in the main text for a typical multi-group energy spectrum calculated by ALEPH). During the MC simulation, the code has only to determine in which energy bin to accumulate the flux. The extra calculation time that this operation takes is so small that it is barely visible, even for our large group structure. During a test with a structure of around 1E+5 groups (10 times more than we actually need) we observed an increase in calculation time of about 2%.

The group cross section s^g_{ijk} itself is calculated analytically by ALEPH using the following formula:

$$\sigma_{ijk}^g = \frac{\int_{E_{g-1}}^{E_g} dE\, \sigma_{ijk}(E)\varphi(E)}{\int_{E_{g-1}}^{E_g} dE\, \varphi(E)} \quad (3)$$

with f (E) the spectrum used to weigh the cross section (which can be a constant spectrum or a spectrum composed of a Maxwellian spectrum, a slowing down spectrum and a fission spectrum).

The total time required to calculate the reaction rates using this formula is constant regardless of the number of particles simulated and is of the order of seconds to minutes (for example, on a dual Xeon 3GHz system, this calculation takes 15 seconds for the entire JEF-2.2 library). The calculation time required depends on the number of reaction rates and the group structure but this is negligible compared to the calculation time of a single MCNP(X) run - unless very few particles are simulated. By using this multi group ALEPH approach we have effectively reduced the calculation time by a factor 30.

3.2 Calculation flow in ALEPH

ALEPH is in essence an interface code between NJOY 99.90, ORIGEN 2.2 and MCNP(X) (we currently use MCNPX 2.5.e) as can be seen in Figure 2. Except for some minor modifications to ORIGEN 2.2 to improve output accuracy (the number of significant digits were increased from 3 to 5) and to improve memory allocation, no changes have been made whatsoever to the source code of the programs involved. ALEPH itself has been written in C++ using a highly modular design to allow for great flexibility. Replacing for instance MCNP(X) by another MC code would be quite easy because of the modular design (we would only have to replace the object responsible for the MCNP(X)-ALEPH interface by a similar object for the new MC code).

The input required by ALEPH is the irradiation history, along with an initial MCNP(X) input file and other code options. Information such as initial material composition, temperatures, volumes, etc. are read from the initial MCNP(X) input file. Before every MCNP(X) run ALEPH generates a new input file based upon the input options of the user. First of all, the material composition of the materials that are being burned are updated. For the purpose of transport calculations we truncate the material composition calculated by ORIGEN using a fractional absorption criterion specified by the user. Only those nuclides responsible for e.g. 99% or 99.9% of all absorptions are included - nuclides that were originally present are added by default and do not necessarily contribute to this fractional absorption criterion. For the BUC IV B benchmark, we used a 99.9% fraction.

If requested by the user, ALEPH will also change the position of burnable materials and replace materials (to represent reshuffling). ALEPH can also change the temperature of any material (both materials that are being burned or materials that are left unchanged) and density and/or composition of a material that is not being burned.

After every MCNP(X) run, the multi group spectra are read from the tally file. ALEPH will now generate the reaction rates required by ORIGEN. ORIGEN makes a distinction between three fundamental types of materials: activation products, actinides (including their daughter nuclei) and fission products. The required input of reaction rates and other data depends upon the type of material. Activation products require cross sections for (n,?) (both to the ground state and the first metastable state), (n,2n) (both to the ground state and the first metastable state), (n a) and (n,p) reactions. In the case of actinides, the (n,a) and (n,p) reactions have been replaced by fission and the (n,3n) reaction. Fission products have the same cross sections as activation products but some of the fission products have direct fission yield data, associated with 8 primary actinides (Th-232, U-233, U-235, U-238, Pu-239, Pu-241, Cm-245 and Cf-252). ALEPH will use an original ORIGEN cross section library and only change the values for isotopes for which data is available. Note that all nuclides represented in WIMS-8a (124 nuclides) are effectively recalculated within ALEPH.

The reaction rates s_{ijk} for the (n,a), (n,p), fission and (n,3n) reactions calculated by equation (2) can be used immediately by ORIGEN. In the case of (n,?) and (n,2n), we still need to distinguish between the reaction rate to the ground state and the first metastable state. For this purpose, ALEPH uses a branching ratio obtained from the original ORIGEN library:

$$\lambda = \frac{\sigma^{0}_{mt}}{\sigma^{0}_{gr} + \sigma^{0}_{mt}} \quad (4)$$

where s^{0}_{gr} is the original ORIGEN-2.2 reaction rate to the ground state and s^{0}_{mt} the one to the first metastable state.
The new reaction rates s_{gr} and s_{mt} will then be given by:

$$\sigma_{gr} = (1-\lambda)\sigma \quad (5)$$

$$\sigma_{mt} = \lambda\sigma \quad (6)$$

in which s is the reaction rate calculated with equation (3) in the main text. The direct use of the cross sections of these reactions to the ground state and the first metastable state (for instance from EAF-99 files or JEFF-3.0A files) is also a possibility.
ALEPH leaves the original yield values from ORIGEN unchanged (the use of energy dependant fission yields is foreseen in the next version of ALEPH).

3.3 Other features of ALEPH

Another significant feature of ALEPH is that it reads microscopic cross sections directly from an ENDF file prepared by NJOY (in linear interpolated form). To automatically generate these ENDF files and the corresponding ACE files (at several different temperatures) for transport calculations, we have created a utility called ALEPH-DLG (Data Library Generator) [**6**]. This way, we ensure that exactly the same nuclear data is used within the entire code system. The probability tables in the unresolved resonance energy region are switched off during the MCNP(X) calculations because the multi group approach in ALEPH cannot use these probability tables like MCNP(X) can as these change the cross section for a single particle while for a collection of particles we see an average cross section. Another approach is being developed to take into account the (small) contribution of probability tables.

The JEF 2.2 nuclear data evaluation (or JEFF-3.0, see section B.6 Effect of using new JEFF3 data) is preferred for use by ALEPH due to its completeness compared to other evaluations (such as ENDF-B6.8) in high energy reactions such as (n,p), (n,?), (n,2n) and (n,3n) that are required by ORIGEN.

ALEPH calculates the required reaction rates, for all nuclides available (with one exception, we do not consider elemental evaluations) in JEF-2.2 (296 nuclides) for use in ORIGEN outside MCNPX. The microscopic point-wise continuous cross sections used by ALEPH to calculate one-group cross-sections are generated by NJOY-99.90 (use of RECONCR and BROADR modules of NJOY-99.90) and these are also used by MCNPX (use of the RECONCR, BROADR, UNRESR, HEATR, THERMR, GASPR, PURR and ACER modules of NJOY-99.90) to perform the required neutron transport calculations. This way, we insure that the same nuclear data is used within the code system.

The MCNPX model is an exact (i.e. no homogenisation of fuel cells) representation of the pin cell, assembly and macro-assembly as described in the benchmark. Each pin is modelled and followed separately.

ALEPH recalculates also, for each pin separately, the fuel composition for each burn-up increment of 1 GWd/t_{HM} (42 time steps of 30 days each for the entire calculation).

We have used JEF-2.2 (296 nuclides) original evaluations to build, with the aid of NJOY99.90, our own linear-linear interpolated continuous (differential) cross sections for MCNPX25e and ALEPH. The fractional reconstruction tolerance used was 0.1% with integral thinning of 5E-8 barns (the only exceptions are Fe 57 and Mo 94 for which a strict fractional reconstruction tolerance of 0.1% was used). If integral thinning is used, NJOY uses a fractional reconstruction tolerance of 1% (i.e. the maximum difference between the exact and the linear interpolated data is lower than 1%). After this, NJOY checks if the difference between the exact and the linear interpolated infinite dilution resonance integral over two consecutive energy points is lower than 5E-8 barns. If so, NJOY stops the process. If not, NJOY uses a higher tolerance up to the 0.1% tolerance.

All materials were Doppler broadened at their respective temperature (900 K for the fuel, 620 K for the cladding and 575 K for the moderator). We generated also S(a,ß) scattering data (THERMR module of NJOY99.90) for H2O at 575K to take into account molecular binding and crystalline effects (coherent scattering) using S(a,ß) functions available in the thermal JEF-2.2 files.

A typical multi-assembly calculation (relative error of about 0.5% on (n,?) reactions) would require about 1 hour of CPU time (40 CPU Xeon, 3GHz, 1GB RAM parallel calculation).
The equivalent cell calculation takes only about 45 minutes on a single processor or a PC.

Fig. App.A.2 shows the complete calculation flow in ALEPH.

Fig. App.A.2 Calculation flow in ALEPH

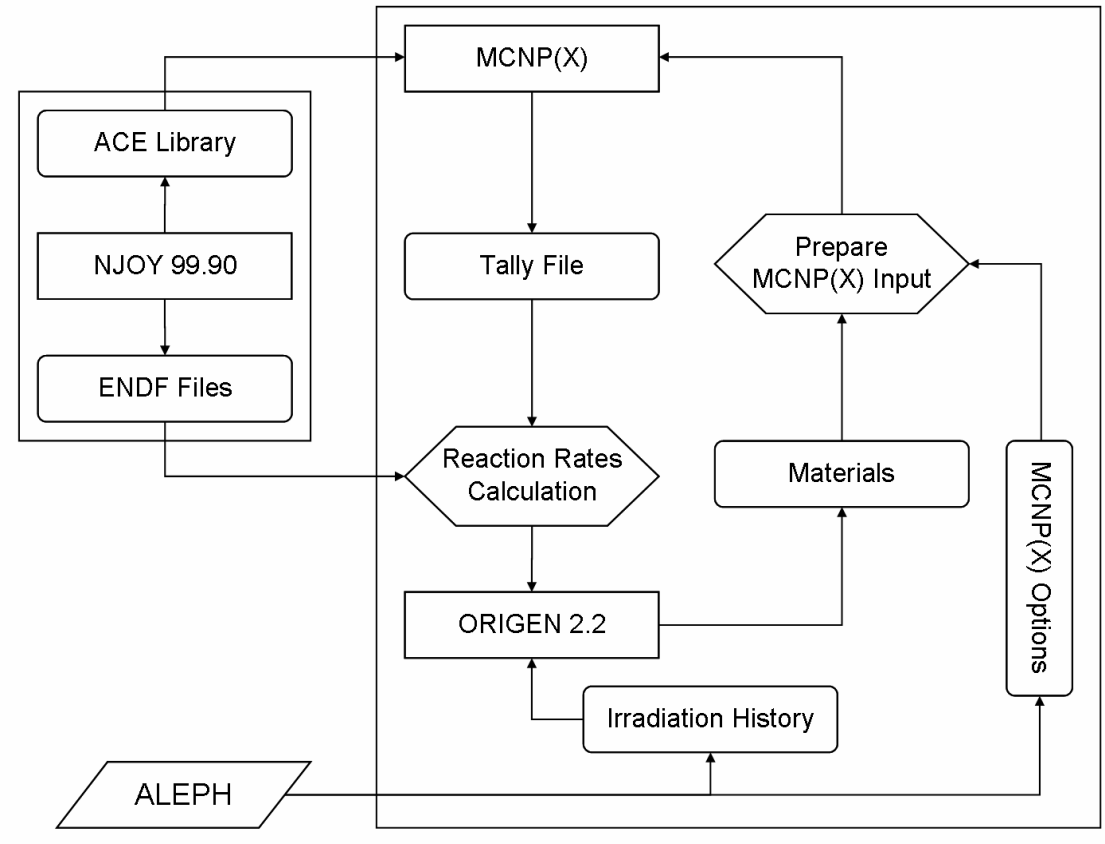

References in this Appendix

1. R. Sanchez, Z. Stankovski, "SILENE & TDT: a code for collision probability calculations in XY geometries," ANS Annual Meeting ,San Diego, USA, June 20-23, 1993.
2. I. Zmijarevic, "Multidimensional discrete ordinates nodal and characteristics methods for the APOLLO2 code, "Proc. Int. Conf. on Math. and Computation, M&C99, Madrid, Spain, Sept. 1999.
3. R. Sanchez, M. Coste, Z. Stanskovski, C. Van der Gucht, "Models for multigroup self-shielded cross sections calculations in the code APOLLO2" Proc. Int. Conf. on the Physics of Reactors, PHYSOR-90, Marseille, France, April 23-27, 1990.
4. A.Santamarina, C. Chabert, A. Courcelle, O. Litaize, G. Willermoz, D. Biron, L. Daudin, "Qualification of the APOLLO2.5/CEA93.V6 code for UOX and MOX fuelled PWRs," Int. Conf. on the Physics of Reactor PHYSOR2002, Seoul, Korea, October 7-10, 2002.
5. J.P. Both, H. Derrienic, B. Morillon, J.C. Nimal, "A Survey of TRIPOLI-4," Proc. Int. Conf. on Radiation Shielding ICRS-8, Arlington, USA, 1994.
6. W. Haeck and B. Verboomen, ALEPH-DLG (Data Library Generator) - Creating a General Purpose Validated Application Library for MCNP(X) and ALEPH, SCK-CEN, BLG n° 1002 (2005)